A SPECTROSCOPIC MECHANISTIC STUDY ON ZIRCONIUM(IV) AND HAFNIUM(IV) COMPLEXES

by

LEBOHANG THEODORE MPHURE

A dissertation submitted to meet the requirements for the degree of

MAGISTER SCIENTIAE

in the

DEPARTMENT OF CHEMISTRY

FACULTY OF NATURAL AND AGRICULTURAL SCIENCES

at the

UNIVERSITY OF THE FREE STATE

Supervisor

Prof. Andreas Roodt

Co-Supervisor

Prof. Hendrik Gideon Visser

Co-Supervisor

Dr Marietjie Schutte-Smith

Acknowledgements

"To God Be the Glory" by Fanny Crosby.

"To God be the glory, great things He hath done; So loved He the world that He gave us His Son,Who yielded His life an atonement for sin, And opened the life gate that all may go in.
Great things He hath taught us, great things He hath done, And great our rejoicing through Jesus the Son; But purer, and higher, and greater will be Our wonder, our transport, when Jesus we see."
With these two stanzas I would like to give God Almighty all the glory for what He has done for me, it is by His grace that I am who I am today.

I would also like to thank my mother Madonna Ngwela and her two sisters Grace Sekaja and Maggie Lebusa for raising me with the little that they had and also for making sure that I received the best education they could get for me. Thank you for your continuous support and prayer for those crystals even though you didn't know what they were.
To Mr and Mrs Seboka my parents away from home thank you for all your efforts and support over the last two years it I am truly a blessed individual to have you in my life . God couldn't have had a better plan

To Prof. Roodt thank you for this opportunity, you believed in me two years ago when most people had written me off. Thank you for your enthusiasm every time I had meeting with you taught me something new you truly are an amazing individual it's a great blessing to have been here in your time. May God continue to bless you to do good.

To Prof Deon Visser thank you for your help, guidance and constant motivation for me to be diligent in my work.

To Dr Marietjie Schutte, thank you for the hard work you did over the December holidays, reading my horrible writing and continuous encouragement. I don't think I would have made it without… Thank you again.

The UFS inorganic group: thank you all for the continuous support and friendship.

To all my friends thank you for your support… Thank you for your candid spirit through all the tough times.

Contents

List of Tables

Table 0: List of abbreviations and meaning.

Abbreviations	
Degrees	°
Degrees Celsius	°C
Angstrom	Å
Acetylacetonate	acac
Deuterated Dimethylformamide	C_3D_7NO
Deuterated Benzene	C_6D_6
DimethyFormamide	DMF
Gram	g
Planck's constant	h
Infrared spectroscopy	IR
Equilibrium constant	K
Boltzman's constant	k_B
Kern Magnetiese Resonans spekstroskopie	KMR
Observed pseudo-first order rate constant	k_{obs}
$mol.dm^{-3}$	M
Methanol	MeOH
Milligram	mg
Millimolar	mM
Sodiumthenoyltrifluoroacetone	N(tta)
Nuclear Magnetic Resonance spectroscopy	NMR
Parts per million	ppm
Time	t
Temperature	T
Thenoyltriflouroacetylacetone	ttaH
Ultraviolet region in light spectrum	UV
Visible region in light spectrum	Vis
Number of molecules in a unit cell	Z
Alpha	α
Beta	β
Gamma	γ
Chemical shift	δ
Extinction coefficient	ε
Thetha	Θ
Wavelength	λ
Stretching frequency on IR	ν
Pi	π
Sigma	σ
Enthalpy	ΔH
Entropy	ΔS
Gibbs Free Energy	ΔG

Abstract

The aim of this study was to synthesize M(*L,L'*)$_4$ type complexes of zirconium(IV) and hafnium(IV) using *N,N'*-diamine and *O,O'*-bidentate ligands. The synthesized complexes were characterized and a kinetic study of the formation of the respective complexes was performed.

Characterization of the successfully synthesized complexes, tetrakis(thenoyltrifluoro-acetylacetone) zirconium(IV) monohydrate ([Zr(tta)$_4$]**.**H$_2$O) and tetrakis(thenoyltrifluoroacetylacetonato) hafnium(IV) ([Hf(tta)$_4$]) was done by infrared (IR), ultraviolet and visible spectroscopy (UV/Vis) and ^{1}H and ^{19}F nuclear magnetic resonance (NMR) spectroscopy. The structure of [Zr(tta)$_4$]·H$_2$O was successfully characterized by single crystal X-ray diffraction while its hafnium counterpart was unsuccessful due to poor crystal quality.

[Zr(tta)$_4$]**.**H$_2$O crystallized in the orthorhombic space group *Pca*2$_1$ with *Z* = 4. The structure of [Zr(tta)$_4$]**.**H$_2$O consists of a zirconium(IV) metal centre coordinated to eight oxygen atoms of four *O,O'*-bidentate ligands, with an average Zr—O bond distance of 2.18(7) Å and an average bite angle of 107(8)˚. Unlike common alternating CF$_3$ groups with respect to the coordinating ligand, the CF$_3$ groups of this structure were clustered in the plane of the molecule. In contrast to a similar structure the thenoyl rings of this structure were connected by a water molecule.

In the kinetic investigations the formation reaction between zirconium(IV) and hafnium(IV) with the Na(tta) ligand at varying metal to ligand ratios were followed by ^{19}F and ^{1}H-NMR. Competition studies were also performed between the two metals and Na(tta). In both the studies the a general observation was made that the formation reaction consisted of two reactions: a fast first reaction and a slow second reaction.

In the individual metal studies it was determined that the observed rate constants for the hafnium(IV) system were ~ 2 times faster than the zirconium(IV) system for the first fast reaction and ~ 7 times faster for the second slow reaction.

In the competition studies between zirconium(IV) and hafnium(IV) integration values of the final spectra showed that more of [Zr(tta)$_4$]**.**H$_2$O was formed compared to [Hf(tta)$_4$] was formed. The observed rate constants for both the fast and the slow reaction were comparable in each case and didn't reflect the observations that were made for the individual metal kinetic runs.

Opsomming

Die doel van hierdie studie was om van M(*L,L'*)$_4$ tipe komplekse van sirkonium(IV) en hafnium(IV) te sintetiseer met *N,N'*-diamien en *O,O'*-bidentate ligande. Die gesintetiseerde komplekse is gekarakteriseer en `n kinetiese studie rakende die vorming van die onderskeie komplekse is uitgevoer.

Karakterisering van die gesintetiseerde komplekse, tetrakis(tenoïeltrifluoor-asetielasetoon) sirkonium(IV) monohidraat ([Zr(tta)$_4$].H$_2$O) en tetrakis(tenoïeltrifluorasetielasetoon) hafnium(IV) ([Hf(tta)$_4$]) is uitgevoer deur middel van infrarooi (IR), ultraviolet en sigbare spektroskopie (UV/Vis) en ^{1}H en ^{19}F kermagnetiese resonans (KMR) spektroskopie. Die struktuur van [Zr(tta)$_4$].H$_2$O is suksesvol deur enkelkristal X-straal diffraksie gekarakteriseer terwyl die karakterisering van die hafnium eweknie enkelkristal diffraksie met X-straal onsuksesvol was as gevolg van swak kristalkwaliteit.

[Zr(tta)$_4$].H$_2$O Dit het gekristalliseer in die ortorombiese ruimtegroep *Pca*2$_1$ met *Z* = 4. Die [Zr(tta)$_4$].H$_2$O kompleks bestaan uit `n sirkonium(IV) metaalkern wat aan die agt suurstofatome van die vier *O,O'*-bidentate ligande gekoördineer is, met `n gemiddelde Zr—O bindingsafstand van 2.18(7) Å en `n gemiddelde bythoek van 107(8)˚. In teenstelling met algemene variasies in die CF$_3$ groepe ten opsigte van die koördinerende ligand, groepeer die CF$_3$ groepe van hierdie struktuur aan die dieselfde kant van die molekuul. Anders as in soortgelyke gepubliseerde strukture word die tenoïelringe van hierdie struktuur met `n water molekuul verbind.

Vir die kinetiese ondersoek is die vormingsreaksie tussen sirkonium(IV) en hafnium(IV) met die Na(tta) ligand met wisselende metaal:ligand verhoudings deur middel van ^{19}F en ^{1}H KMR gevolg. Kompetisiestudies is uitgevoer tussen die twee metale en die Na(tta) ligand. In beide die studies is die algemene waarneming gemaak dat die vormingsreaksie uit twee reaksies bestaan: `n vinnige eerste reaksie en `n stadige tweede reaksie.

In die individuele metaalstudies is vasgestel dat die waargenome tempokonstantes vir die hafnium(IV) reaksies ~ 2 keer vinniger is as die sirkonium(IV) reaksies vir die eerste, vinnige reaksie, en ~ 7 maal vinniger vir die tweede, stadige reaksie.

In die kompetisiestudies tussen sirkonium(IV) en hafnium(IV) het integrasiewaardes van die finale spektra getoon dat meer [Zr(tta)$_4$] as [Hf(tta)$_4$] gevorm het. Die waargenome

tempokonstantes vir beide die vinnige en stadige reaksies was vergelykbaar in elke geval en weerspieël nie die waarnemings wat vir die individuele metaal studies gemaak is nie.

1 Introduction

1.1 General

Zirconium and hafnium are the two elements on the periodic table that are more similar than any other pair, therefore they have been referred to as the twins.[1] ^{40}Zr has a metallic grey appearance; it is a hard, malleable, strong metal that can withstand highly corrosive environments. ^{72}Hf is positioned directly below ^{40}Zr on the periodic table, in the titanium-triad. ^{72}Hf has the same physical appearance and most of the chemical properties of zirconium but zirconium is naturally more abundant than hafnium, because these two elements are so similar, separation is complicated and expensive.

These two metals have been had many applications in various industries since their discovery in 1789 and 1923 respectively. The most important application in recent years has been in the nuclear energy production, due to the physical difference in their thermal neutron absorption cross section. Trace amounts of one element in the other lead to the inefficiency of their application in the nuclear energy production. Zirconium is utilized in zirconium alloys that are used as cladding material for containing nuclear fuel such as UO_2 ($U^{235} \approx 3.5\%$ and $U^{238} \approx 97\%$) or plutonium-239. It allows for neutrons to be transmitted through the cladding material where the fission reaction takes place. On the other hand hafnium is used in the manufacturing of the control rods that control the amount of neutrons made available for the fission reaction, by neutron absorption.

[1] Chemistry Explained Foundations and Applications, Zirconium, Available: http://www.chemistryexplained.com/elements/T-Z/Zirconium.html (Last accessed 05/ 01/ 2014).

1.2 Nuclear Energy

South Africa forms part of a group of 12 countries called the Southern African Power Pool (SAPP). It contributes 80% of SAPP's power in addition to the 95% it supplies to itself.[2] 4% of this energy is produced from nuclear powered power stations.[2] South Africa constructed its first nuclear power station in the 1970s and now possesses two operating nuclear reactors. The energy consumption of the SAPP countries and South Africa itself has been increasing since the 1980s and it has been projected that South Africa needs to generate 63 GW more by 2025 to maintain its distribution capabilities to the growing demand. 9.6 GW of the electricity required will have to come from nuclear powered power stations. [2]

For this reason South Africa now considers to construct new nuclear power plants. South Africa is not the only country that has been reported to be considering building nuclear power plants to assist with the growing power demand. Other African countries that are also considering nuclear power plant construction include Nigeria, Ghana, Kenya, Senegal, Namibia, Sudan and Uganda.[3] This growing interest means that there will be a higher demand for refractory metals such as zirconium and hafnium. Therefore development of more efficient and cost effective methods for separating such metals will be vital in the near future.[3]

1.3 Separation of Zirconium and Hafnium

The use of these two elements in nuclear power plant reactors and the growing demand for this form of energy generation has made the separation of these elements an necessary problem to solve.[4] The difficulties associated with separating zirconium and hafnium will be discussed in more detail in Chapter 2 along with the methods that have been developed. These methods include Ion Exchange and Liquid-Liquid Extraction.

[2] World Nuclear Association: Nuclear Power in South Africa. Available. http://www.world-nuclear.org/info/country-profiles/countries-o-s/south-africa/ (Last accessed 7/ 12/ 14).
[3] Barber, D.A., Africa's Nuclear Energy Hopefuls Learning From South Africa. Available: http://afkinsider.com/75817/africas-nuclear-energy-hopefuls-learning-south-africa/ (Last accessed 7/ 12/ 14).
[4] Machlan, L. A., Hague, J. L., *J. of Research of the National Bureau of Standards—A. Physics and Chemistry*, **66A**, 517-520, 1962.

1.4 Aim of this Study

The general coordination chemistry of zirconium and hafnium is well established.[5] However investigations into the different aspects like crystallization, reactivity, solubility etc. of similar coordination compounds have not been explored to a large extent. Subtle differences could potentially lead to cleaner separation processes.[6,7]

Keeping the above in mind the following aims for this study can be summarized:

- To utilize *O,O'*-bidentate and *N,N'*-diamine ligand systems to synthesize zirconium(IV) and hafnium(IV) complexes.
- To fully characterize the respective complexes using NMR, IR and UV/Vis spectroscopy, and to try and find small differences in the structure/property relationships that could be manipulated for separation in the future.
- X-Ray Diffraction characterization will be pivotal as it provides unique three dimensional visualization of the complexes synthesised. This will allow for accurate structural differences to be easily identified and exploited.
- To conduct ^{19}F-NMR solution studies of the zirconium(IV) and hafnium(IV) complex formation with an asymmetrical bidentate ligand. Hopefully the formation of the intermediate species may be identified. Any obvious differences in the reactivity of these two metals with a bidentate ligand could be used in future separation studies.
- To investigate whether one of the two metal ions in solution has a higher affinity for the bidentate ligand by designing different competition ^{19}F-NMR studies.

[5] Bruno, I. J., Cole, J. C., Edgington, P. R., Kessler, M., Macrae, C. F., McCabe, P., Pearson, J. and Taylor, R., *Acta Cryst*. **B58**, 389-397, 2002.
[6] Steyn, M., MSc Dissertation: *Speciation And Interconversion Mechanism Of Mixed Halo And O,O'- And O,N-Bidentate Ligand Complexes Of Zirconium.* University of the Free State. UFS, 2009.
[7] Viljoen, J. A., MSc Dissertation: *Speciation And Interconversion Mechanism Of Mixed Halo And O,O'- And O,N-Bidentate Ligand Complexes Of Hafnium.* University of the Free State. UFS, 2009.

2 Literature Study

2.1 Brief History

Zirconium, element number 40, was discovered in 1789 by the German chemist Martin Klaproth while hafnium, element number 72 was discovered in 1923 by George Charles de Hevesy and Dirk Coster.[1,2] The delay in the discovery of hafnium was due to its chemical similarity to zirconium. There are earlier references to zirconium and hafnium that date back to ancient Arabia. These references refer to zirconium as "Zargun" meaning gold-like or gold colour.[3] The name Hafnium is derived from the Latin word "Hafnia" meaning Copenhagen, the capital city of Denmark, where hafnium was first discovered.[4]

The similarity of zirconium and hafnium is associated with their chemical properties. Zirconium and hafnium occur in the same group on the periodic table and therefore have similar electron configurations (Zr: $4d^2\ 5s^2$ and Hf: $5d^2\ 6s^2$).[5] Their ionic and atomic radii are almost identical, even though hafnium is expected to have a larger ionic radius, since it has 32 more electrons than zirconium. Due to lanthanide contraction, the ionic radius of hafnium is decreased to almost that of zirconium. Lanthanide contraction is a term introduced by Victor Goldschmit and is a phenomenon that causes a decrease in ionic radii of the lanthanides.[6] Lanthanide contraction further affects the ionization energies, which also leads to the ionization energies of hafnium and zirconium to be similar.[7] The two elements' physical properties also have distinct similarities.

[1] Schemel, J. H., *ASTM Manual on Zirconium and Hafnium*, ASTM International, 1977.
[2] Roza, G., *Zirconium*, Rosen Publishing Group Inc. 2009.
[3] Stwertka, A., *A Guide to the Elements*, 2nd Ed, Oxford UniversityPress Inc, 2002.
[4] Haynes, W. M., *CRC Handbook of Chemistry and Physics*, Ed. 93, 2012.
[5] Brown, T. E., LeMay, E. H., Bursten, B. E., Murphy, C., Woodward, P., *Chemistry The Central Science* 13th Ed, Prentice Hall, 2014.
[6] Kauffman, G. B., *The Chemical Educator*, **2(**5), 1-26, 1997.
[7] Huang, C-H., *Rare Earth Coordination Chemistry: Fundamentals and Applications*, John Wiley & Sons (Asia) Pte Ltd, 2010.

In 1949 a satisfying reason for the need to separate hafnium from zirconium was first acknowledged when the need of materials for future energy demands were reported by Larsen from S. Pike's discussion.[8] It was indicated that zirconium and hafnium were the metals of choice over other similar refractory metals like titanium, due to their chemical and physical properties. Zirconium has a low thermal neutron absorption cross-section while hafnium's is high.[9] A thermal neutron absorption cross-section is a cross section area in an atom that represents the probability of neutron interaction with the atom and it is measured in barns*.[9,10] Zirconium and hafnium can withstand high temperatures and corrosion and for these reasons they were proposed to be the materials of choice for future nuclear fuel cladding material.[8,11]

2.2 Chemical Properties of Zirconium and Hafnium

Zirconium and hafnium are in the titanium triad on the periodic table and have similar chemical properties.[1,12] Both zirconium and hafnium metal have a silver metallic appearance and are malleable. Their external features resemble steel when they are compacted.[1,2,12] It is rare to find pure hafnium in its natural state.[13] The chemical and physical properties of zirconium are affected to a large extent by the 'impurity' i.e. hafnium.

There are, however, two significant physical differences between hafnium and zirconium. Firstly the density of zirconium is half that of hafnium; secondly, hafnium has an absorption cross section for thermal neutrons that is estimated to be six hundred times greater than that of zirconium.[14] A concentration larger than 100 ppm of hafnium present in a zirconium alloy will cause the fuel cladding zirconium to absorb thermal neutrons, thus essentially 'poisoning' it. Table 2.1 notes some of the significant physical properties of hafnium and zirconium.[15,16,17]

* Barn is an unofficial SI unit often abbreviated (bn) that is extensively used by nuclear physicists for expressing the cross sectional area of nuclei.

[8] Larsen, E. M., *J. Chem. Ed.*,529-535, 1931.
[9] Gusakov-Stanyukovich, I. V., Poluektov, P. P., Radchenko, M. V., Atomic Energy, **108** (5), 393-394, 2010.
[10] Measurement unit: barn. Available: http://www.convertunits.com/info/barn. (Last accessed 18/ 01/ 2014).
[11] *Chem. Eng. News*, **28** (47), 4112-4115, 1950.
[12] Wiberg, E., Wiberg, N., *Holleman-Wiberg's Inorganic Chemistry* 1st Ed, Academic Press, 2001.
[13] Lowe, A. L., *Zirconium in the Nuclear Industry*, ASTM International, 1984.
[14] Ritter, S. K., *C&EN*, **85** (41), 42-43, 2007.

Table 2.1: Some of the physical properties of hafnium and zirconium.[15,16,17]

Property	Hafnium	Zirconium
Atomic Number	72	40
Atomic Weight (g/mol)	178.49	91.22
Atomic Radius (Å)	1.442	1.452
Density **(**g/cm^3)	13.28	6.5107
Thermal neutron cross section (barns)	105	0.18
Melting Point (˚C)	2222	1852
Boiling Point (˚C)	5400	3580

There are several isotopes of hafnium that range from mass atomic number 153 to 186. Of these isotopes only six occur naturally.[18] The most unstable isotope has a half-life of 400 ms and the most stable isotope has a half-life of 10 years. A nuclear isomer of hafnium (^{178m2}Hf) emits gamma rays with energies totalling to 2.45 MeV.[16,19] It is estimated that one gram of this isotope would be able to emit 1330 MJ of energy that would be proportionate to an explosion of 317 grams of TNT*.[19]

Zirconium also has several isotopes ^{90}Zr, ^{91}Zr, ^{92}Zr, ^{94}Zr, and ^{96}Zr with respective natural abundances of ~52, ~11, ~17, ~17 and ~3% (Table 2.2).[9,20] The preferred isotope for nuclear reactor construction is the one with the lowest ability to absorb thermal neutrons, namely ^{90}Zr. ^{90}Zr has a thermal neutron absorption cross-section that is 10 times larger than that of ^{91}Zr.[20] The removal of this isotope would increase the efficiency of the nuclear reactor container that zirconium is used for. A laser isotope process is used where a sample of zirconium is exposed to a particular wavelength. The radiation from the laser is absorbed by the isotope of interest and will react with a scavenger which will then form a product that is easily separated from the other

*TNT is an abbreviation for trinitrotoluene, an explosive chemical compound also known as dynamite.

[15] Bloomer, R. C., Werner, H. J., Geology of the Blue Ridge Region in Central Virginia: *Geol. Soc. America*, **66** (5), 579-606, 1955.
[16] Othmer, K., *Encyclopaedia of Chemical Technology* 3rd Ed. **12**.
[17] Othmer, K., *Encyclopaedia of Chemical* Technology 3rd Ed. **24**.
[18] Rank, J., *Hafnium: Chemical Elements*. Available: http://www.chemistryexplained.com/elements/C-K/Hafnium.htmL. (Last accessed 8/ 10/ 2014).
[19] Becker, J. A., Gemmell, D. S., Schiffer, J. P., Wilhelmy, J. B., *The 178m2 Hf Controversy*, Lawrence Livemore National Labratory, 2003.
[20] Chiang, P. T., Lahoda, E. J., Burgman, H. A., *Process for separating zirconium isotopes*. Patent US4584183A, Dec 21, 1983.

isotopes. This process is efficient but it is very expensive and difficult, as a result it is not employed on an industrial scale.[20,21]

Table 2.2: Natural abundances of the isotopes of zirconium and their thermal neutron capture cross sections.[20,21]

Isotope of Zr	Occurrence %	Thermal Neutron Capture Cross Section (Barns x 10^{-28})
90	51.45	0.03
91	11.32	1.14
92	17.32	0.21
94	17.28	0.055
96	2.76	0.02

The most prevalent oxidation state of hafnium and zirconium is the tetravalent +4 oxidation state, and in this oxidation state these metals form many inorganic compounds. This is also the most stable oxidation state for both metals.[22] There are certain instances where hafnium and zirconium have been reported to have a +1, +2 and +3 oxidation state.[22] These lower oxidation states are rare and are obtained with difficulty.[22] In aqueous solutions zirconium and hafnium exist solely in the quadrivalent +4 oxidation state. They react with halogens to form tetra halogen compounds and at high temperatures zirconium and hafnium also react with oxygen, nitrogen, carbon, sulphur, boron and silicon.[22]

2.3 Applications

2.3.1 Application of Zirconium in the Nuclear Energy Industry

Hafnium-free zirconium is produced almost solely for the application in the nuclear construction industry for the manufacturing of metal alloys called zirconium alloys.[1] Alloying elements like Nb, Fe, Sn, Ni etc. help to improve some physical aspects of these alloys like an increase in resistance to corrosion, the ability to withstand high temperatures and a low absorption cross section for thermal neutrons.[1,23] The zircaloys are used for structural parts (cladding material) of

[21] Monrocville, P. D. C., Peterson, S. H., Boro, M., *Zirconium Isotope Separation*. Patent US 4,389,292, Jun. 21, 1983.
[22] Kozak, C. M., Mountford, P. *Encyclopedia of Inorganic Chemistry Zirconium & Hafnium: Inorganic & Coordination Chemistry*, Wiley, 2006.

the core of a water moderated nuclear reactor, the cladding of cylinders used to contain the uranium nuclear fuel rods from the modulator. In order to contain the fuel rods, the cladding needs to withstand harsh conditions and at the same time not interfere with the nuclear reaction by having as little as possible interaction with the neutrons.[23,24,25] Zirconium is very well suited for this application as it possesses all the required properties for cladding material. Depending on the type of nuclear reactor, a specific type of zirconium alloy is employed which differ in specifications. Table 2.3 below shows a list of Zircaloys™ that have been developed with the different specifications to suit a nuclear reactor. [25,27,28] Table 2.3 was adopted from Krishnam *et al.*[26]. The importance of adding niobium to the zirconium alloys was discussed even though the percentage composition was not tabulated. Niobium forms a significant percentage of the alloying metals in zirconium alloys 2 and 4 and it improves the resistance to corrosion and radiation.

Table 2.3: Percentage Composition of the Different Zircaloys.[27, 28]

Zircaloy™	Zr %	Cr %	Sn %	Fe %	Ni %	O %
Zircaloy-1	97.5	-	2.5	-	-	
Zircaloy 2	98.25	0.10	1.45	0.06	0.01	0.01
Zircaloy-3	99.5	-	0.25	0.25	-	
Zircaloy-4	98.17	0.10	1.60	0.23	-	0.01

Zircaloy-1 is not being employed in reactor construction since the break-away transition is not improved with the alloying. Zircaloy-1 also had very low corrosion resistance.

Zircaloy-2 was an accidental discovery, where the corrosion resistance was improved compared to Zircaloy-1 but the mechanical strength was still the same and for this reason Zircaloy-2 was and still is employed in the construction of the Boiling Water Reactor.

Zircaloy-3 was a result of an increase of iron and decrease of tin in Zircaloy-2. The mechanical strength was reduced with these changes and thus Zircaloy-3 was abandoned.

---

[23] *Development of Radiation Resistant Reactor Core Structural Materials*. Available: http://www.iaea.org/About/Policy/GC/GC51/GC51InfDocuments/English/gc51inf-3-att7_en.pdf. (Last accessed 11 /08/2014).

[24] Azevedo, C.R.F., *Engineering Failure Analysis*, **18,** 1943-1962, 2011.

[25] Olander, D. R., *J. Nucl. Mater*., **389**, 1-22, 2009.

[26] Krishnan, R., Asundi, M. K., *Proc. Indian Acad. Sci.(Engg. Sci.),* **4**, Pt. 1, 41-56, 1981.

[27] Moan, G. D., Rudling, P., *Zirconium in the Nuclear Industry: Thirteenth International Symposium*, **1423**, ASTM International, 2000.

[28] Broy, Y., Garzavolli, F., Seibold, A., Van Swam, L. F., *ASTM STP*, **1354,** 609-722, 2000.

Zircaloy-4 came with the accidental note that nickel was hydrogen absorbing and this affected the mechanical properties of the Zircaloy. Due to this, nickel was removed. The iron content was increased and this resulted in Zircaloy-4. Compared to Zircaloy-3, Zircaloy-4 has good mechanical strength, absorbs hydrogen and is employed in the construction of the Pressurised Water Reactor*.

2.3.2 Application of Hafnium in the Nuclear Energy Industry

A common method of maintaining the required state of fission within a reactor in the nuclear energy production industry is the introduction or withdrawal of control rods.[29] The control rods assist with the fission chain reaction to stay active and prevent it from accelerating beyond control.[29] Besides maintaining the fission reaction it also helps to remove the neutrons that are not capable of triggering new fission reactions.[29] For this function, the control rod needs to have a large cross section for absorption of neutrons as one of its principal properties. Hafnium free of zirconium serves just that purpose. There are other elements with a larger thermal neutron cross section like boron that is a better neutron absorber but it has inferior physical and mechanical properties to hafnium, therefore boron needs to be alloyed with other metals to be utilized. Hafnium is preferred over boron because it can be used without being alloyed.[29] Another factor that makes hafnium unique and ideal to use in nuclear control rods is the fact that its various isotopes' thermal neutron cross sections are very similar.[30,31] Hafnium is produced almost for the sole purpose of manufacturing control rods for the construction of nuclear reactors.[32,33]

2.3.3 Application of Zirconium and Hafnium in Other Industries

Hafnium became available as a pure metal with the popularity that came with hafnium free zirconium.[34] It is produced at approximately 70 tons per year.[35] Hafnium is employed as an

*Pressurised Water Reactor (PWR) is a type of a nuclear reactor, in which the fuel is uranium oxide cladded in zircaloy™ the coolant and moderator are water at high pressure, so that it does not boil at the operating temperature of the reactor.

[29] http://web.mit.edu/nrl/Training/Absorber/absorber.htm (Last accessed 12/11/2014).
[30] Gambogi, J., *Zirconium and Hafnium*, USGS Minerals Yearbook 2010.
[31] Lamarsh, J., *Introduction to Nuclear Engineering*, Addison-Wesley, 1983.
[32] Elanchezhian, C., Saravanakumar, L., Ramnath, B. V., *Power Plant Engineering*, I.K.International Publishing House, 2007.
[33] Bodansky, D., *Nuclear Energy: Principles, Practices, and Prospects*, Springer, 2004.
[34] Parry, G.W., *Zirconium in the Nuclear Industry: 3rd International Conference, Quebec, Proceedings*, ASTM, 1976.

alloying agent, in the manufacturing of superalloys. Superalloys are mixtures of metals that can withstand high stress levels, water corrosion effects, high pressure, high temperature and mechanical stress.[36] Hafnium increases grain boundary strength (the interface between two crystallites in a polycrystalline material), improves creep (tendency for solids to slowly move or deform under stress) and tensile strength.[37] Hafnium containing superalloys are used in turbine blades of jet engines and they work very well at temperatures between 600-700 ^{o}C.[38] The high temperatures help reduce emissions since the combustion cycle is nearer to completion.[38] Zirconium metal is used to manufacture metal wire, sheets, pressed disks, seamLess tubes, welded tubes and foil. The different forms of zirconium metal find different applications in various industries.[39] The steel industry uses zirconium for the manufacturing of moulds for steel bars.[40] The zirconium increases the mould's resistance to metal steel penetration.[40] The ceramic industry uses zirconia as an opacifier because it has good light reflectivity properties.[2] Zirconium was employed extensively in photography in photographic flash bulbs which were manufactured out of zirconium foil.[1,2] In optometry, the zirconium compound slurry in water is used in the polishing of optical glasses.[41] The medical industry employs zirconium compounds to counteract the effects of plutonium poisoning by preventing skeletal disposition.[42]

2.4 Chemical Separation Processes of Zirconium and Hafnium

It has been mentioned that separating hafnium and zirconium is difficult because of their similarity in chemical behaviour. Formal attempts to separate hafnium and zirconium were initiated in the 1920s by G. de Hevesy and D. Coster who succeeded using X-ray techniques and

---

[35] *Seeking Alpha, Hafnium: Small Supply, Big Applications.* Available: http://seekingalpha.com/article/255689-hafnium-small-supply-big-applications. (Last accessed 12/ 11/ 2014).
[36] Blackford, J., *Engineering of Superalloys*, Available: http://www.cmse.ed.ac.uk/AdvMat45/SuperEng.pdf (Last accessed 12/11/2014).
[37] Donachie, M. J., Donachie, S. J., *Superalloys: A Technical Guide*, 2nd Ed, ASM International, 2002.
[38] Podrog, D. J., Hafnium turbine engine and method of operation Patent US20130300120 A1, Nov 14, 2013.
[39] Haley, A., Danley, B., How Things are Made. Available: http://www.madehow.com/Volume-1/Zirconium.htmL (Last accessed 12/11/2014).
[40] Mishra, B., *Review of Extraction, Processing, Properties, and Applications of Reactive Metals: 1999 TMS Annual Meeting, San Diego, CA, February 28 - March 15, 1999*, LDS TMS, 2010.
[41] Riedl, R. and Randin, J., *Substrate with first hard layer of titanium, zirconium or hafnium nitride containing aluminum, carbon, group Vb or VIb element second layer of mixed palladium and indium*, Patent US 5445892A, Aug 29, 1995.
[42] Stellman, J. M., *Encyclopaedia of Occupational Health and Safety: Industries and Safety*, 4th Ed, **3,** International labour Relations Geneva, 1998.

reported the discovery of element number 72.[1,2,43] A large interest and drive to separate hafnium and zirconium on an industrial scale started in the 1950s. This came with the knowledge that hafnium and zirconium were ideal materials to use in nuclear reactor construction and naval submarines. Since then an increased number of methods for separating hafnium and zirconium have been proposed.[44] Fractional crystallisation, precipitation, sublimation, distillation, selective chlorination of oxides, reduction of chlorides, ion exchange, selective liquid extraction and many others have been employed in the separation of hafnium and zirconium.[45,46,47,48] Ion exchange and liquid-liquid extraction are used for the separation of zirconium and hafnium. The Kroll process and electrowinning also referred to as electroextraction are two methods used to prepare zirconium metal and hafnium metal respectively. These processes for separation and preparation of the two metals will be discussed in the subsections that follow.[2,49,50,51] Although there are many different techniques available for separating these two metals, separating hafnium and zirconium is still complex and difficult because of their similarities. The other challenge in the separation of zirconium and hafnium is the negative environmental effects that these extraction processes have. Some separation processes produce large quantities of ammonium chloride and ammonium sulphate. Others produce water soluble thiocyanate ions and ketone solvents that render drinking water undrinkable and can poison marine life.[16]

2.4.1 Ion exchange of Zirconium and Hafnium

Ion exchange is a process of separating different ions.[50] The separation is based on different attractions of the ions to the solid phase (ion exchanger) and the polarity of the solutions used for eluting the ions and the polarity of the ions of interest.

[43] Weintraub, B., Shamoon S., Beersheva, A., *George de Hevesy (1885-1966): Hafnium and Radioactive Tracers.* Available: Bob@sce.ac.il. (Last accessed 12/11/2014).
[44] Murphy, P., Frick, L., *Zirconium and Hafnium*. Available: www.segemar.gov.ar/bibliotecuintemin/LBROSDIGITALES/Industrialminerals&rocks7ed/pdffiles/papers/075.pdf. (12/11/2014).
[45] Vinarov, I. V., *Modern Methods of Seperating Zirconium and Hafnium Rus. Chem. Rev*. **36** (7) 522-536, 1967.
[46] Bromberg M. L., Purification of zirconium tetrachlorides by fractional distillation., Patent US2852446 A, Dec 7, 1956.
[47] Adams, R. W., Holness, H., *Analyst*, **89**, 603-607 1964.
[48] Newnham, I. E., *J. Am. Chem. Soc*., **79** (20), 5415-5417, 1957.
[49] Von Bichowsky, F., *Process for electrowinning zirconium and hafnium*. Patent US2820748 A, Nov 15, 1956.
[50] Smolik, M., Jakóbik-Kolon, A., Porański, M., *Hydrometallurgy*, **95,** 350-353, 2009.
[51] Deorkar, N.V., Khopkar, S.M., **245**, 27-33, 1991.

There are a few variations of ion exchange techniques like activated gel chromatography, partition chromatography, cation exchange and many others that have been proposed for separating hafnium and zirconium.

- In activated gel chromatography hafnium and zirconium are introduced into the column and are adsorbed to activated silica gel resin (solid phase). Activation of the silica gel is done by heating it to a temperature of 300 ^{o}C for two hours. After the metals have been introduced to the activated silica gel and adhered to it, the column is treated with an anhydrous solution of hydrochloric acid and methanol. Zirconium has an affinity for a hydrochloric acid and methanol solution and the solution will detach the zirconium from the activated silica gel resin leaving the hafnium adsorbed to the activated silica gel resin. An aqueous sulphuric acid solution is then used to detach the hafnium from the column. This ion exchange method has been reported to be efficient, simple, cost effective and employable on an industrial scale.[52]
- Partition chromatography is a chromatographic technique that employs impregnation of a cellulose mass with an aqueous zirconium nitrate solution. The impregnation process is followed by treating the cellulose mass with an eluent consisting of diethyl ether and nitric acid in a ratio of 7:1, and the zirconium gets eluted first followed by the hafnium.[53,54]
- Cation exchange takes advantage of the instability of zirconium and hafnium complexes in the presence of strong acids on a cation exchange resin. In this process a Dowex-50 resin with sulphonic acid groups is treated with a solution containing zirconium and hafnium oxide chlorides in the presence of an acid. This acidic environment will then render the zirconium and hafnium cations and they are eluted with hydrochloric acid. The hafnium is eluted first, followed by the zirconium.[55,56,57]

[52] Mukherji, A. K., Belcher, R. and Frieser, M., *Analytical Chemistry of Zirconium and Hafnium*, Pergamon Press Inc. Ergamon Press, 1970.
[53] Ueno, K., Hoshi, M., *Bulletin of the Chemical Society of Japan*., **39**, 2183-2187, 1966.
[54] Hudswell, F. M., Hutcheon, *J., Extraction and Refining of the Rarer Metals*, Atomizdat, Moscow, **22**, 490, 1960.
[55] Lister, B.A. J., McDonald, L.A., *J.Chem.Soc*, 4315, 1952.
[56] Belyavskaya, T. A., Mu Ping-we"n., Vestnik Moskov.Univ., Ser.Mat.Mekhan., Astron., Fiz., i Khim., **207** 1959.
[57] Newnham, I.E., *J. Amer. Chem.Soc*, **73**, 5899 (1951).

2.4.2 Liquid-Liquid Extraction of Zirconium and Hafnium

This selective extraction technique is now seen as the most modern technique for the separation of hafnium and zirconium.[51] Liquid-Liquid extraction is a separation technique that exploits the solidity differences between different molecules in order to separate them. Two liquids that are immiscible are utilized during this separation process. Generally an organic solvent with an aqueous solvent or a polar solvent with a non-polar solvent. Even though they are immiscible they work together to separate and select the different compounds from each other. The product is usually drawn into the organic phase.

For the separation of hafnium(IV) and zirconium(IV) the liquid-liquid extraction method has been thoroughly researched. Various compositions of the aqueous phase have been utilized with a variety of partially immiscible organic phases. The process of liquid-liquid is governed by the distribution coefficient. A distribution coefficient is a quantitative measure of how the organic compound will be distributed between the aqueous and the organic phase.

Similar to chromatographic methods, several versions of liquid-liquid extraction techniques that exploit certain properties have been proposed to try and optimise the efficiency of the separating ability of these methods. The methods that seem to take the prime spot in liquid-liquid extraction are those that are based on extraction employing neutral organic reagents. Depending on the organic phase and the aqueous phase combination utilized the product will extracted into the accordingly:

Thiocynates of zirconium(IV) and hafnium(IV) can be distributed between solution of 1,3-diketones (2-thenoltriflouroacetone, 2pyrrylfluoroacetone and 2-fluoroyltrifluoroacetone) and a hydrochloric acid solution as the aqueous of the two solvents that are being contacted. When these two phases are mixed the zirconium(IV) will be extracted into the organic phase.

2.4.3 The Kroll Process for the Preparation of Zirconium Metal

The Kroll Process is a reduction process of metal halides with magnesium.[2,58] The Kroll process is the most common method for acquiring zirconium metal but it is not limited only to zirconium, a similar method was reported by Thomas *et al*.[59] for acquiring hafnium. The Kroll Process can be briefly described as follows:

[58] Seetharaman, S., *Treatise on Process Metallurgy, Vol 3: Industrial Processes*, 1st Ed, Elsevier, 2013.
[59] Thomas, D. E., Hayes E. T., *(Eds) The Metallurgy of Hafnium U.S.A.E.C*, Washington, 1960.

Zirconium tetrachloride is sublimated in the presence of carbon in an electric furnace until a hot mixture is formed. The sublimated zirconium tetrachloride is then reduced to metallic zirconium with magnesium. This process is performed in an inert atmosphere. The reduction process follows the reaction illustrated in Scheme 2.1 below.[60]

Scheme 2.1: Reaction scheme of the Kroll Process.

The reaction will stop with at least 30% excess magnesium left. The magnesium chloride that results from the reduction process along with the excess magnesium is then distilled off.[61] At this point the zirconium may contain minute impurities of nitrogen and oxygen and this can be removed by a process called the Crystal Bar Process. In this process the zirconium containing the impurities is heated to 200 ^{o}C in the presence of small amounts of iodine. Zirconium iodide (ZrI_4) gas is formed and the nitrogen and oxygen impurities remain in the solid state. A filament made of tungsten in the container is heated to 1300 ^{o}C and the zirconium iodide (ZrI_4) decomposes due to the temperature and pure zirconium crystals condense on the tungsten filament.[2]

The Kroll Process is also referred to as the magnesium reduction process. This process was developed by William Kroll, who initially envisioned it to separate titanium from its ores. When compared to other methods that were developed to separate hafnium and zirconium the Kroll Process is an economically viable method to employ on an industrial scale for separating hafnium and zirconium.[62] The Kroll Process is very efficient for refining zirconium, which is acceptable for application in various fields of nuclear construction.[63] Unfortunately the quality of hafnium produced through this process is not acceptable for application in the nuclear reactor control rods' construction. The hafnium produced through this process does not meet the standards required for corrosion resistance and hardness specifications.

---

[60] Gedemann, S. J., *Advanced Materials & Processes*, 41, 2001.

[61] Hani, A. M., Abodishish, R. J., Steven R. K., *Separation of magnesium from magnesium chloride and zirconium and/or hafnium subchlorides in the production of zirconium and/or hafnium sponge metal*., US5098471 A., Mar 24, 1992.

[63] Othmer, K., *Encyclopaedia of Chemical Technology 3rd Edition*, **24**, 873.

2.4.4 Electrowinning for Preparation of Hafnium Metal

Electrowinning, also referred to as electroextraction, is an electrochemical process that is conducted almost solely in non-aqueous media and molten salts are used.[49] In this electrolysis process the chemical reaction is accompanied by electron transfer. The electrolysis takes place in a reactor with non-consumable anodes, that are made up of inert material that does not get affected by chemicals and electrochemical attack, are utilized.[64]

This electrochemical process had been utilized primarily in the extraction of refractory metals. For a while it was considered to be the one process that would replace the Kroll Process or to be a better alternative. A prototype cell was constructed and zirconium was produced electrochemically through it.[65]

2.5 The Chemistry of Zirconium and Hafnium Coordination Complexes

The aim of this study is to attempt to develop and investigate separation methods for hafnium and zirconium utilizing various ligands in ligand assisted separation of hafnium and zirconium. This may lead to an effective and easy separation method compared to methods already available.[66] Separating hafnium and zirconium by ligand assisted methods exploit the differences between the chemical properties of the complexes synthesized with similar ligands. Careful attention needs to be given to the type of ligand selected for the purpose of separating the two metals. The ligand must form complexes that allow for extensive characterization and mechanistic studies. Hafnium and zirconium form part of a group of metals called early transition metals along with scandium, titanium, rutherfordium, lanthanides and actinides.[2] This group of metals has been reported to show an affinity for *O,O', N,O'* and *N,N'* (pyrophosphates) donor ligands. These donor ligands are 'hard' sigma donors and strong nucleophiles. A variety of hafnium and zirconium complexes with these types of ligands have been reported in literature and some are discussed in the following paragraphs.

---

[64] Sadoway, D. R., *The Electrochemical Processing of Refractory Metals*, 16, 1991. Available: http://web.mit.edu/dsadoway/www/58.pdf (Last accessed 13 / 11/ 2014).
[65] *Zrhf Newsletter*, Amax Speciality Metal Corp., Akron, N.Y., Sept. 1973.

[66] Steyn, M., MSc Thesis: *Speciation And Interconversion Mechanism Of Mixed Halo And O,O'- And O,N-Bidentate Ligand Complexes Of Zirconium*, University of the Free State, UFS, 2009.

2.5.1 Zirconium and Hafnium Complexes with *O,O'*-donor Ligands

β-Diketonates make up a large number of the molecules of the form $R_1C(-OH)C(-R_3)(=O)R_2$ (Figure 2.1)[67] and have been used as effective chelating ligands. β-Diketonates coordinate typically to form six membered rings as illustrated in Figure 2.2.

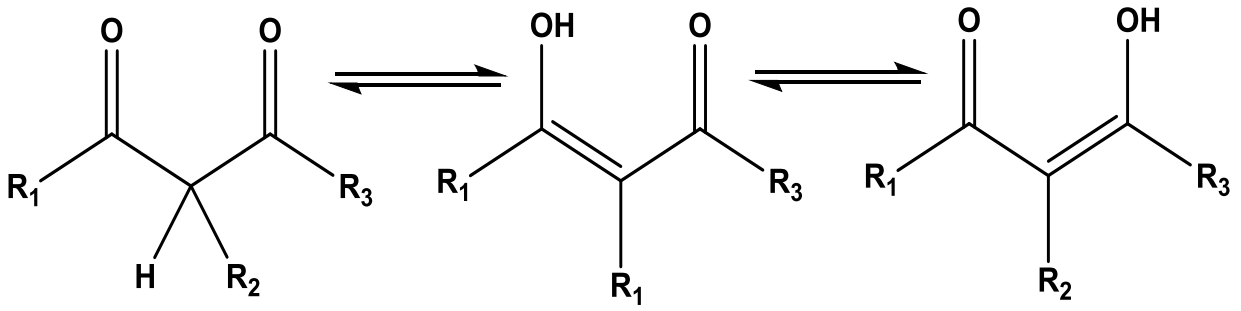

Figure 2.1*: O,O'*-donor ligands (β-diketones) in the form $R_1C(-OH)C(-R_3)(=O)R_2$.

Zirconium, hafnium and other metals with coordination numbers greater than 2 can form complexes with acetylacetone.[68] Zirconium and hafnium have been reported to exhibit coordination numbers of six, seven and eight. The six, seven and eight coordinated complexes of zirconium and hafnium are important because they show stereochemical rigidness on NMR scale.[67] Zirconium and hafnium β-diketonates have been popular for years and have been extensively studied. Some of these acetylacetonates will be discussed in the following sections.

2.5.2 Tetrakis Complexes of Zirconium(IV) and Hafnium(IV) with *O,O'*-donor Ligands

In 1998 Fausto Carderazzo *et al.*[69] published the structure of tetrakis(hexafluoroacetylacetonato) zirconium(IV) ($Zr(hfacac)_4$). In the X-ray diffractometric and EPR* study they discussed early transition metals and their affinity for oxygen containing bidentate ligands. They also reported how they synthesized [$Zr(hfacac)_4$] by reacting $ZrCl_4$ with Tl(hfacac) (hfacac = hexafluoroacetylacetone) and reported the crystal structure (Figure 2.2). It crystalized in a square

*Electronic Paramagnetic Resonance also known as Electron Spin Resonance is a technique for studying materials with unpaired electrons. The basic concept of EPR is analogous with Nuclear Magnetic Resonance (NMR) but its electrons spin are excited instead of spins of atomic nuclei.

[67] Bierschenk, E. J., Wilk, N. R., Jr., Hanusa, T. P., *Inorg. Chem*., **50**, 12126-12132, 2011.
[68] Flatau, K., Musso, H., *Angew Chem*., **82,** 390, 1970.
[69] Calderazzo, F., Englert, U., Maichle-Mössmer, C., Marchetti F., Pampaloni, G., Petroni, D., Pinzino, C., Strähle, J., Tripepi, G. *Inorg. Chim. Acta*, **270**, 177-188, 1998.

antiprismatic coordination around the zirconium, with four hexafluoroacetylacetonato groups surrounding the zirconium atom.

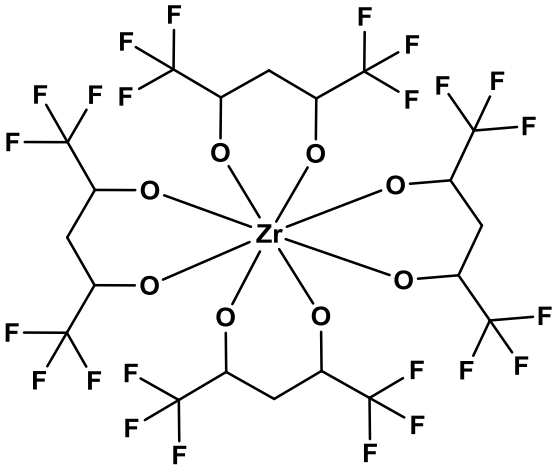

Figure 2.2: Graphical representation of a typical fluorinated tetrakis *β*-diketone zirconium(IV) complex, [Zr(hfacac)$_4$].

In 2008 R. Pothiraya *et al.*[70] reported the structures of several zirconium and hafnium complexes in a study based on the development of precursors for MOCVD (metal-organic vapor deposition) *via* HfO_2 and ZrO_2. They synthesized the zirconium and hafnium complexes by reacting metal amides with different malonate ligands (L = dimethyl malonate (HdmmL), diethyl malonate (HdemL), di-tert-butyl malonate (HdbmL) and bis(trimethylsilyl) malonate (HbsmL)). They were able to isolate ML_4 tetrakis complexes of hafnium with all the malonate ligands mentioned above (Figure 2.3 c and d illustrate two of the strucures) but they were only able to isolate ML_4 tetrakis complexes of zirconium with (HdmmL) and (HdemL) (Figure 2.3 a and b).

[70] Pothiraya, R., Milanov, A., Parala, H., Winter, M., Fischer, R. A., Devi, A., *Dalton Trans*., 654-663, 2009.

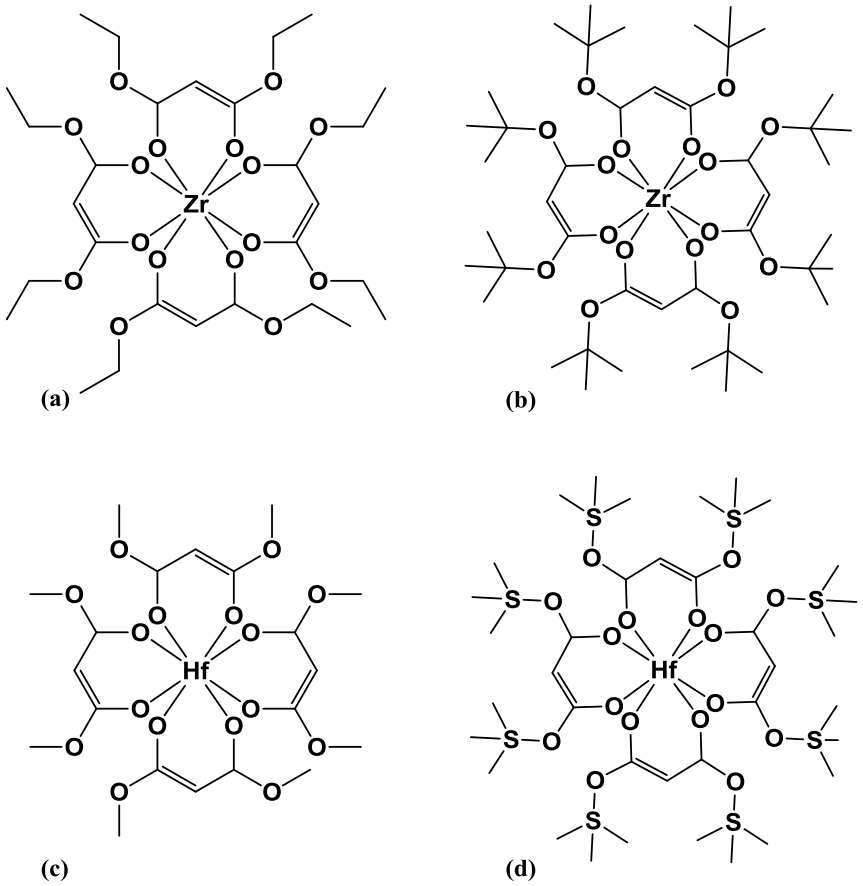

Figure 2.3: Graphical representation (a) [Zr(demL)$_4$], (b) [Zr(dbmL)$_2$], (b)[Zr((c)[Hf(dmmL)$_4$ and (d)[Hf(bsmL)$_4$].

2.5.3 Zirconium(IV) and Hafnium(IV) complexes with *N,O*-donor Ligands

In 1996 Bastinini *et al.*[71] published the β-ketoimine complexes, [Zr(enTFA$_2$)$_2$] and [Zr(trimenTFA$_2$)$_2$] (Figure 2.4). In the study they investigated the application of these types of complexes in MOCVD since it showed more stability and volatility and also possessed nitrogen that could be exploited for tailoring the reactivity. The complexes were synthesized by adding the diamine to an ethanolic solution of trifluoroacetylacetone (Htfac) and by refluxing it. The resulting white crystalline material was then recrystallized in water.

[71] Bastianini, A., Battiston, G. A., Benetollo, F., Gerbasi, R., Porchia, M., *Polyhedron*, **16**(7), 1105-1110, 1997.

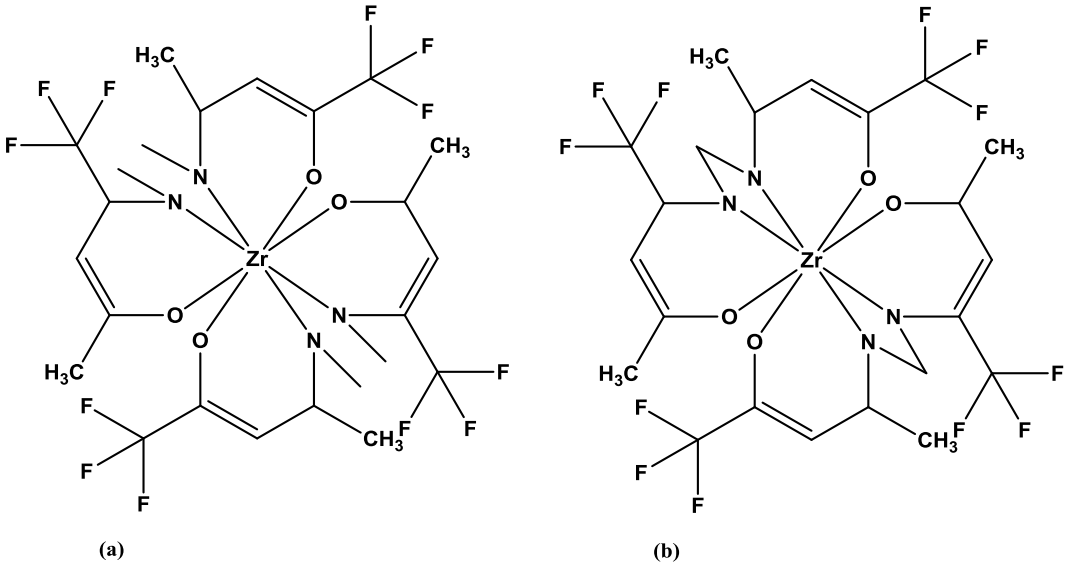

Figure 2.4: Graphical representations of (a) di[bis-trifluoroacetylacetone-ethylenediiminato]zirconium IV, [$Zr(enTFA_2)_2$] and (b) di[bis-trifluoroacetylacetone-trimethylenediiminato]zirconium, [$Zr(trimenTFA_2)_2$].

In 2010 Kathirgamanathan *et al.*[72] reported the structure of two phases of β and α zirconium tetrakis(8-hydroxyquinolinolate) (Figure 2.5). They investigated the properties of these complexes for application in organic light emitting diodes (OLED) based display. This has become significant in panel display technologies. They synthesized the complexes by refluxing zirconium isopropyl in toluene for the alpha complex and refluxing zirconium tetrachloride in ethanol for the beta complex. The white crystalline material that was obtained after refluxing was recrystallized by quadruple sublimation at 280 ˚C under vacuum.

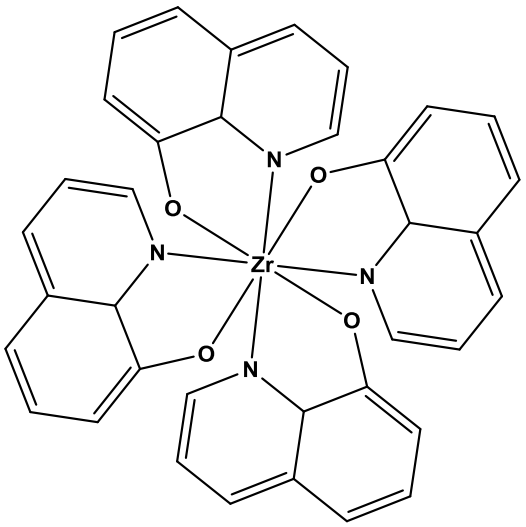

Figure 2.5: Graphical representation of the structure of zirconium tetrakis(8-hydroxyquinolinolato).

[72] Kathirgamanathan, P., Surendrakumar, S., Antipan-Lara, J., Ravichandran, S., Reddy, V. R., Ganeshamurugan, S., Kumaraverl, M., Arkley, V., Blake A. J., Bailey, D., *J. Mater. Chem.*, **21**, 1762-1771, 2011.

2.5.4 Zirconium(IV) and Hafnium(IV) Complexes

In the period 2009-2014 M. Steyn[66] and J. A. Viljoen[73] reported several structures of zirconium(IV) and hafnium(IV) complexes illustrated in Figure 2.6 with the selected bond distances and angles of the various complexes tabulated in Table 2.4. This was a parallel study in which the Steyn/Viljoen pair investigated the chelating behaviour of zirconium(IV) and hafnium(IV) with various organic bidentate ligands namely: 1,1,1-trifluoro-acetylacetone (TfacacH),1,1,1,5,5,5-hexafluoro-acetylacetone (HfacacH), 8-hydroxy quinoline (OxH), 5,7-dichloro-8-hydroxyquinoline (diClOxH), 5-chloro-7-iodo-8-hydroxyquinoline (CliOxH) and 5-chloro-8-hydroxyquinoline (5-ClOxH). They conducted the following synthetic procedures:

- $[Hf(Tfacac)_4]$ and $[Zr(Tfacac)_4]$ were synthesized by adding Natfaa to a suspension of the respective metal slurry in toluene and refluxing the mixture for ~20 hrs.
- $[Hf(Hfacac)_4]$ was synthesized by adding hexafluoroacetone drop-wise to a suspension of $[HfCl_4]$ and refluxing the mixture for ~12 hrs.
- $[Hf(Ox)_4]$ and $[Zr(Ox)_4]$ were synthesized by dissolving the respective metal in a minimal amount of DMF while stirring at room temperature and slowly adding a separately dissolved 8-hydroxy quinolone solution to the metal.
- $[Zr(diClOx)_4]\cdot 2DMF$ was synthesized by combining $[ZrCl_4]$ with 5,7-dichloro-8-quinoline (diClOxH) in 11 mL of DMF.
- $[ZrCl(ClOx)_2(DMF)_2O]_2$ was synthesized by combining $[ZrCl_4]$ with 5-chloro-7-iodo-8-hydroxyquinoline (ClOxH) in 12 mL DMF.
- $[Zr(5\text{-}ClOx)_4]\cdot 2DMF$ was synthesized by adding 5-chloro-8-hydroxyquinoline (5-clOxH) to $[ZrCl_4]$ in 10 mL DMF.

The complexes synthesized in this parallel study were compared to identify differences in chelating behaviour, reaction rates, solubility, coordination modes and equilibrium behaviour. The attempted identification of differences was done with the foresight of exploiting them and using them in developing a novel separation method for zirconium(IV) and hafnium(IV).

[73] Viljoen, J. A., MSc Thesis: *Speciation And Interconversion Mechanism Of Mixed Halo And O,O'- And O,N-Bidentate Ligand Complexes Of Hafnium.* University of the Free State. UFS, 2009.

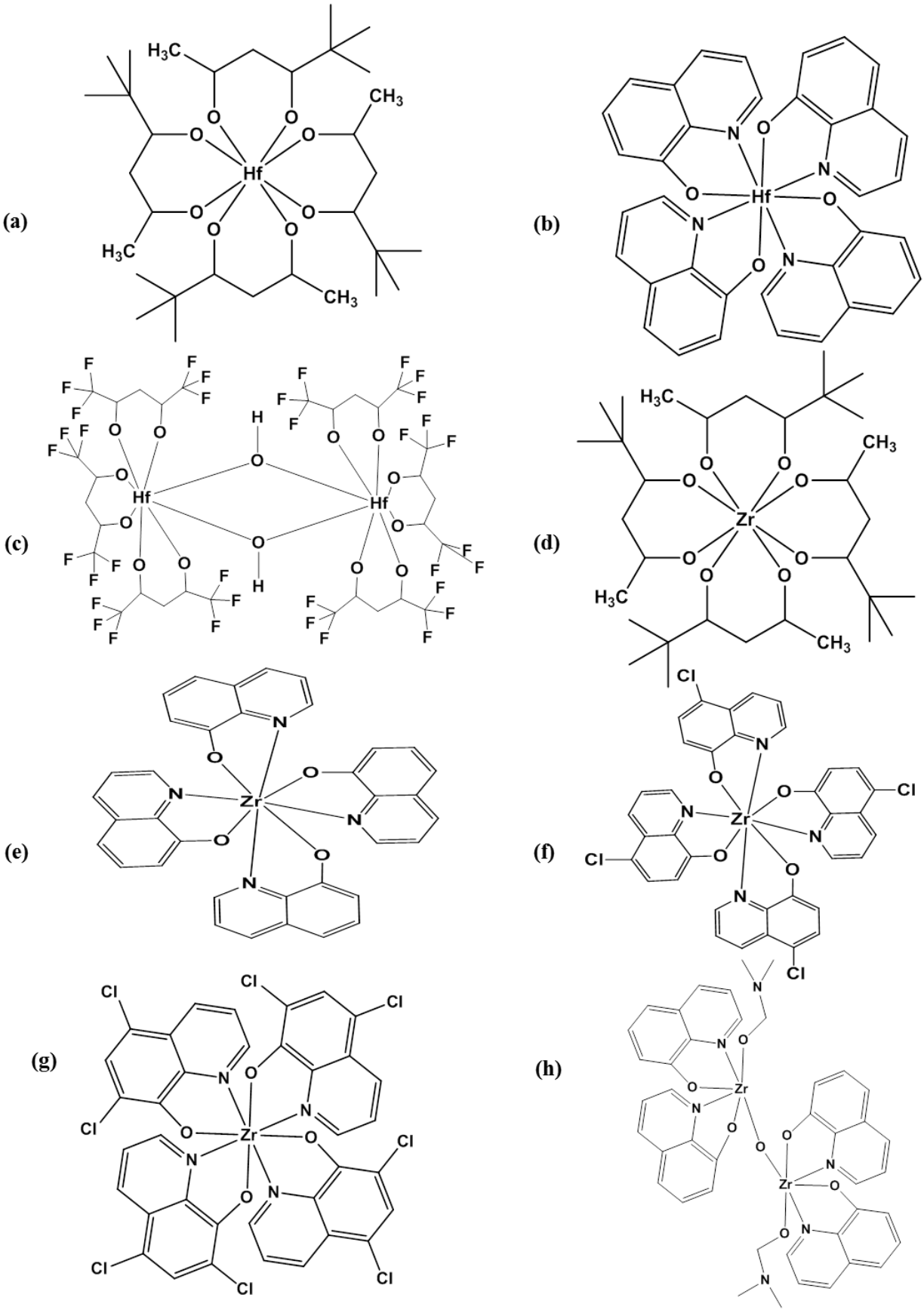

Figure 2.6: Graphical representation of (a) $[Hf(Tfacac)_4]$, (b) $[Hf(Ox)_4]$, (c) $[Hf(Tfacac)_4]$, (d) $[Zr(Tfacac)_4]$, (e) $[Zr(Ox)_4]$, (f) $[Zr(diClOx)_4]$, (g) $[ZrCl(ClOx)_2(DMF)_2O]_2$ and (h) $[Zr(5\text{-}ClOx)_4]$.

Table 2.4: Zirconium(IV) and Hafnium(IV) complexes bond distances and band angles (˚).

Figure 2.6	Complex	Bond	Bond (Å)	Angle	Bond Angles (°)
a	$[Hf(tfaa)_4]\cdot 2C_7H_8$	Hf—O	2.15(1) - 2.19(1)	O—Hf—O	75.5(5)-143(4)
b	$[Hf(Ox)_4]\cdot(HCON(CH_3)\cdot(H_2O)$	Hf—O	2.07(6)-2.11(5)	O—Hf—N	70.7(2)-71.2(14)
		Hf—N	2.38(5)-2.40(7)	O—Hf—O	3.10(2)-0.902(2)
c	$[Hf(OH)(Hfacac)_3]_2\cdot(CH_3)_2CO$	Hf—O	2.09(7)- 2.25(8)	O—Hf—O	66.6(4)-112(6)
		Hf-Hf	3.51(7)		
d	$[Zr(Tfacac)_4]$	Zr—O	2.16(13)-2.20(15)	O—Zr—O	75.4(5)-142(7)
e	$[Zr(ox)_4]\bullet(HCON(CH_3)_2)\bullet(H_2O)$	Zr—O	2.08(2)-2.10(2)		
		Zr—N	2.41(2)-2.43(2)	O—Zr—N	70.1(8)-70.0(8)
f	$Zr(5ClOx)_4]\cdot 2DMF$	Zr—O	2.09(4)-2.10(4)	O—Zr—N	69.5(15)-70.3(14)
		Zr—N	2.41(4)-2.44(4)		
g	$Zr(diClOx)_4]\cdot 2DMF$	Zr—O	2.08(2)-2.11(2)	O—Zr—N	69.1(7)-70.4(7)
		Zr—N	2.07(2)-2.11(2)		
h	$ZrCl(diClOx)_2](DMF)_2O]\cdot 2DMF$	Zr—O	2.41(3)-2.42(3)	O—Zr—O	88.5(8)-141(1)
		Zr—N	1.93(2)-2.22(3)	N—Zr—N	143.0(3)
				O—Zr—N	73.5(1)-147(1)
				O—Zr—Cl	86.9(7)-170(3)

Efforts to attempt to quantify previously unknown/unobtainable structures for comparative purposes were initiated *via* computational chemistry techniques. The comparisons, as with those done with XRD, yielded information on significant differences that could contribute to the development of a solid or solution state separation method for these two metals.

More importantly are the solution studies that were published from the parallel study. The zirconium(IV) and hafnium(IV) compounds' formation mechanisms were evaluated *via* UV/Vis kinetics and reaction modelling. These investigations were done with the intention to aid with the comprehension of equilibrium influences in the formation process of these complexes. The information gathered from the investigations would also contribute to the development of a novel solution extraction method for separating the two metals from each other.

Steyn stressed that the mono coordinated bidentate ligand complexes with zirconium(IV) would be difficult to isolate in solid state, since the first phase of the reaction occurred rapidly. It was

also reported in the study that the complexes of zirconium(IV) and hafnium(IV) preferred to form complexes in the maximum coordination mode. The rate at which the formation of this higher coordination complexes took place could possibly be limited by the presence of excess original halide ligand.

Viljoen expected a reaction mechanism consisting of four separate steps. He reported a reaction mechanism that consisted of a fast reaction followed by three slower ones for the hafnium(IV) system. The fast reaction was studied by stop-flow techniques and the slower reactions by normal UV/Vis. Due to the high complexity of the substitution reaction that were observed in this investigation, a detailed discussion of the reaction rate constants were not attempted. However the steps analysed in the investigation agreed well with the determined observed rate constants.

2.6 Fluorine NMR Kinetic Studies of Zirconium and Hafnium

In 1965 Thomas *et al.*[74] published a paper where they studied ligand exchange for group IVb β-diketonates. In the study they investigated whether the square antiprism nature of eight-coordinated zirconium, hafnium and other metals would persist in solution. Through fluorine nuclear magnetic resonance spectroscopy they discovered that the complexes undergo rapid intermolecular rearrangement. To further investigate this rapid rearrangement they followed a kinetic experiment where [$Zr(acac)_4$] and [$Zr(tfac)_4$] were added in a 1:1 ratio illustrated by the reaction scheme below (Scheme 2.2), along with the ^{19}F-NMR spectra (Figure 2.7).

$$Zr(acac)_4 + Zr(tfac)_2(acac)_2 \overset{K_1}{\rightleftharpoons} 2Zr(tfac)(acac)_3 \quad ...2.2$$

$$Zr(tfac)(acac)_3 + Zr(tfac)_3(acac) \overset{K_2}{\rightleftharpoons} 2Zr(tfac)_2(acac)_2 \quad ...2.3$$

$$Zr(tfac)_2(acac) + Zr(tfac)_4 \overset{K_3}{\rightleftharpoons} 2Zr(tfac)_3(acac) \quad ...2.4$$

Scheme 2.2: Reaction scheme of the ligand exchange equilibria.

[74] Pinnavaia, T. J., Fay, R. C., Nuclear Magnetic Resonance Studies of Ligand Exchange for Some Group IVb 6-Diketonates, **5**(2), 233-239, 1966.

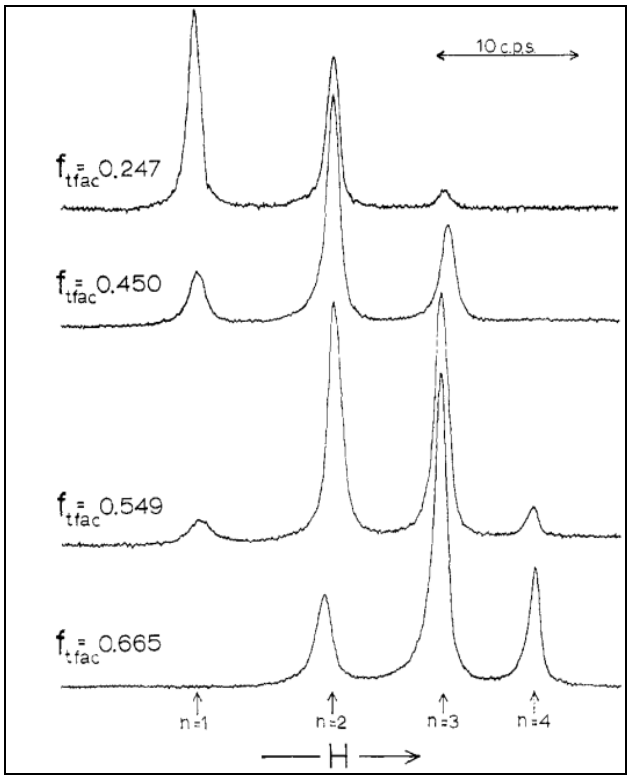

Figure 2.7: The ^{19}F-NMR spectrum of [Zr(tfac)$_4$] and [Zr(acac)$_4$] in benzene at 31°C.

The fluorine kinetic study spectra shows a maximum of four signals as observed in Figure 2.7.[74] The signals represent the CF_3 groups of each [Zr(tfac)$_n$] molecule. The lowest field line is of [Zr(tfac)$_2$(acac)$_2$] followed by the [Zr(tfac)$_3$(acac)] and [Zr(tfac)$_4$] respectively. During this study it was also found that the spectrum for the hafnium system was identical to the one represented in Figure 2.7 and was found to be temperature dependent. The equilibrium quotients for this study are tabulated in Table 2.5. All three quotients were 2.5 times higher than they had anticipated. They supported these high quotients by postulating that the reactions were exothermic. They further supported this claim by studying the temperature dependence of these equilibrium quotients. From the least square analysis, free energies and entropies were calculated. The results from this study are tabulated in Table 2.5 along with the ΔS values.

Table 2.5: Thermodynamic data in benzene at 25 ˚C for reaction 1, 2 and 3 (Scheme 2.2).The temperature dependence of the average equilibrium quotients in carbon tetrachloride for the [$Zr(tfac)_4$] and [$Zr(acac)_4$] system were determined at varying temperatures.

Reaction	ΔH (kcal/mol)	ΔF (kcal/mol)	Statistical ΔS (e.u)
1	0.05 ± 0.54	-1.10 ± 0.14	1.95
2	-0.05 ± 0.08	-1.10 ± 0.08	1.61
3	0.02 ± 0.26	1.15 ± 0.9	1.95

Average values of equilibrium quotients			
Temp (˚C)	K_1	K_2	K_3
-18.5	5.9 ± 0.5	5.4 ± 0.3	8.8 ± 0.7
-7.8	5.7 ± 1.2	6.4 ± 0.4	8.1 ± 1.3
7.2	6.0 ± 0.7	7.0 ± 0.4	7.7 ± 0.9
20.7	0	6.3 ± 0.4	7.4 ± 1.0
31.7	5.9 ± 0.6	6.0 ± 0.8	8.0 ± 1.1
41.0	5.8 ± 0.9	6.1 ± 0.5	7.6 ±1.1
51.6	5.6 ± 0.1	6.9 ± 0.9	8.1 ±0.8
63.4	5.5 ± 0.5	6.5 ± 0.5	0
79.8	5.6 ± 1.1	0	0

They superimposed the ^{19}F-NMR spectra of the hafnium(IV) and zirconium(IV) complexes with the ligand trifluoroacetylacetone (Figure 2.8) and discovered that the spectrum observed for the hafnium(IV) system was essentially identical to the one observed for the zirconium(IV) system after the impurities were subtracted.

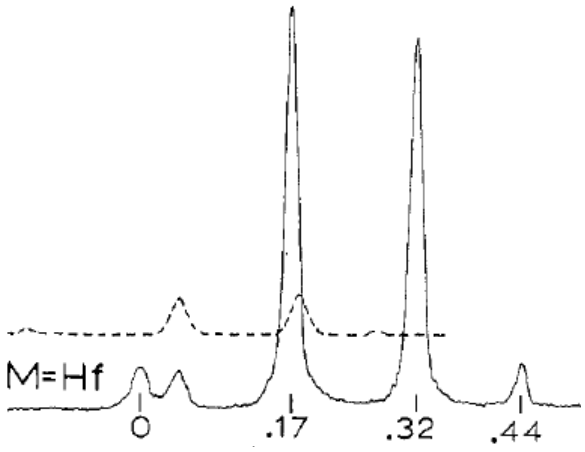

Figure 2.8: ^{19}F-NMR spectrum for equilibrium mixture of $M(tfac)_4$ $M(acac)_4$ (M=Hf) in benzene solution at 31 ˚C [0.25 M]. The dotted spectrum is the spectrum of the eqilibrium mixture of $Zr(tfac)_n(acac)_{4-n}$ which was present as an impurity.

2.7 Summary

Zirconium and hafnium have many applications, some of which have been mentioned here. The aim of this study is to attempt to develop a basis of separating zirconium and hafnium. Extraction and separation of zirconium and hafnium from mineral ores that possess very stable structures require decomposition by high temperature and aggressive chemical processes. The problem with these methods and those mentioned earlier in the text, is that they are relatively expensive and some have competing reactions that lead to the decomposition of the chemicals that are meant to aid in separating the zirconium and hafnium.

The basis for separating zirconium and hafnium in this study will be ligand assisted separation where oxygen and nitrogen containing chelating agents will be utilized to synthesize a heterocyclic ring chelate compound with zirconium or hafnium. The chelate compound will possess a $M(L\text{-}L')_4$ formula which is graphically represented in Figure 2.9.

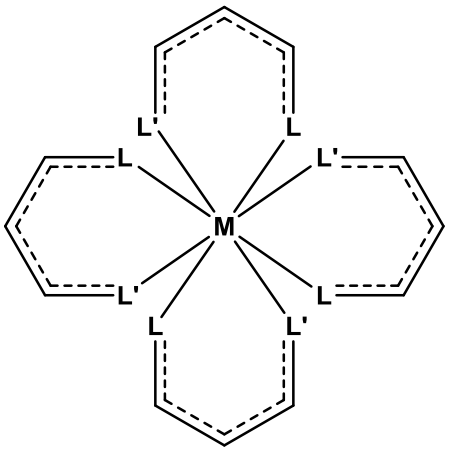

Figure 2.9: Schematic representation of the ML_4 chelate compound of zirconium or hafnium.

In Figure 2.9, M is the zirconium or the hafnium metal centre and *L,L'* would be the chelating acetylacetone (*O,O'*) or *N,N'*-diamine based ligands. Once the respective complexes are successfully synthesized, mechanistic studies by NMR, aided by crystallographic techniques will be used to identify mechanistic differences for complex formation or structural differences to exploit for separation.

3 Theory on Characterization Methods

3.1 Introduction

The characterization of compounds in research forms an important part of the research project as it qualitatively and quantitatively identify the synthesized compounds. This chapter focuses on the basic concepts of characterization techniques. Characterization techniques are divided into two distinctive groups namely destructive and non-destructive techniques.[1,2,3] Destructive techniques consume the sample and the sample cannot be recovered. There are several destructive techniques available; Inductively Coupled Plasma (ICP) and Elemental Mass Spectroscopy (EMS) are two examples of destructive techniques that are used in a characterization process. None of these destructive techniques will be covered in the scope of this chapter. Non-destructive techniques do not consume the sample and the sample can be recovered after the characterizations were performed. Infrared Spectroscopy (IR), Single Crystal X-ray Diffraction (XRD), Nuclear Magnetic Resonance Spectroscopy (NMR) and Ultraviolet and Visible spectroscopy (UV/Vis) are examples of non-destructive techniques which will be discussed in this chapter. Some theory on chemical kinetics is also reported.[4]

3.2 Infrared Spectroscopy (IR)

Infrared light forms part of the electromagnetic spectrum that is not visible to the human eye, along with radio waves, microwaves, ultraviolet, alpha and gamma rays.[5] The infrared region of

[1] Alder, L., Holland, P.T., Lantos, J., Lee, M., MacNeil, J. D., O'Rangers, J., van Zoonen, P., Ambrus, A., *Guidelines for Single-Laboratory Validation of Analytical Methods for Trace-level Concentrations of Organic Chemicals in Principles and Practices of Method Validation, Fajgelj, A., & Ambrus, A*., The Royal Society of Chemistry, Cambridge, UK, pp. 179-248, 2000.
[2] Helmenstine, A. M., *Analytical chemistry definition", Analytical Biochem*. *Res*., 123, 14-19, 2009.
[3] Gill N. S., Kumari P., *Pharmacophore*, **2** (3), 186-194, 2011.
[4] Martineza, I., Aursanda, U. M., Eriksona, T. E., Singstadb, E., Veliyulin, B., van der Zwaag, C., *Destructive and non-destructive analytical techniques for authentication and composition analyses of foodstuff Trends in Food Science & Technology*, **14**, 489-498, 2003.

the electromagnetic spectrum is divided into the near, mid and far infrared regions as illustrated in Figure 3.1.

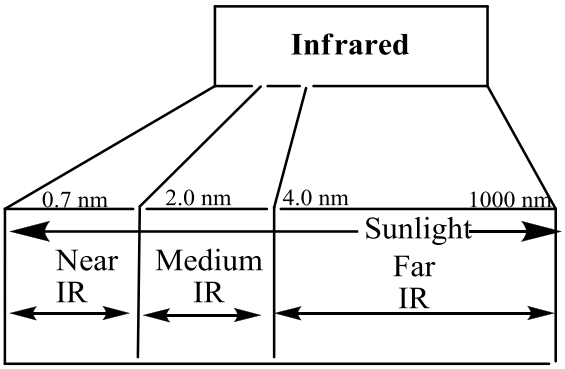

Figure 3.1: The infrared region of the electromagnetic spectrum.

Infrared spectroscopy is a qualitative technique that is often used where moderate accuracy is required. Infrared spectroscopy is a characterization technique with basic operations that are based on the vibration of atoms of a molecule. The sample is radiated with an infrared beam, the fraction of the infrared radiation that is absorbed by the molecules at certain energy values is determined and a spectrum is produced.[5] The absorption spectrum have peaks appearing at certain energies. These peaks correspond to frequencies of vibration of certain parts of the molecule. When a sample is irradiated with an infrared beam of an initial intensity (I_o), certain parts of the molecule will absorb the radiation. The absorbing parts of the molecule need to possess an electric dipole moment change that is at the same frequency as that of the infrared radiation.[5] For energy to be transferred or absorbed, the infrared radiation energy needs to correspond to the molecules' inherent stretching, bending or vibrational frequency. Absorption of infrared irradiation or energy transfer results in the excitation from the ground state (E_0) to an excited state (E_f). The frequency of the absorbed energy transfer is validated by Planck's Law and can be used to calculate the vibrational frequencies.

Vibrations in a molecule result in changes in bond length and bond angles between two atoms. The change in bond length is referred to as stretching and the change in the angle between two atoms is referred to as bending. Stretching of a molecule's bonds can occur in-phase or out-of-phase. When stretching is in-phase, it is referred to as symmetrical stretching and when stretching is out-of-phase, it is referred to as asymmetric stretching. There are several modes of bending namely scissoring, rocking, wagging and twisting. Bending and stretching vibrations are

[5] Stuart, B. H., *Infrared Spectroscopy: Fundamentals and Applications*, John Wiley & Sons Ltd, 2004.

significant factors that contribute to how the infrared absorption spectrum will ultimately look like. For example, two molecules that have similar bond angles and bond lengths might differ in inherent vibrations, due to the difference in vibrational environments and this phenomenon will result in two different infrared spectra. When a molecule has absorbed the infrared radiation it can vibrate in several ways. The several ways of vibrations are referred to as vibrational modes or vibrational degrees of freedom. The nature of the molecule dictates the degrees of freedom that a molecule will have. Linear molecules have (3N-5) vibrational degrees of freedom, where N is the number of atoms the molecule contains. Therefore a linear molecule with two atoms will have one vibrational degree of freedom and non-linear molecules have (3N-6) degrees of vibrational freedom.[5]

3.3 Ultraviolet/Visible Spectroscopy (UV/Vis)

Ultraviolet/Visible spectroscopy is a highly accurate quantitative identification characterization technique. Qualitative characterization with UV/Vis is limited and needs to be performed in conjunction with NMR, XRD or IR. UV/Vis has gained increasing popularity over the past thirty five years because of accuracy, efficiency and economic viability for performing rapid kinetic studies and monitoring reaction profiles of corresponding formation and disappearance of coloured samples in a chemical reaction. UV/Vis also forms part of the electromagnetic spectrum as illustrated in Figure 3.2.[6]

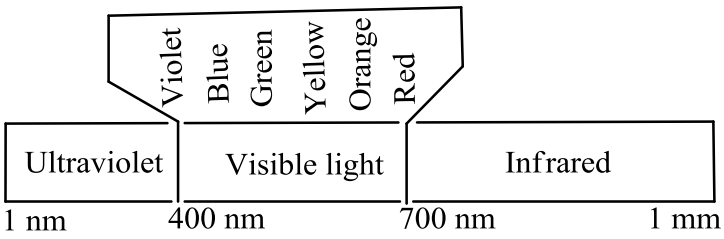

Figure 3.2: The Ultraviolet and Visible light region of the electromagnetic spectrum.

UV/Vis spectroscopy is based on the absorbance of the radiation by the sample. When the sample absorbs UV/Vis light, electronic transitions take place in a molecule. Absorbance of UV/Vis radiation will lead to the increase in energy of the atoms thereby exciting them to a higher energy level. For example the atom's energy will move from the ground state E_0 to the excited state E^*.

[6] Marczenko, Z., Balcerzak, M., *Analytical Spectroscopy Library-10 Separation, Preconcentration and Spectrophotometry in Inorganic Analysis*, Elsevier Science B. V. for the English edition only, 2000.

In the molecule the atoms can rotate or vibrate with respect to one another. The rotations and vibrations have discrete energy levels and they can be envisioned as being packed on top of each other. If the photons of the UV/Vis radiation have enough energy they will cause transition to the electronic energy levels of the atoms. Energy changes can occur in a molecule and these changes are due to changes in energy levels of the electrons. The total energy of a molecule is made up of electronic, vibrational and rotational energy that are independent of the other. Rotational spectra are observed for molecules with a permanent dipole moment and vibrational spectra for molecules with a change in the dipole moment during a vibration. Electronic spectra are observed for all molecules.

Atoms have three types of valence electrons namely sigma valence electrons which take part in single bonds and, π valence electrons which take part in double bonds and triple bonds. π valence electrons can also be non-bonding valence electrons that exist as lone pairs that do not take part in bonding. σ valence electrons have the lowest energy, followed by π valence electrons that have higher energy and the non-bonding electrons that have the highest energy. When absorption of UV/Vis radiation occurs the electrons get excited to higher energy levels, usually to anti-bonding orbitals.[6]

Characterising a sample using UV/Vis is most efficiently performed with a liquid solution of the sample because only a small amount of absorbing species is required. The solvent that is used to dissolve the sample should have minimal absorbing capabilities. When a sample is irradiated with UV/Vis light it can scatter, reflect, absorb or a photochemical reaction can occur. During characterization *via* UV/Vis, a UV/Vis beam is passed through the solution (sample) in a small cell of approximately 1 cm in width called a cuvette. The beam passes through the sample and through the reference cell containing only the solvent used to dissolve the sample at the same time. The radiation that is transmitted is detected and the absorption is recorded by comparing the difference between the transmitted beam of the sample and the reference. Absorption of UV/Vis radiation occurs according to absorbance laws guided by Beer's Law (defined as: absorbance is proportional to concentration) (Equation 3.1) and Lambert's Law (defined as: absorbance is proportional to thickness of the solution) (Equation 3.2).

$$A = \frac{k''c}{2.303} \text{ or } \log\frac{I_0}{I_T} = \frac{k''c}{2.303} \qquad \textbf{...3.1}$$

$$A = \frac{k'b}{2.303} \text{ or } \log\frac{I_0}{I_T} = \frac{k'b}{2.303} \quad \text{...3.2}$$

Where *k* is a proportionality constant, *c* is the concentration, b is the thickness of the solution (path-length) and A is the absorbance. I_o is the intensity of the incident light and I_T is the intensity of the transmitted light. Combining these two laws helps to derive the Beer-Lambert Law (Equation 3.3). The combination of these laws provides us with an absorption value that can be read directly from the spectrum.[7]

$$A = log_{10}\frac{I_o}{I_T} = \epsilon\, l\, c \quad \text{...3.3}$$

In Equation 3.3, ϵ is the molar absorptivity, a constant that can be denoted by ($\sigma \times 6.023 \times 1020$)/2.303) and l is the path length of the sample.The transitions from lower energy to higher energy levels lead to narrow absorbance bands at wavelengths characteristic to the absorbing species. Absorption peaks on a UV/Vis spectrum are not sharp but appear as broad peaks. This is due to several vibrational and rotational energy levels that are available for absorption. Absorption can be affected by solvents for instance polar solvents can cause some molecules to absorb at a higher wavelength more than non-polar solvents would.[6]

3.4 Nuclear Magnetic Resonance Spectroscopy (NMR)

Nuclear Magnetic Resonance (NMR) is an absorption characterization technique and its flexibility and high degree of accuracy has made it a corner stone for characterization of samples. NMR has become one of the most invaluable characterization techniques to modern research science.[8] Both qualitative and quantitative identification of sample molecules can be performed on an NMR instrument with mastery of some basic theory on the interpretation of NMR spectra. NMR is not limited to one nuclide, there are several nuclei that can be studied namely H, C, N, P, Si, Al, Pt and several others. NMR is fast and it provides detailed information for the selected nuclei and chemical bonds of the molecule in question.

[7] Mehta, A., Ultraviolet-Visible (UV-Vis) Spectroscopy – Derivation of Beer-Lambert Law, Posted in: Analytical Chemistry, Notes, April 22, 2012, Available: http://pharmaxchange.info/press/2012/04/ultraviolet-visible-uv-vis-spectroscopy-%E2%80%93-derivation-of-beer-lambert-law/ (Last accessed 11/11/2014).

[8] Bertini, I., Luchinat, C., Parigi, G., *Solution NMR of Paramagnetic Molecules - Applications to Metallobiomolecules and Models*, Vol 2, Elsevier Science B.V., 2001.

CHAPTER 3

Nuclear Magnetic Resonance takes advantage of the magnetic field of an atom created by the spinning charge. The magnetic field has an angular momentum that is expressed as a quantum spin number (I). I can be one of the following numbers: 0; $\frac{1}{2}$; 1 or 2. Table 3.1 lists some of the nuclei that are NMR observable on an NMR instrument, and their quantum spin numbers.[9]

Table 3.1: Spin quantum numbers for selected nuclei.

Nuclei	Spin Quantum number (I)
^{12}C, ^{16}O, ^{32}S,	0
^{1}H, ^{19}F, ^{31}P, ^{13}C,	$\frac{1}{2}$
^{2}H, ^{14}N	1
^{127}I, ^{11}B, ^{35}Cl, ^{79}Br	$\frac{3}{2}$
^{17}O, ^{91}Zr,	$\frac{5}{2}$
^{177}Hf	$\frac{7}{2}$

A nuclide with I = 0 will result in a magnetic moment ($\mu = Ih / 2\pi$) of zero. The magnetic moment μ is a vector that can be manipulated in the presence of an external magnetic field B_o. A magnetic moment of zero will cause the nuclide not to be observable by NMR. One can imagine a paper of iron filling randomly scattered on a piece of paper in the absence of a magnet and how they get arranged with respect to the north and south poles of the magnet. The electrons almost work in a similar way in the presence and the absence of an external magnetic field.

Most nuclides that are popular for NMR observation have a quantum spin number of $\frac{1}{2}$. Nuclides with a quantum spin number of $\frac{1}{2}$ can assume certain orientations in the presence of a static magnetic field B_o. The external magnetic field can be $+\frac{1}{2}$ which is the lower (ground state) energy level and $-\frac{1}{2}$ which is the higher (excited) energy level The energy is given by Equation 3.4 where h is Planck's constant, γ is the magnetogyric ratio and B_o is the strength of the magnetic field at the nucleus. The nuclides with a quantum spin number of 1 and greater have an uneven charge distribution which leads to asymmetry that will further affect the spectra that is produced.[9]

[9] Balci, M., *Basic ^{1}H-NMR and ^{13}C-NMR Spectroscopy*, 1st Ed, Elsevier Science, 2005.

$$\Delta E = h\gamma/2\pi B_o \quad \text{...3.4}$$

When the nuclides have orientated themselves in their respective energy levels in the static magnetic field the nuclide's magnetic moment, which is a vector that has been aligned in this external magnetic field, can be manipulated. Manipulation is done by pulsing the nuclides with radio frequency energy (ν). The nuclides will absorb the radio frequency and the system will go into resonance. The nuclides in the lower energy level get excited and saturate the upper energy level. When the excited nuclides relax from the upper energy to the lower energy level, they emit a signal that is detected as a free induction decay signal. An NMR signal is then produced from this signal. The produced NMR spectrum peaks are observed at their respective positions relative to the sample.[9]

The positions where peaks appear on the NMR spectrum are referred to as chemical shifts, a phenomenon referred to as deshielding or shielding of the static magnetic field by local fields produced by circulating sigma, pi or lone pair electrons. The peaks are observed at different chemical shifts because of their magnetic distinction in the molecule. If nuclei have identical chemical environments, they will produce a single peak that integrates for the total number of observed nuclei that are present in the chemically identical environments.[9]

NMR spectroscopy alongside many other spectroscopic techniques has become a principal tool to research chemists for the characterization of both solid and liquid samples.[10] Abou-Handam *et al.*[11] prepared and characterized a range of complexes with a general formula $[M^{*}O(X)(CN)_4)^{n-}$ using ^{13}C, ^{15}N, ^{17}O, and ^{99}Tc-NMR. ^{13}C-NMR (Figure 3.3) was used to characterize $[TcO_2(^{13}CN)]^-$ where a broad ^{13}C peak was observed due to the significant quadrupolar moment of the ^{99}Tc nucleus. This was contrary to typical ^{13}C-NMR spectra obtained for the other metals (very sharp lines that show long relaxation times of several seconds).

[*] M = the respective metal used in the study (Re(V), Tc(V), W(IV),Mo(IV) and Os(VI)

[10] Claridge, T. D. W., *High-resolution NMR Techniques in Organic Chemistry*, 1st Ed, Elsevier Ltd. 1999.
[11] Abou-Hamdan, A., Roodt, A., Merbach, A. E., *Inorg. Chem.* **37**, 1278-1288, 1998.

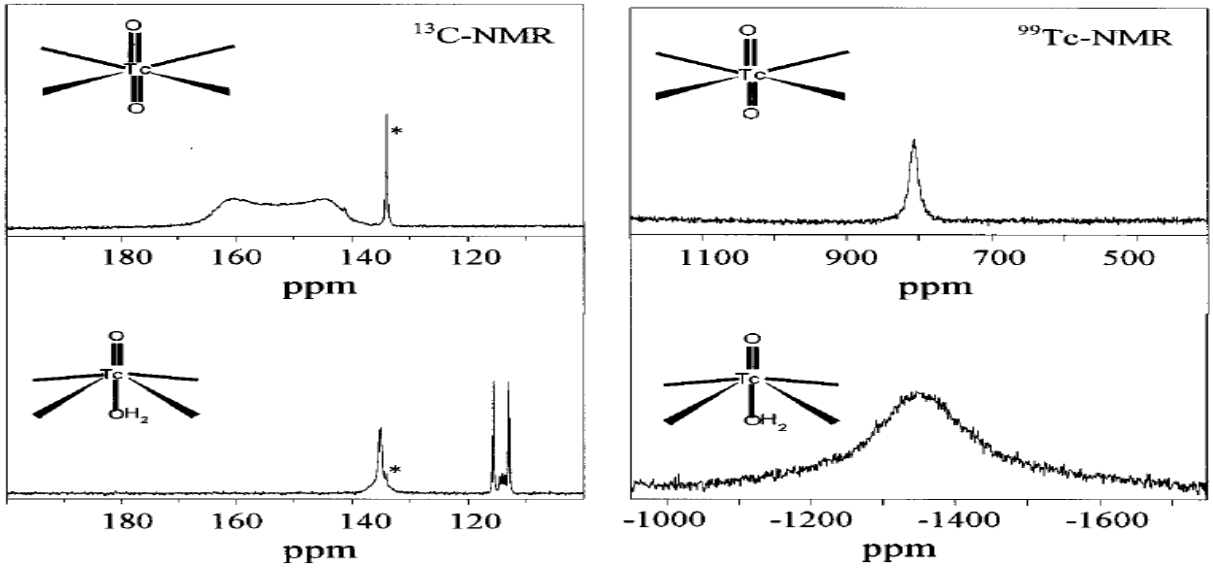

Figure 3.3: ^{13}C and ^{99}T spectra at T = 25 ˚C of $[TcO_2(^{13}CN)_4]^{3-}$. (Note the signal structure of free HCN due to proton-carbon and deuterium-carbon couplings), illustrating the quadrupolar effect introduced by ^{99}Tc (I = 9/2, 100%) and the effect of reduced symmetry upon protonation. The asterisked signal is the $[Re_2O_3(CN)_8]^4$ complex.[11]

In the same study a correlation between structural data from X-ray determinations (W-CN bond lengths) and NMR first order coupling constants between ^{183}W and ^{13}C in equatorial cyano ligands was done to aid in the characterization (Figure 3.4). The correlation found was that as the equatorial M-CN bond lengths decreased the coupling constants increased with ~10 Hz.

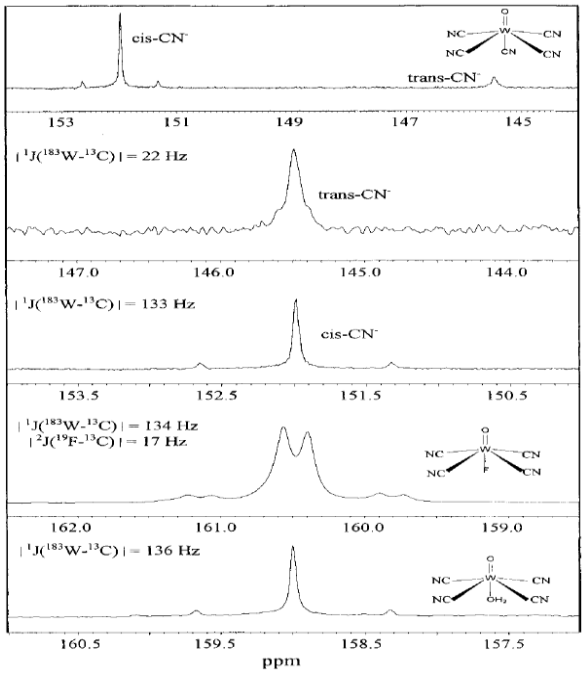

Figure 3.4: ^{13}C-NMR spectra for $[WO(X)(^{13}CN)_4]^{m-}$ illustrating the variation in chemical shift. δ$[Re_2O_2(CN)_8^{4-}]$ = external reference $|^1J(^{183}W\text{-}^{13}C)|$ coupling constants for $[WO(^{13}CN)_5]^{3-}$.[11]

More importantly, especially for the purpose of this study, is utilizing NMR as a tool to perform chemical kinetic studies and to determine the rate data. Utilizing NMR for these purposes has been gaining popularity among researchers since the 1980s.[12] Plutino *et al*.[13] reported fast kinetic reaction studies on the reaction mechanism of olefin exchange. They performed repetitive scans on a reaction and determined the line broadening in the NMR scans of the reactions to aid them in calculating the rate of the reactions constants (Figure 3.5) show two H-NMR stacked plots (a) represents the experimental data and (b) represents the simulated data. They observed the relation between the coordinated and non-coordinated species from the decrease of the line widths of the signal.

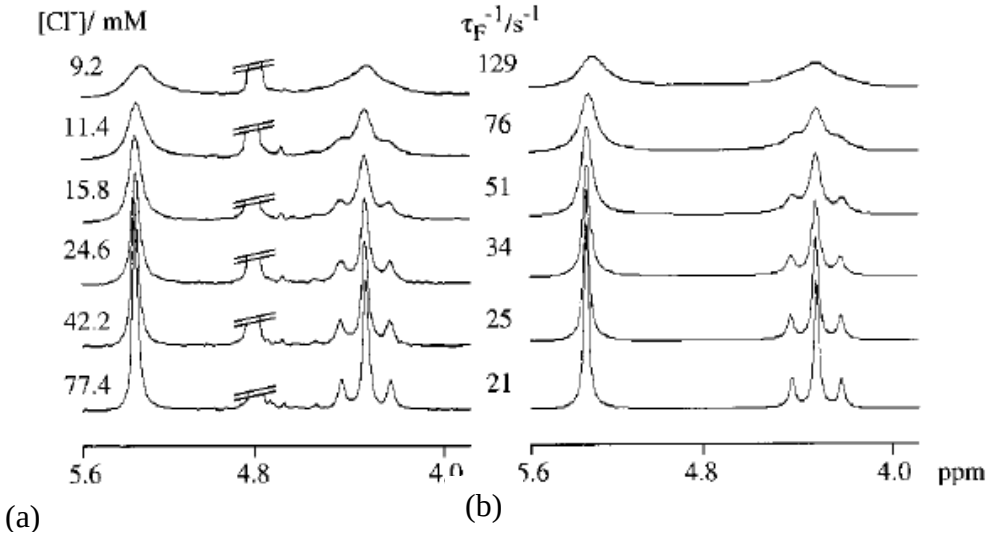

Figure 3.5: ^{1}H-NMR: Stacked plot (a) is the experimental plot and stacked plot (b) is the simulated plot showing the decrease in one of the reactants used in the experiment with increasing concentration of the other reactant.

3.5 X-ray Diffraction Spectroscopy (XRD)

Single crystal X-ray diffraction was discovered in 1912 and since then the technique has been extensively employed in material characterization. XRD characterization is an effective qualitative method. Identification of a molecule with XRD techniques is based on the crystal rather than the chemical composition. Since identification is based on the crystal, different compounds with the same chemical composition can be differentiated and characterized with high accuracy, however suitable crystals are required.

[12] Kaufman, D., Sterner, C., Masek, B., Svenningsen, R., Samuelson, G., *J Chem. Ed.* **59**, (10), 885-886, 1982.
[13] Plutino, M. R., Otto, S., Roodt A. Elding, L. I., *Inorg. Chem*., **38**, 1233-1238, 1999.

The X-ray diffractometer produces X-ray beams of a single wavelength (produced by a X-ray tube) to examine a sample crystal. The X-ray beam's incident angle continuously changes to allow for a spectrum of intensity *versus* angle data points (angle between the incident beam and the diffracted beam) to be recorded. A preliminary experiment is performed obtaining information of a unit cell, geometry and symmetry. Thereafter intensity is measured and the crystal structure is solved and refined. These processes are discussed in detail in the following subsections.[14]

3.5.1 Bragg's Law

Bragg's Law is a law that was developed by two English physicists, Sir W.H. Bragg and his son Sir W.L. Bragg. They developed this law to explain how atomic planes within a crystal appear to reflect X-ray beams at particular angles of indices. They explained this by assuming that X-rays are reflected by atoms that act as mirror planes. X-rays are not completely reflected by a single atomic mirror plane, at times they pass through to deeper atomic mirror planes and are reflected from deeper within the sample crystal. X-rays that are either reflected from the same atomic mirror plane which could lie shallow or deeper within the sample crystal, get reflected in phase. When the X-rays are reflected in phase, trough to trough or crest to crest interactions are summative and this results in an increase of intensity of the trough or the crest. The X-rays that are reflected from different atomic mirror planes whether shallow or deeper within the sample crystal get reflected out of phase. When the X-rays are reflected out of phase then crest to trough or trough to crest interaction between waves is subtractive and it results in a decrease in intensity of the trough or the crest.

Bragg's Law was developed to correct the X-rays that are reflected out of phase. This law is the basic law that is used by all methods to obtain the unit cell geometry from the derived geometry.

$$n\lambda = 2d \sin\theta \qquad \text{... 3.5}$$

Equation 3.5 is a mathematical representation of Bragg's Law.[14] In this equation d denotes the distance between the atomic mirror planes or layers in the sample crystal, λ is the wavelength of

[14] Leng, Y., *Material Characterization Introduction to Microscopicand Spectroscopic Methods*., JohnWiley & Sons (Asia) Pte Ltd, 2008.

the incident X-ray beam, n is the integer and θ is the angle of incidence of the reflected X-ray beam. Bragg's Law as it is derived by Equation 3.5 does not satisfy the mirror reflection analogy and it needs to be modified slightly. n is converted to hkl and Bragg's Law is written as derived in Equation 3.6 to satisfy the mirror reflection analogy.[14]

$$\lambda = 2d_{hkl}sin\theta \quad \text{... 3.6}$$

3.5.2 The structure factor

The structure factor (F|hkl|) of a diffracted wave is a resultant of waves being scattered by all the atoms (*j*) in a unit cell compared to an electron with the directions of the hkl reflections. The structure factor is defined by two numerical values: the amplitude denoted F|hkl| which relates to the height of the crest of the diffracted wave and it is measured in electrons and the phase denoted by φ relates to the horizontal shift with respect to the particular origin. The structure factor is mathematically expressed by Equation 3.7 where g_j is the temperature-corrected atomic scattering factor that is sometimes also denoted as f_j. This factor accounts for each of the N atoms in a given unit cell.[15,16]

$$F|hkl| = \sum j\text{^}N = g_j\ exp(i\varphi\_j\ ) \quad \text{..3.7}$$

Equation 3.7 can also be written as Equation 3.8 where g_j is the scattering factor of the j^{th} atom with x_j, y_j and z_j as fractional coordinates.

$$F|hkl| = g_j \exp[i2\pi(hx_j + ky_j + Iz_j)] \quad \text{...3.8}$$

This series of coordinates can be expressed in terms of sine and cosine waves called a Fourier series, because X-rays are waves (see Equation 3.9).

$$F_{hkl} = 2\sum f_j cos2\pi(hx_n + ky_n + Iz_n) \quad \text{...3.9}$$

[15] Azàroff, L.V., *Elements of X-ray Crystallograph*, New York, McGraw Hall. Inc., 1968.
[16] Brink, A., MSc Dissertation: *Rhodium(I) Betadiketone Complexes As Model Catalysts In Methanol Carbonylation*. University of Free State, UFS 2007.

The electron distribution within the crystal is a Fourier Transform of the structure factor ($F|hkl|$), therefore it is possible to calculate the electron density distribution. The electron distribution can be expressed by Equation 3.10 that is a three-dimensional Fourier series, where ρ(x, y, and z) is the electron density position in a unit cell and V denotes the volume of the unit cell.

$$\rho(x,y,z) = 1/V \sum_h \sum_k \sum_l F_{hkl} \quad e^{-2\pi(hx_n+ky_n+Iz_n)} \qquad \text{...3.10}$$

The intensity of the hkl reflections is directly proportional to the square of the structure factor (Equation 3.11).

$$F|hkl|^2 \propto I_{hkl} \qquad \text{...3.11}$$

Therefore the modulus of the structure factor is obtained by the taking the root of the structure factor (Equation 3.12).[15,16]

$$F|hkl| = \sqrt{I_{hkl}} \qquad \text{...3.12}$$

3.5.3 Phase Problem

The phase problem occurs when we take the root of the structure factor, therefore the magnitude is known but not the sign. This will result in the loss of phase information. The phase information is required for the determination of the positions of the atoms and the electron density distribution. The phase problem can be overcome by creating trial phases for the structure factor using either the Patterson Function or the Direct Method.[15,16]

3.5.3.1 The Patterson Function

The Patterson Function works on the basis of determining one or more heavy atoms in a unit cell to help solve a crystal structure. The Patterson Function is a Fourier transform of the intensities of the structure factors. It is determined by the multiplication of coordinates (x, y, and z) with electron densities at (x+u, y+v, z+y) and the product is then multiplied by *dxdydz* and integrated over the volume of the unit cell (Equation 3.13). The Patterson function is then derived by substituting every electron density into Equation 3.14.[15,16]

$$\iiint \rho(x,y,z) * \rho(x+u, y+v, z+u) dxdydz \qquad \text{...3.13}$$

$$\rho(uvw) = \sum\sum\sum F|hkl|^2 cos2\pi(hu + kv + lv) \quad \text{...3.14}$$

3.5.3.2 The Direct Method

The Direct Method works on the basis of determining several atoms with similar scattering abilities in a unit cell. A mathematical probability for phase values and an electronic density map is created to help in the refining process for solving the sample crystal structure. This method is particularly good for determining phase information for crystal structures that contain light atoms i.e. organic molecules.[15,16]

3.5.4 Least-Squares Refinement

Least-Squares Refinement is a direct comparison of the calculated structure against the observed or the experimental structure. The mathematical representation of this comparison is given by Equation 3.15, the residual index. A good comparison between the calculated structure and the experimental structure should give a residual index value of approximately 0.02 to 0.07.

$$R = \frac{\sum||F_o|-|F_c||}{\sum|F_o|} \quad \text{...3.15}$$

3.6 Chemical Kinetics

Chemical kinetics is a process that is used to determine the rate of a chemical reaction and the mechanistic pathway(s) that occur during a chemical reaction. Chemical kinetics also gives insight into the type of activation process that takes place in the transition state during the formation of the products.

3.6.1 Theoretical Principles of Chemical Kinetics

The rate law gives the relationship between the concentration and the reaction rate that is experimentally determined. The transition state is the entity that can form the products or revert back to form the reactants. The transition state can be defined at a position at the apex of the

potential energy graph and is usually short lived. The transition state theory is further discussed in Section 3.6.5. The structure of the transition state and the solvent molecules that are involved in the transition state cannot be determined from the rate law. The rate law also does not provide information on the reactants before and after the transition state. For a generalized chemical reaction (Equation 3.16) the rate law can be derived (Equation 3.17),

$$aA + bB \longrightarrow cC \qquad \textbf{…3.16}$$

$$R = -\frac{\Delta[A]}{\Delta[t]} = -\frac{\Delta[B]}{\Delta[t]} = \frac{\Delta[C]}{\Delta[t]} \qquad \textbf{... 3.17}$$

where t denotes the time and the concentration is denoted by the square brackets. The rate of the chemical reaction is directly proportional to the concentration and generally it is expressed as Equation 3.18,[17]

$$R = k\,[A]^x[B]^y \qquad \textbf{…3.18}$$

where the superscripts x and y denote the order of the reaction and are independent of the temperature and the stoichiometric coefficients in the chemical reaction. The sum of the two exponents gives the order of the reaction, and can add up to zero. In a first and second order reaction *k* denotes the rate constant and its magnitude is an indication of how slow or how fast the reaction is. A large rate constant indicates a fast reaction while a small rate constant indicates a slow reaction. The rate constant is unique for every reaction at a given temperature and it is temperature dependent. This is best described by the Arrhenius equation (Equation 3.19),

$$k = Ae^{-E_a/RT} \qquad \textbf{…3.19}$$

where E_a is the activation energy and it denotes the energy barrier that has to be overcome in order for the chemical reaction to occur, and A is the frequency factor. Not only does the activation energy need to be overcome for the reaction to form products but the molecules need to be in a particular orientation. This variable A is an expression of the orientation of the molecules when they collide with one another. The larger the value of A, the more likely a

[17] Jordan, R.B., *Reaction Mechanism of Inorganic and Organometallic Systems*., Oxford, Oxford University Press. Inc. 1991.

successful collision can occur in a chemical reaction. R is the universal gas constant and T denotes the temperature.

3.6.2 The Differential Laws and Integrated Rate Law

For a specific chemical reaction (Equation 3.20) we can determine the rate law and differentiate it to give the differential rate law (Equation 3.21)

$$aA \longrightarrow cC \quad \textbf{…3.20}$$

$$-\frac{\Delta[A]}{\Delta[t]} = k[A]^n \quad \textbf{... 3.19}$$

The differential rate law can be integrated to give the integrated rate laws (Equation 3.22 - 3.24) with limits $[A_o]$ at time 0 as the initial concentration and [A] as the final concentration at the respective final time. Depending on the magnitude of n that denotes the order of the reaction, the integration will give a direct relation of the concentration with respect to time. For a zero order reaction the integrated rate law will be determined as:

$$[A] = [A_o] - kt \quad \textbf{... 3.22}$$

For a first order reaction the integrated rate law will be determined as:

$$\ln[A] = -kt + \ln[A_o] \quad \textbf{... 3.23}$$

And for a second order reaction the integrated rate law will be determined as:

$$\frac{1}{[A]} = kt + \frac{1}{[A_o]} \quad \textbf{...3.24}$$

The experimental raw data that is collected is fitted to these integrated rate laws to get the best fit and the rate constant *k* is obtained from the slope with the best fit.

3.6.3 The Reaction Half-Life ($t_{1/2}$)

The reaction half-life is the period of time that is needed for the reaction to consume half of the original reactants. The relationship between the rate constant and the half-life of a first order reaction is given by Equation 3.25 and it is independent of the initial concentration [A_o] while it is dependent on the rate constant.

$$t_{1/2} = \frac{ln2}{k} \quad \textbf{...3.25}$$

Second order reactions however depend on both the initial concentration [A_o] and the rate constant *k* and given is by Equation 3.26. [16, 17]

$$t_{1/2} = \frac{1}{k[A_o]} \quad \textbf{…3.26}$$

3.6.4 Reaction Thermodynamics

The Arrhenius equation (Equation 3.19) gives a relationship between the temperature and the rate of the reaction. Thermodynamic equations are independent of time as illustrated in Figure 3.6.

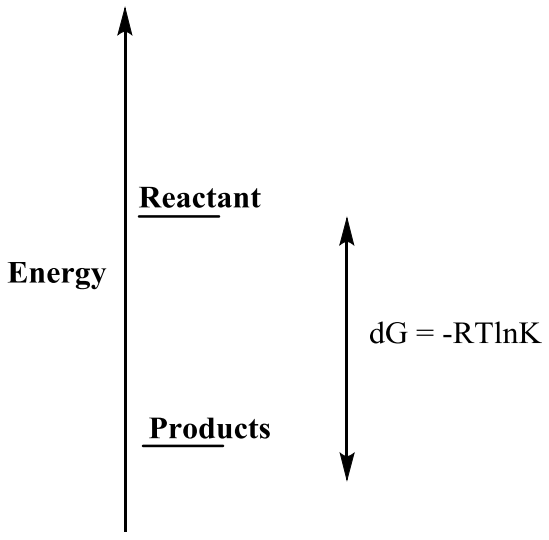

Figure 3.6: The energy difference between the reactants and the products formed.[18]

[18] *Kinetics and Thermodynamics*., Available: http://web.stanford.edu/~kaleeg/chem32/kinT/ (Last accessed 12/11/2014).

From Figure 3.6 the energy difference is represented in terms of the Gibbs Energy at constant pressure and temperature. The thermodynamic equation can also be given in terms of the rate constant *k* (Equation 3.27 – 3.28).

$$k = \exp(-\Delta G^o/RT) \quad \textbf{…3.27}$$

$$k = \exp(-\Delta S^o/R)\exp(-\Delta H^o/R) \quad \textbf{...3.28}$$

Where ΔG^o, ΔH^o and ΔS^o denote the change of the standard free energy, standard enthalpy and standard entropy of the reaction respectively and exp is the exponential function e^x also referred to as the inverse of ln.

3.6.5 The Transition State Theory

The transition state theory is a topic that focuses on a certain stage in the chemical reaction called the transition state or the activated complex that exists between the reactants and the products. It is assumed that the activated complex is in equilibrium with the reactants and the products. This assumption gives rise to Equation 3.29.

Figure 3.7 is a reaction coordinate diagram, a representation of how a chemical reaction proceeds from reactants to products. With the intermediate (activated complex) represented at the apex of the graph.

$$[\text{X-Y}] \underset{}{\overset{K_{\#},\, k_1}{\rightleftharpoons}} [\text{X--Y}] \xrightarrow{k_2} \text{X} + \text{Y} \quad \textbf{...3.29}$$

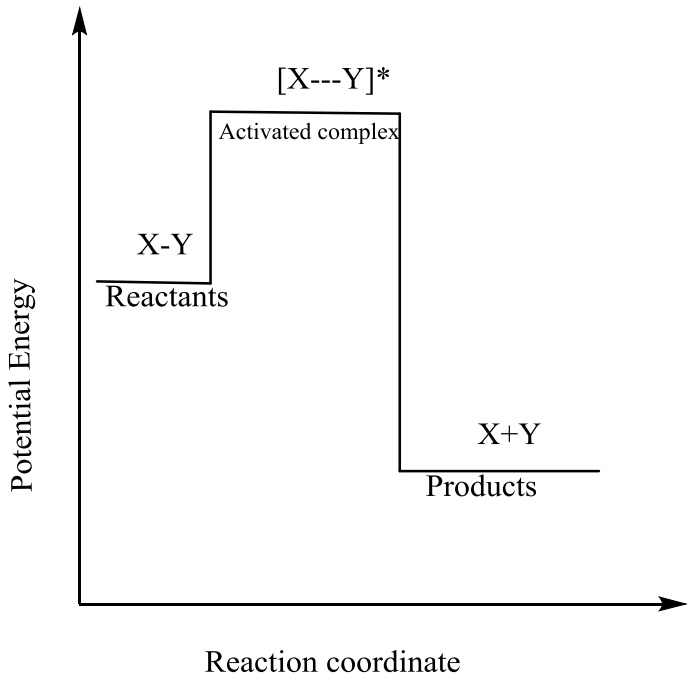

Figure 3.7: Graphical representation of how a reaction proceeds through the transition state [X- - -Y]* to form the products X+Y.

When there is sufficient thermal energy to overcome the activation energy barrier, the activated complex favours the forward reaction and the products are formed as the reactants are consumed. This way the vibrational frequency will equal the rate constant. With *k* the rate constant, the following (Equation 3.30) can be derived:

$$\frac{d[Y]}{dt} = k_3[X--D]^* = k_3K^*[X-D] \quad \text{...3.30}$$

and

$$lnK^{\#} = -\frac{\Delta G^{o\neq}}{RT} = -\frac{\Delta GH^{o\neq}}{RT} = -\frac{\Delta S^{o\neq}}{RT} \quad \text{...3.31}$$

From Equation 3.30, Equation 3.31 can be derived. The logarithmic form of Equation 3.29 gives rise to Equation 3.32 which aids in the determination of the rate constant at different temperatures. Plotting a graph from the Eyring Equation should result in a linear plot. Deviation from a linear graph is a reflection of equilibria, parallel or back to back reactions.

$$Kexp = \frac{kT}{h}K^{\neq} = \frac{kT}{h}\exp(\frac{\Delta G^{o\neq}}{RT}) \quad \text{... 3.32}$$

$$\ln\left(\frac{Kexp}{T}\right) = \ln\left(\frac{k}{h}\right) - \frac{\Delta H^{o\neq}}{RK} + \frac{\Delta S^{o\neq}}{R} \quad \text{... 3.33}$$

By plotting a linear graph from Equation 3.33 the value of $\frac{\Delta H^{o\neq}}{RK}$ can be determined from the gradient of the graph and the y intercept gives the value of $\frac{\Delta S^{o\neq}}{R}$.[18,16,19]

3.7 Summary

The characterization methods discussed in the preceding subsections were paramount in the characterization of the synthesized compounds in this study. NMR, IR, and UV/Vis data for the synthesized compounds are reported in Chapter 4.

X-ray diffraction described in this chapter were utilized to determine the crystal structures of the selected compound reported in Chapter 5.

[19] Laidler, K. J., Meiser, J. H., Sanctuary, B. C., *Physical Chemistry*, 4th Ed., Houghton Mifflin., 2000.

4 Synthesis and Spectroscopic Characterisation of Zirconium(IV) and Hafnium(IV) Complexes

4.1 Introduction

This chapter will focus on the synthesis and characterization of *N,N'*-diamine and *O,O'*-based bidentate ligands and their employment in various synthetic procedures. The complexes synthesized were designed with the aim of potentially employing them in the separation of zirconium and hafnium for application in the nuclear industry. Several methods and solvents were used in an attempt to grow the best possible crystals of the zirconium and hafnium complexes for identification with X-ray diffraction. The characterization techniques used to characterize the compounds in this chapter include Nuclear Magnetic Resonance Spectroscopy (NMR), Infrared Spectrocospy (IR), Ultraviolet and Visible Spectroscopy (UV/Vis) and single crystal X-ray Diffraction (XRD). The basic theory of these characterization techniques was discussed in Chapter 3.

4.2 Synthesis of Ligands

4.2.1 Synthesis of *N,N'*-bis(pyridine-2-ylmethyl)cyclohexamine (BPMH)

In an oxygen atmosphere, pyridine-2-carbaldehyde (1.85 g, 1.46 mL, 17.281 mmol) was added to a solution of cyclohexamine (0.812 g, 0.938 mL, 8.185 mmol) in dichloroethane (10 mL). The reaction mixture was stirred for 30 min at 50 ˚C and then cooled to room temperature. Sodium triacetoxyborohydride (3.662 g, 17.27 mmol) was dissolved in dichloroethane (10 mL) and kept in an ice bath. This mixture was slowly added, in small portions, to the reaction mixture and was stirred overnight at room temperature. The reaction mixture was then quenched with a 2% sodium bicarbonate solution (100 mL). The organic layer containing the product was separated from the aqueous later then dried over aqueous sodium sulphate and filtered to give the product

(Figure 4.1). This synthetic method was adopted from the methods reported by Sato *et al.*[1] previously reported by Toftlund *et al.*[2] as well as Andereg *et al.*[3]

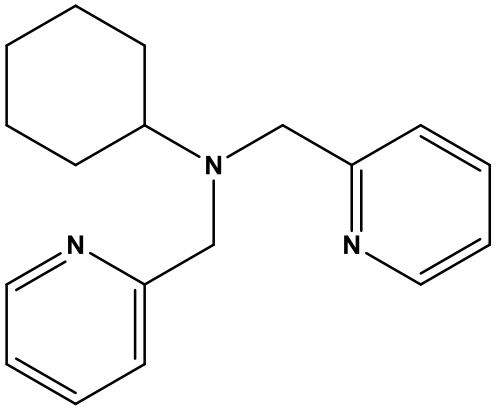

Figure 4.1: Diagram of the structure of *N,N'*-bis(pyridin-2-ylmethyl)cyclohexanamine (BPMH).

Spectroscopic data: ^{1}H 300 MHz NMR (Chloroform-D): δ = 8.49 (d, 2H), 7.59 (m, 4H), 7.12 (t, 2H), 3.90 (s, 4H), 2.52(tt, 1H), 1.94 (d, 2H), 1.77(d, 2H), 1.62(d, 1H), 1.33(m, 2H), 1.15(m, 3H).
IR : v(NC) = 3003 cm^{-1}.
UV/Vis: λ_{max} = 425 nm, ε = 1.080 x10^3 M^{-1}cm^{-1}.

4.2.2 Attempted Synthesis of N^1,N^1,N^2,N^2-tetrakis(pyridin-2-ylmethyl)ethane-1,2-diamine (TPEN) and Formation of 2,2'-((2-(pyridin-2-yl)imidazolidine-1,3-diyl)bis(methylene))-dipyridine (PIBD)

In an oxygen atmosphere, pyridine-2-carbaldehyde (1.85 g, 1.46 mL, 17.2 mmol) was added to a solution of ethylenediame (0.260 g, 0.280 mL, 4.32 mmol) in dichloroethane (10 mL) and the reaction mixture was stirred for 30 min at 50 ˚C and then cooled to room temperature. Sodium triacetoxyborohydride (3.66 g, 17.3 mmol) was dissolved in dichloroethane (10 mL) and kept in an ice bath and slowly added in small portions to the reaction mixture. After the reaction mixture was stirred overnight at room temperature, it was quenched with a 2% sodium bicarbonate solution (100 mL) and the organic layer containing the product was dried over aqueous sodium sulphate and filtered to give the unexpected product 2,2'-((2-(pyridin-2-yl)imidazolidine-1,3-diyl)bis(methylene))-dipyridine (PIBD) (Figure 4.3).

[1] Sato, M., Mori, Y. Iida, T., *Synthesis*, **6**, 539-540, 1992.
[2] Toftlund, H., Yde-Andersen, S., *Acta Chem. Scand. Ser*. A, **35**, 575-581, 1981.
[3] Anderegg, G., Wenk, F., *Helv. Chim. Acta*, **50**, 2330-2332, 1967.

Figure 4.2 below illustrates the expected structure for this synthetic procedure that was unfortunately not obtained. Instead ring closure was favoured and 2,2'-((2-(pyridin-2-yl)imidazolidine-1,3-diyl)bis(methylene))-dipyridine illustrated in Figure 4.3 was obtained. This conclusion was made by single crystal X-ray diffraction.

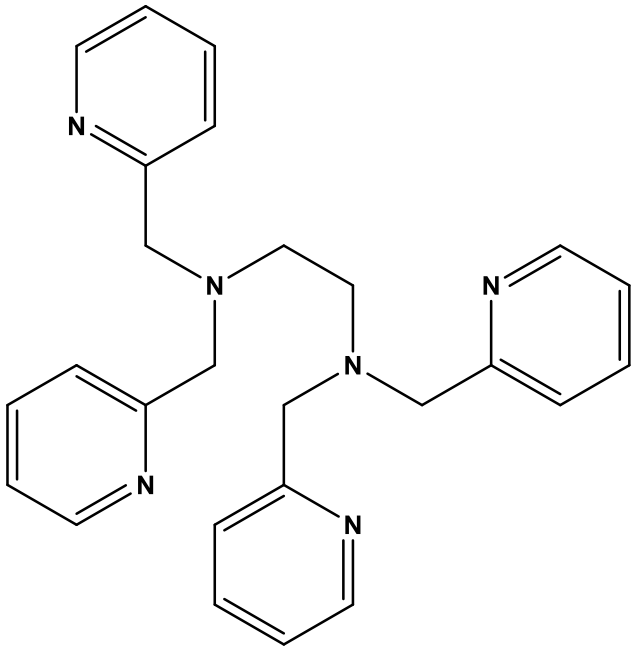

Figure 4.2: Diagram of the expected structure of N^1,N^1,N^2,N^2-tetrakis(pyridin-2-ylmethyl)ethane-1,2-diamine (TPEN).

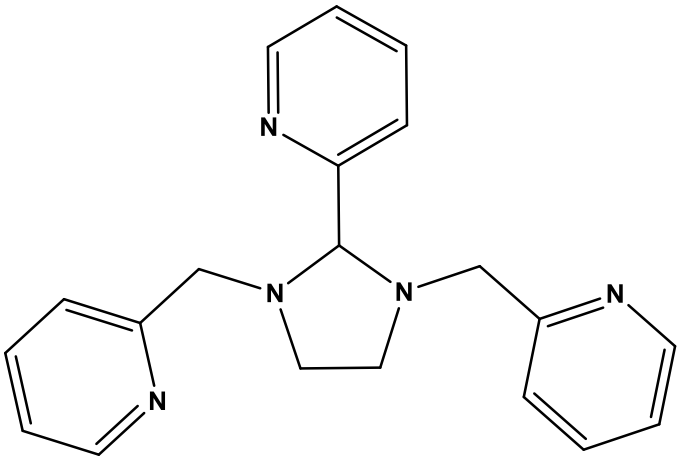

Figure 4.3: Diagram of the unexpected structure of 2,2'-((2-(pyridin-2-yl)imidazolidine-1,3-diyl)bis(methylene))-dipyridine (PIBD) that was obtained.

Spectroscopic data: ^{1}H 300 MHz NMR (Chloroform-D): δ = 8.49 (dm, 3H), 7.87 (d, 1H), 7.72 (t, d, 1H), 7.47 (d, 1H), 7.38(d, 1H), 7.21(m, 1H), 7.12(m, 2H), 4.3 (s, 1H) 3.92 (s, 1H), 3.79(s, 2H), 3.74 (d, 3H), 3.34 (td, 1H).

IR : ν(NC) = 2926 cm^{-1}.

UV/Vis: λ_{max} = 425 nm, ε = 1.080 x10^3 M^{-1}cm^{-1}.

4.3 Bench Top Synthesis of Zirconium(IV) and Hafnium(IV) Complexes with *N,N'*-diamine Based Ligands

The following synthetic procedure was adopted from Steyn[4] and Viljoen.[5] The synthetic procedure involved addition of the solid metal (zirconium(IV) and hafnium(IV)) to a solvent at room temperature to form a metal slurry. Several solvents were utilized: dimethylformamide, Methanol, Acetonitrile, Toluene, Water and THF. The solvents were used as received from the supplier without further purification or drying. The ligand, dissolved in the solvent was added to the metal in a variety of molar ratios. The reaction mixture was then heated and stirred overnight.

4.3.1 Attempted Synthesis of Zr(BPMH) – 1: 1

$ZrCl_4$ (0.0693 g, 2.90 x 10^{-1} mmol) was added to BPMH (0.0844 g, 3.00 x 10^{-1} mmol) in 5 mL of DMF. The transparent metal solution turned yellow after 5 min. An oily brown product was obtained after the solvent was removed *in vacuo.* (Yield: 22 mg, 18 %)

Spectroscopic data: ^{1}H 300 MHz NMR (Chloroform-D): δ = 8.48 (dd, 2H), 7.62 (d, 4H), 7.12 (m, 2H), 4.01 (s, 4H), 2.63(t, 1H), 2.57 (m, 2H), 1.77(d, 2H), 1.58(d, 1H), 1.39(m, 2H), 1.14(m, 3H).

IR : ν(NC) = 3078 cm^{-1}.

UV/Vis: λ_{max} = 425 nm, ε = 1.080 x10^3 $M^{-1}cm^{-1}$.

4.3.2 Attempted Synthesis of $Zr(BPMH)_2$ – 1: 2

$ZrCl_4$ (0.0701 g, 3.0 x 10^{-1}mmol) was reacted with BPMH (0.168 g, 5.98 x 10^{-1}mmol) in 5 mL of DMF. The transparent metal solution turned yellow after 5 min. An oily brown product was obtained after the solvent was removed *in vacuo*. (Yield: 30.5 mg, 18 %)

---

[4] Steyn, M., MSc Dissertation: *Speciation And Interconversion Mechanism Of Mixed Halo And O,O'- And O,N-Bidentate Ligand Complexes Of Zirconium.* University of the Free State. UFS, 2009.

[5] Viljoen, J. A., MSc Dissertation: *Speciation And Interconversion Mechanism Of Mixed Halo And O,O'- And O,N-Bidentate Ligand Complexes Of Hafnium.* University of the Free State. UFS, 2009.

Spectroscopic data: ^{1}H 300 MHz NMR (Chloroform-D): δ = 8.47 (md, 2H), 7.56 (m, 4H), 7.09 (m, 2H), 3.87 (s, 4H), 2.50(tt, 1H), 1.96 (d, 3H), 1.75 (d, 2H), 1.60 (d, 2H), 1.31 (m, 2H), 1.13 (m, 3H).

IR : ν(NC) = 3078 cm^{-1}.

UV/Vis: λ_{max} = 425 nm, ε = 1.080 x10^3 M^{-1}cm^{-1}.

4.3.3 Attempted Synthesis of Zr(BPMH)$_3$ – 1: 3

$ZrCl_4$ (0.0695 g, 2.98 x 10^{-1} mmol) was added to BPMH (0.338 g, 8.94 x 10^{-1} mmol) in 5 mL of DMF. The transparent metal solution turned yellow brown after 5 min. An oily brown product was obtained after the solvent was removed *in vacuo.* (Yield: 34 mg, 13.5 %)

Spectroscopic data: ^{1}H 300 MHz NMR (Chloroform-D): δ = 8.46 (d, 2H), 7.57 (m, 4H), 7.09 (m, 2H), 3.88 (s, 4H), 2.51 (t, 1H), 1.93 (d, 2H), 1.67 (m, 9H), 1.14 (m, 9H).

IR : ν(NC) = 3078 cm^{-1}.

UV/Vis: λ_{max} = 425 nm, ε = 1.080 x10^3 M^{-1}cm^{-1}.

4.3.4 Attempted Synthesis of Hf(BPMH) – 1: 1

$HfCl_4$ (0.0738 g, 2.31 x 10^{-1} mmol) was added to BPMH (0.258 g, 2.31 x 10^{-1} mmol) in 5 mL of DMF. The transparent metal solution turned yellow brown after 5 min. An oily brown product was obtained after the solvent was removed *in vacuo.* (Yield: 29 mg, 21.8 %)

Spectroscopic data: ^{1}H 300 MHz NMR (Chloroform-D): δ = 8.59 (d, 2H), 7.88 (d, 2H), 7.81 (t, 2H), 7.33 (t, 2H) 4.72 (s, 4H), 3.26 (t, 1H), 2.39 (d, 2H), 1.90 (d, 2H), 1.65 (d, 3H), 1.24 (m, 3H).

IR : ν(NC) = 2930 cm^{-1}.

UV/Vis: λ_{max} = 425 nm, ε = 1.080 x10^3 M^{-1}cm^{-1}.

4.3.5 Attempted Synthesis of Hf(BPMH)$_2$ – 1: 2

$HfCl_4$ (0.0740 g, 2.31 x 10^{-1} mmol) was added to BPMH (0.1293 g, 4.60 x 10^{-1} mmol) in 5 mL of DMF. The transparent metal solution turned yellow brown after 5 min. An oily brown product was obtained after the solvent was removed *in vacuo.* (Yield: 42 mg, 27 %)

Spectroscopic data: ^{1}H 300 MHz NMR (Chloroform-D): δ = 8.57 (d, 2H), 7.87 (d, 2H), 7.78 (t, 2H), 7.30(t, 2H) 4.69 (s, 4H), 2.38 (d, 2H), 1.88 (d, 2H), 1.63 (m, 3H), 1.22 (m, 3H).

IR : ν(NC) = 2930 cm^{-1}.

UV/Vis: λ_{max} = 425 nm, ε = 1.080 x10^3 M^{-1}cm^{-1}.

4.3.6 Attempted Synthesis of $Hf(BPMH)_3$ – 1: 3

$HfCl_4$ (0.0738 g, 2.31 x 10^{-1}mmol) was added to BPMH (0.194 g, 6.90 x 10^{-1} mmol) in 5 mL of DMF. The transparent metal solution turned yellow brown after 5 min. An oily brown product was obtained after the solvent was removed *in vacuo.* (Yield: 22 mg, 18 %)

Spectroscopic data: ^{1}H 300 MHz NMR (Chloroform-D): δ = 8.04 (d, 2H), 7.85 (s, 2H), 7.37 (s, 2H), 4.65 (s, 4H) 3.22 (t, 1H), 1.90 (d, 2H), 1.62 (m, 3H), 1.22 (m, 3H).

IR : ν(NC) = 2930 cm^{-1}.

UV/Vis: λ_{max} = 418 nm, ε = 9.233 x10^3 $M^{-1}cm^{-1}$.

4.3.7 Attempted synthesis of Zr(PIBD) – 1: 1

$ZrCl_4$ (0.0110 g, 4.70 x 10^{-1}mmol) was added to PIBD (0.0201 g, 4.70 x 10^{-1} mmol) in 5 mL of DMF. The transparent metal solution turned yellow brown after 5 min. An oily brown product was obtained after the solvent was removed *in vacuo.* (Yield: 3.45 mg, 11%)

Spectroscopic data: ^{1}H 300 MHz NMR (Chloroform-D): δ = 8.49 (dm, 3H), 7.87 (d, 1H), 7.72 (t, d, 1H), 7.47 (d, 1H), 7.38 (d, 1H), 7.21 (m, 1H), 7.12 (m, 2H), 4.3 (s, 1H) 3.92 (s, 1H), 3.79 (s, 2H), 3.74 (d, 3H), 3.34 (td, 1H).

IR : ν(NC) = 3090 cm^{-1}.

UV/Vis: λ_{max} = 418 nm, ε = 9.233 x10^{-3} $M^{-1}cm^{-1}$.

4.3.8 Attempted Synthesis of $Zr(PIBD)_2$ – 1: 2

$ZrCl_4$ (0.109 g, 4.70 x 10^{-1}mmol) was added to PIBD (0.399 g, 9.4 x 10^{-1} mmol) in 5 mL of DMF. The transparent metal solution turned yellow brown in colour after 5 min. An oily brown product was obtained after the solvent was removed *in vacuo.* (Yield: 2.9 mg, 9.6%)

Spectroscopic data: ^{1}H 300 MHz NMR (Chloroform-D): δ = 8.49 (dm, 3H), 7.87 (d, 1H), 7.72 (td, 1H), 7.47 (d, 1H), 7.38 (d, 1H), 7.21 (m, 1H), 7.12 (m, 2H), 4.3 (s, 1H) 3.92 (s, 1H), 3.79 (s, 2H), 3.74 (d, 3H), 3.34(td, 1H).

IR : ν(NC) = 3090 cm^{-1}.

UV/Vis: λ_{max} = 418 nm, ε = 9.233 x10^3 $M^{-1}cm^{-1}$.

4.3.9 Attempted synthesis of Hf(PIBD) – 1: 1

$HfCl_4$ (0.281 g, 9.0 x 10^{-1}mmol) was added to PIBD (0.3901 g, 9.0 x 10^{-1}mmol) in 5 mL of DMF. The transparent metal solution turned yellow after 5 min. An oily brown product was obtained after the solvent was removed *in vacuo.* (Yield: 3.9 mg, 6%)

Spectroscopic data: ^{1}H 300 MHz NMR (Chloroform-D): δ = 8.49 (dm, 3H), 7.87 (d, 1H), 7.72 (td, 1H), 7.47 (d, 1H), 7.38 (d, 1H), 7.21 (m, 1H), 7.12 (m, 2H), 4.3 (s, 1H) 3.92 (s, 1H), 3.79 (s, 2H), 3.74 (d, 3H), 3.34 (td, 1H).
IR : ν(NC) = 3090 cm^{-1}.
UV/Vis: λ_{max} = 418 nm, ε = 9.233 x10^3 M^{-1}cm^{-1}.

4.3.10 Attempted synthesis of Hf(PIBD)$_2$ – 1: 2

$HfCl_4$ (0.279 g, 9.0 x10^{-1}mmol) was added to PIBD (0.772 g,1.82 x 10^{-1}mmol) in 5 mL of DMF. The transparent metal solution turned yellow brown after 5 min. An oily brown product was obtained after the solvent was removed *in vacuo.* (Yield: 4.1 mg, 6.4%)
Spectroscopic data: ^{1}H 300 MHz NMR (Chloroform-D): δ = 8.49 (dm, 3H), 7.87 (d, 1H), 7.72 (dt, 1H), 7.47 (d, 1H), 7.38 (d, 1H), 7.21 (m, 1H), 7.12 (m, 2H), 4.3 (s, 1H) 3.92 (s, 1H), 3.79 (s, 2H), 3.74 (d, 3H), 3.34 (td, 1H).
IR : ν(NC) = 3090 cm^{-1}.
UV/Vis: λ_{max} = 418 nm, ε = 9.233 x10^3 M^{-1}cm^{-1}.

From the various attempts with different ratios of *N,N'*-diamine base ligands, no conclusive evidence was obtained with regards to ligand to metal coordination ratios for the respective metals. The IR spectra that were collected could only provide basic fingerprints of the compounds synthesised. The ^{1}H spectra that were collected were very similar to the free ligands spectra, but with slight chemical shifts. No crystallographic data could be collected as the products were oily residues.

4.4 Attempted Synthesis of Zr(IV) and Hf(IV) complexes with *O,O'*-based Bidentate Ligands

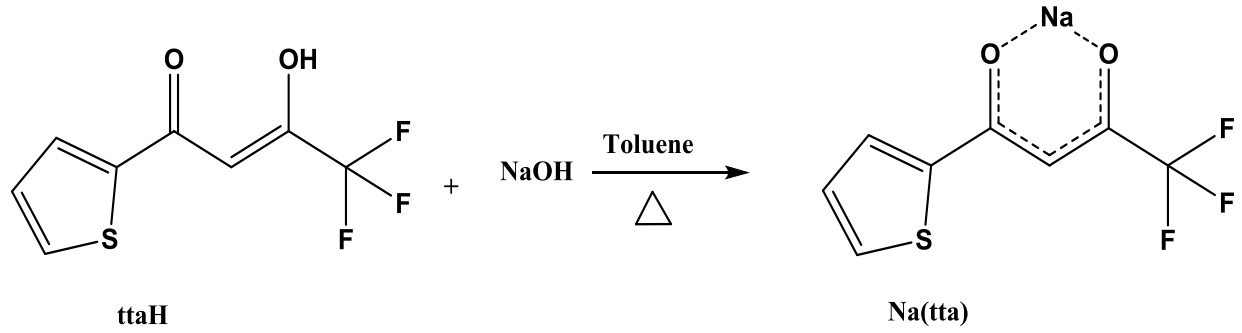

ttaH **Na(tta)**

Reaction scheme 4.1: Deprotonation of 4,4,4-trifluoro-3-hydroxy-1-(thiophen-2-yl)but-2-en-1-one.

The ligand salt [Na(tta)] was prepared by adding 4,4,4-trifluoro-3-hydroxy-1-(thiophen-2-yl)but-2-en-1-one, (ttaH) (5.55 g, 25.0 mmol) drop-wise to NaOH (1.05 g, 25.0 mmol) over a period of 3 minutes. The resulting white solid was washed with toluene to produce an isotropic mixture and was dried *in vacuo.*

Spectroscopic data: ^{1}H 300 NMR (Benzene-*D6*): δ = 1.66 (s, 3H), 5.86 (s, 1H).

^{19}F 300 NMR (Benzene *D6*):δ = 75.5 (s, 12F).

IR : ν(CO) = 1640.08 cm^{-1}.

UV/Vis: λ_{max} = 343 nm.

4.4.1 Dean Stark * Synthesis of Zirconium and Hafnium Complexes with ttaH

In this equilibrium reaction water was produced and the solvents also contain a certain percentage of water. Zirconium and hafnium are known to readily react with water to form derivatives like oxychlorides. The metals are also prone to hydrolise and then precipitate to form $Zr(OH)_4$ and $Hf(OH)_4$. The precipitation and formation of oxychlorides lead to the metals not being favourable for these coordination reactions. To counteract this and to increase the probability of successful chemical reactions with these metal salts, the Dean Stark apparatus was employed. The synthetic procedure involved the addition of the metal salt to toluene in the refluxing Dean Stark assembly. The solution was stirred vigorously at 115 ˚C until the metal salt was dissolved. Two batches of moisture (water and toluene) were collected from the Dean Stark outlet.

4.4.1.1 Synthesis of [Zr(tta)$_4$] ($ZrCl_4$ and Na(tta) (1 : 4))

$ZrCl_4$ (0.102 g, 4.36 x10^{-1} mmol) was dissolved in 15 mL toluene. [Na(tta)] (ttaH (0.384 g, 1.73 mmol) and NaOH (0.0635 g, 1.60 mmol)) dissolved in 15 mL toluene were slowly added to the metal salt solution. The transparent metal solution turned light yellow from a cloudy white colour upon addition of the ligand. The reaction mixture was allowed to reflux at 113 ˚C overnight. The reaction mixture was filtered and the toluene filtrate was allowed to crystalize. Hexagonal colourless crystals were obtained. (Yield: 11.4 mg, 60 %). A schematic representation of the product is given in Figure 4.4.

Spectroscopic data: ^{1}H 300 NMR (Benzene-D*6*): δ = 1.66 (s, 3H), 5.86 (s, 1H).

^{19}F 300 NMR (Benzene *D6*): δ = 76.86 (s, 12F).

* The Dean Stark is also referred to as the Dean-Stark receiver or a distilling trap is used in combination with a reflux condenser, It is a piece of laboratory glassware used to collect water during a reaction.

IR : ν(CO) = 1607.28 cm^{-1}.

UV/Vis: λ_{max} = 340 nm, ε = 1.017 $x10^3$ $M^{-1}cm^{-1}$.

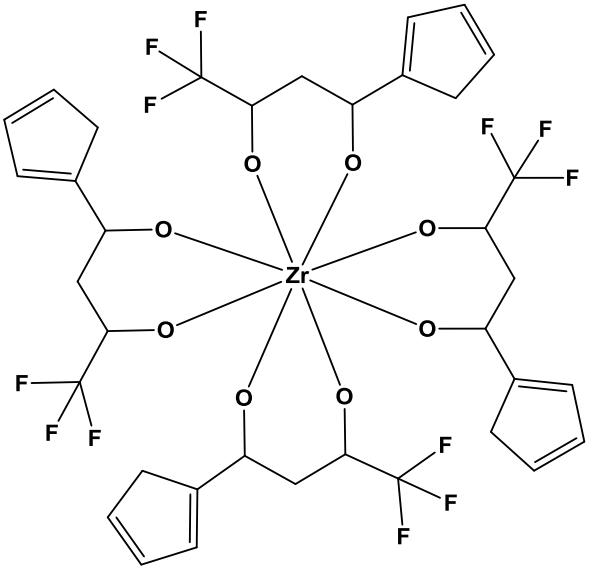

Figure 4.4: Diagram of Tetrakis(thenoyltrifluoroacetylacetonato)Zirconium(IV) [$Zr(tta)_4$].

4.4.1.2 Synthesis of $Hf(tta)_4$ $HfCl_4$ and Na(tta) (1 : 4)

$HfCl_4$ (0.202 g, 6.30 $x10^{-1}$ mmol) was dissolved in 15 mL toluene. [Na(tta)] (ttaH (0.551 g, 2.48 mmol) were NaOH (0.103 g, 2.56 mmol)) dissolved in 15 mL toluene and slowly added to the metal salt solution. The cloudy-white metal solution turned light yellow upon addition of the ligand solution. The reaction mixture was allowed to reflux at ~ 113 ˚C overnight. The reaction mixture was filtered and the toluene filtrate was allowed to crystalize and transparent cuboidal crystals were obtained. (Yield: 26 mg, 63%). A schematic representation of the product is given in Figure 4.5.

Spectroscopic data: ^{1}H NMR (Benzene-D*6*): δ = 1.66 (s, 3H), 5.86 (s, 1H).

^{19}F 300 NMR (Benzene-*D6*): δ = 76.86 (s, 12F).

IR: ν(CO) = 1598 cm^{-1}.

UV/Vis: λ_{max} = 342 nm, ε = 1.089 x 10^3 $M^{-1}cm^{-1}$.

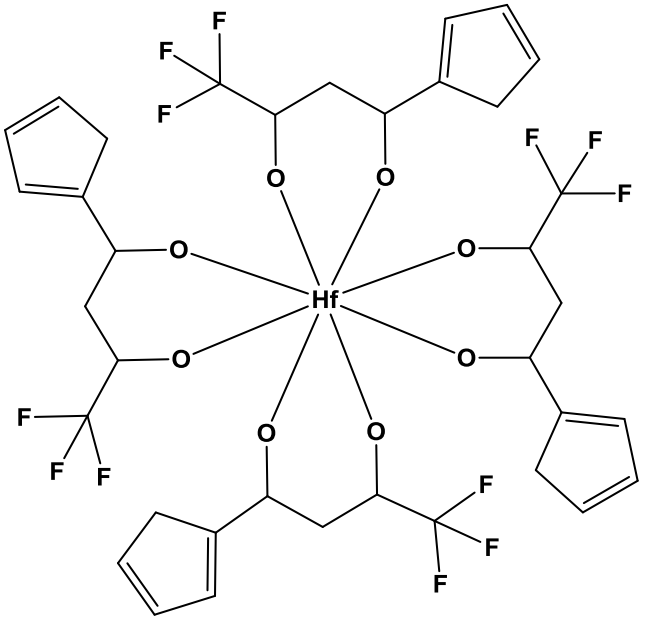

Figure 4.5: Diagram of Tetrakis(thenoyltrifluoroacetylacetonato)Hafnium(IV) [Hf(tta)$_4$].

4.4.2 Bench Top Synthesis of Zirconium and Hafnium Complexes with ttaH

The Dean Stark reaction that was employed was successful for the synthesis of the tetrakis complexes of zirconium and hafnium and was performed in toluene (Paragraph 4.2.3), but the The metal salts were not entirely soluble at room temperature. DMF was employed for the bench top synthesis of the compounds since it was established in the preceding synthetic programs that DMF dissolved both metal salts completely. The employment of DMF also brought the advantage of the compound synthesis without refluxing at high temperature.

The synthetic procedure involved separately dissolving both the metal salt and the ligand. Both were stirred until completely dissolved and homogeneity was reached. The ligand was added to the metal salt solution at room temperature and a colour change was observed. The reaction mixture was stirred overnight at room temperature. The solvent was evaporated *in vacuo*.

4.4.2.1 Synthesis of [Zr(tta)$_4$] $ZrCl_4$ and Na(tta) (1 : 4)

$ZrCl_4$ (0.0508 g, 2.18 x 10^{-1} mmol) was dissolved in 10 mL DMF. [Na(tta)] (ttaH (0.192 g, 8.64 x 10^{-1} mmol) and NaOH (0.0345 g, 8.63 x 10^{-1} mmol)) dissolved in 10 mL DMF were added to the metal solution. The transparent metal solution turned orange almost immediately. After the solvent was removed the product was crystalized in toluene and hexagonal colourless crystals were obtained.

(Yield: 10.8 mg, 59 %)

Spectroscopic data: ^{1}H NMR (Benzene-D6): δ = 1.66 (s, 3H), 5.86 (s, 1H).

^{19}F 300 NMR (Benzene-*D6*): δ = 76.86 (s, 12F).

IR: ν(CO) = 1607.28 cm^{-1}.

UV/Vis: λ_{max} = 340 nm, $\varepsilon = 1.017 \times 10^3$ M^{-1}cm^{-1}.

4.4.2.2 Synthesis of [Hf(tta)$_4$] HfCl$_4$ and Na(tta) (1 : 4)

HfCl$_4$ (0.101 g, 3.15 x 10^{-1} mmol) was dissolved in 10 mL DMF and was [Natta] (ttaH (0.2774 g, 1.25 mmol) and NaOH (0.0505 g, 1.263 mmol)) dissolved in 10 mL DMF was added to the metal solution. The transparent metal solution turned a pale yellow colour immediately. After the solvent was removed the product was crystalized in toluene and hexagonal colourless crystals were obtained. (Yield: 24.7 mg, 60 %)

Spectroscopic data: ^{1}H NMR (Benzene-D*6*): δ = 1.66 (s, 3H), 5.86 (s, 1H).

^{19}F 300 NMR (Benzene-*D6*): δ = 76.86 (s, 12F).

IR : ν(CO) = 1598 cm^{-1}.

UV/Vis: λ_{max} = 342 nm, $\varepsilon = 1.089 \times 10^3$ M^{-1}cm^{-1}.

Only the metal to ligand ratio of 1:4 was attempted here. This was done with the knowledge reported by Steyn and Viljoen, that these metals have a tendency to prefer a tetrakis coordination (See Chapter paragraph) with *O,O'*-bidentate ligand systems regardless of the ratio. The synthesis of a tetrakis zirconium(IV) and hafnium(IV) complex was successful and were characterized by ^{1}H and ^{19}F-NMR, UV/Vis and Infrared Spectroscopy. Furthermore the crystal structures were studied by XRD. The hafnium(IV) crystals gave poor data during data collections due to decomposition.

4.5 Conclusion

From the various synthetic procedures performed in this study, valuable synthetic information was obtained on zirconium(IV) and hafnium(IV) complexes. It was established that the utilization of neutral ligand systems, though they may contain strong nucleophile donor atoms like nitrogen, will not result in successful coordination between the ligand and the zirconium or hafnium metal centre. There were attempts of synthetic procedures with different ligand ratios, Subsection 4.2.3, where it was expected that different coordination systems with respect to the number of ligands coordinating to the metal centre would be obtained. The only significant outcome from these attempts was a slight increase in the chemical shifts of the product peaks. Charged ligands systems containing strong nucleophilic donor atoms are better suited for the complex synthesis of these two metals.

Although similar zirconium and hafnium complexes were synthesized by Baskin,[7] a different synthetic procedure was utilized to synthesize the complexes reported in this study. Due to advancements in technology and instrumentation, more accurate determinations of the atom interactions, bond angles and bond lengths of both the zirconium complexes with the *O,O*-bidentate donor ligand could be determined.

The synthesis and attempted synthesis posed some challenges:

- The presence of moisture in the reaction vessel during synthesis resulted in the metal salts forming oxo species. That hindered desired coordination of the metal center with the ligands systems.
- Crystallization was a major problem and after this problem was overcome obtaining crystals of good quality for data collection was a challenging.
- The crystals that were obtained especially for the hafnium systems were very sensitive. They decomposed very easily regardless of the various methods that were attempted to retain them i.e.
    - Keeping the crystals in an inert environment on bench top,
    - Keeping the crystals refrigerated in an inert environment,
    - Keeping the crystals in the mother solvent under the same conditions they were grown under and replenishing solvent as it evaporated.
- Retaining crystals for good quality was also problematic for the crystallographers who had to mount and collect the crystals. As crystals would sometimes decompose during data collections. This resulted in poor data collections which was exceptionally difficult to refine and solve.
- The *N,N*'-diamine based ligands that were initially synthesized, characterized and utilized in the synthesis of zirconium and hafnium complexes afforded crystallization problems and an *O,O'*-bidentate ligand system was employed. The presence of moisture during the initial synthetic attempts yielded unsatisfactory results which lead to the use of the Dean Stark apparatus in the synthetic procedure.

^{19}F-NMR kinetic studies were performed and this will give further insight to the chemical behaviour of zirconium and hafnium bidentate complexes. The crystallographic determinations and mechanistic study are reported in Chapter 5 and 6 respectively.

[7] Baskin, Y., Prasad, N.S. K., *J. Inorganic and Nuclear Chemistry*, **25**, (8), 1011-1019, 1963.

5 Crystallographic Study of Tetrakis(thenoyltrifluoroacetacetonato)zirconium(IV) Monohydrate $[Zr(tta)_4].H_2O$

5.1 Introduction

The aim of this study was to synthesize complexes of zirconium(IV) and hafnium(IV) and to characterise them in an effort to determine if significant differences exist which might assist with the separation of these two elements. *O,O*-bidentate ligands were utilized for the synthesis of the complexes according to the methods described in Chapter 4. In this chapter the solid state characterisation of the tetrakis(thenoyltrifluoroacetylacetonato)zirconium(IV) monohydrate $[Zr(tta)_4].H_2O$ compound is reported.

5.2 Experimental Procedure

The X-ray intensity data was collected on a Bruker X8 ApexII 4K Kappa CCD area detector diffractometer, equipped with a graphite monochromator and MoKα fine focus sealed tube (λ = 0.71073 Å, T = 100(2) K) operated at 2.0 kW (50 kV, 40 mA). The initial unit cell determinations are performed by the SMART[1] software package. All collected frames were integrated using a narrow-frame integration algorithm and reduced with the Bruker SAINT-Plus and XPREP software packages,[2] respectively. Analysis of the data showed no significant decay during the data collection. The data was corrected for absorption effects using the multi-scan technique SADABS[3], and the structure was solved by the direct methods package SIR97[4] and

[1] Bruker SMART-NT Version 5.050. Bruker AXS Inc. Area-Detector Software Package; Madison, WI, USA, 1998.
[2] Bruker SAINT-Plus Version 6.02 (including XPREP), Bruker AXS Inc. Area-Detector Integration Software, Madison, WI, USA, 1999.
[3] Bruker SADABS Version 2004/1. Bruker AXS Inc. Area Detector Absorption Correction Software, Madison, WI, USA, 1998.
[4] Altomare, A., Burla, M, C., Camalli, M., Cascarano, G, L., Giacovazzo, C., Guagliardi, A.,

refined using the WinGX[5] software incorporating SHELXL.[6] The final anisotropic full-matrix least-squares refinement was done on F^2. The methine, methylene and aromatic protons were placed in geometrically idealized positions (C–H = 0.93 – 0.98 Å) and constrained to ride on their parent atoms with $U_{iso}(H) = 1.2\ U_{eq}(C)$. Non-hydrogen atoms were refined with anisotropic displacement parameters. The graphical illustrations were obtained using the DIAMOND[7] program with 25% probability ellipsoids for all non-hydrogen atoms.

5.3 Tetrakis(thenoyltrifluoroacetylacetonato) zirconium(IV) Monohydrate, $[Zr(tta)_4].H_2O$

5.3.1 Introduction

The crystal structure of tetrakis(thenoyltrifluoroacetylacetonatido)zirconium(IV) was first reported in 1963 by Baskin *et al*.[8] They synthesized the complex by adding a less than required alcoholic solution of thenoyltrifluoacetone to zirconium nitrate, leaving an excess of metal ion in solution. The complex that formed was precipitated by dilution of the alcoholic solution with water. The precipitate was recrystallized in benzene.

In this study tetrakis(thenoyltrifluoroacetylacetonato)zirconium(IV) monohydrate ($[Zr(tta)_4].H_2O$) was synthesized according to the method reported in Chapter 4. Colourless hexagonal crystals were obtained. The X-ray data was collected at a lower temperature in an effort to yield more accurate data. Similarities in bond lengths and bond angles were observed during the comparison to the original data collection.

The title compound crystallized in the orthorhombic space group $Pca2_1$ with four molecules in the unit cell. The numbering scheme is presented in Figure 5.1 where the hydrogen atoms have been omitted for clarity. The general crystal data of $[Zr(tta)_4].H_2O$ is tabulated in Table 5.1 while the selected bond distances and bond angles are tabulated in Table 5.2. A complete list of bond distances, bond angles, hydrogen coordinates, atomic coordinates and anisotropic coordinates are reported in Appendix.

Moliterni, A, G,G., Polidori, G., Spagna; R., *J. Appl. Cryst.*, **32**, 115, 1999.
[5] Farrugia, L.J., *J. Appl. Cryst.*, **32**, 837, 1999.
[6] Sheldrick, G.M., SHELXL97. Program for crystal structure refinement, University of Göttingen, Germany, 1997.
[7] Brandenburg, K., Putz H. *DIAMOND*, Release 3.0e, Crystal Impact GbR, Bonn, Germany, 2006.
[8] Baskin Y., Krishna N. S., *J. Inorg. Chem*, **25**, 1011-1019, 1963.

Table 5.1: Crystallographic and Refinement Details for the structure of $[Zr(tta)_4].H_2O$.

Crystal Formula	$[Zr(tta)_4].H_2O$
Empirical formula	$C_{32}\ H_{16}\ F_{12}\ O_8\ S_4\ Zr$
Formula weight ($g.mol^{-1}$)	959.78
Crystal system	Othorhombic
Space Group	$Pca2_1$
Unit cell dimensions:	
a, b, c (Å)	20.4(5), 10.7(5), 17.2(5)
α, β, γ	90.0(5), 90.0(5), 90.0(5)
Volume ($Å^3$),	3763(2)
Z	4
Density (calculated) Mg/m^3	1.694
Crystal morphology	Hexagonal
Crystal Colour	Colourless
Crystal size	0.33 × 0.22 × 0.20 mm
Absorption coefficient μ mm^{-1}	0.621
F(000)	1872
Theta range (˚)	1.898 to 28.000
Index ranges	$-26 \leq h \leq 26$ $-14 \leq k \leq 14$ $-22 \leq l \leq 22$
Reflections collected	111680
Independent Reflections	9083
R_{int}	$[R_{(int)} = 0.0807]$
Completeness to 2θ (°, %)	25.242 ,99.90
Data, restraints, parameters	9083 / 1 / 516
Goodness-of-fit on F^2	1.056
Final R indices [I>2sigma(I)]	$R_1 = 0.0918$, $wR_2 = 0.2164$
R indices (all data)	$R_1 = 0.1073$, $wR_2 = 0.2403$
Absolute structure parameter	0.15(10)
Extinction coefficient	0.012(2)
Largest diff. peak and hole $e.Å^{-3}$	7.231 and -0.801

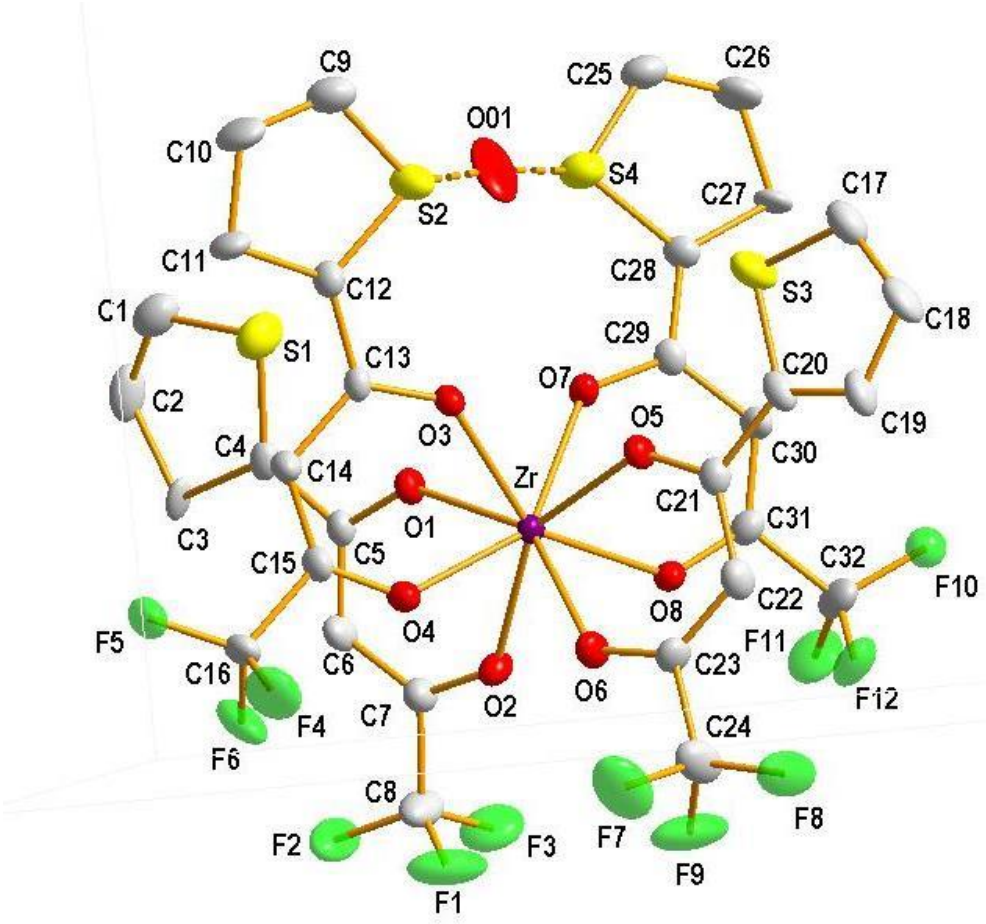

Figure 5.1: Illustration of the Molecular structure of tetrakis(thenoyltrifluoroacetylacetonato)zirconium(IV) monohydrate indicating the numbering scheme. Hydrogen atoms omitted for clarity 25% ellipsoid probability.

Table 5.2: Selected bond distances (Å) and angles (°) of $[Zr(tta)_4].H_2O$.

Bond Distances (Å)					
Zr(1)-O(1)	2.167(7)	C(4)-C(5)	1.442(14)	C(7)-C(8)	1.533(15)
Zr(1)-O(2)	2.208(7)	C(12)-C(13)	1.442(15)	C(14)-C(15)	1.330(14)
Zr(1)-O(3)	2.197(6)	C(20)-C(21)	1.454(13)	C(24)-C(23)	1.508(17)
Zr(1)-O(4)	2.156(8)	C(29)-C(28)	1.436(13)	C(32)-C(31)	1.480(14)
Zr(1)-O(5)	2.183(7)	O(1)-C(5)	1.275(11)	O(2)-C(7)	1.248(12)
Zr(1)-O(6)	2.193(7)	O(3)-C(13)	1.285(10)	O(4)-C(15)	1.268(12)
Zr(1)-O(7)	2.215(6)	O(5)-C(21)	1.261(11)	O(6)-C(23)	1.276(12)
Zr(1)-O(8)	2.157(7)	O(7)-C(29)	1.234(11)	O(8)-C(31)	1.284(12)
Bond Angle (°)					
O(1)-Zr(1)-O(2)	74.8(3)	O(4)-Zr(1)-O(3)	74.1(2)		
O(2)-C(7)-C(8)	113.2(10)	O(4)-C(15)-C(16)	112.6(9)		
C(7)-C(6)-C(5)	120.9(9)	C(15)-C(14)-C(13)	122.2(10)		
O(1)-C(5)-C(6)	122.5(9)	O(3)-C(13)-C(14)	120.5(9)		

5.3.2 Results and Discussion

The asymmetric unit consists of one [Zr(tta)$_4$] molecule and a distorted H_2O solvent molecule. The four bidentate ligands coordinated *via* eight oxygen atoms to the zirconium(IV) metal centre to form an approximate square anti-prismatic polyhedron (Figure 5.2). All the above bond distances and angle reported in Table 5.2 are similar to what was reported before for a similar complex.[8]

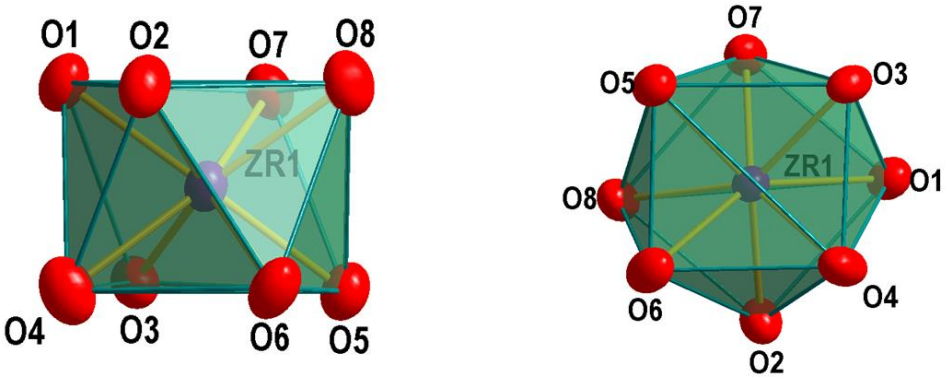

Figure 5.2: Antiprismatic polyhedron structure formed by the inner coordination sphere of [Zr(tta)$_4$].H_2O. Hydrogen atoms omitted for clarity 25% ellipsoid probability.

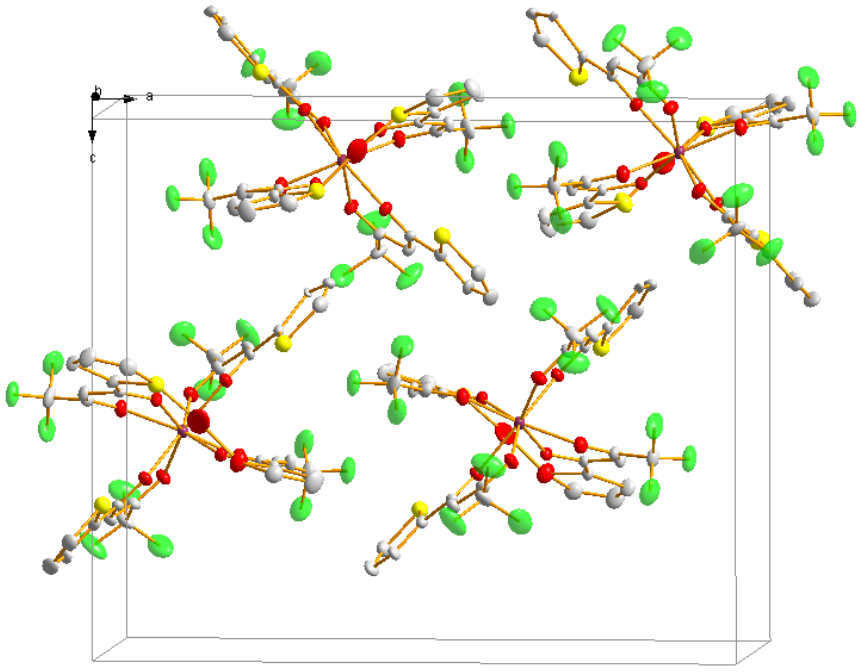

Figure 5.3: Graphical representation of molecular packing within the unit cell for the title compound viewed along the b-axis. Hydrogens omitted for clarity, 25% probability displacement ellipsoids.

Interestingly the CF_3 substituents on the ligand backbones are arranged in such a way that all four appear to be on the same side of the molecule, with the thenoyl groups arranged on the

opposite side (Figure 5.1). This can be attributed to the presence of the solvent H_2O between S_2 and S_4. It forces the rings to all be in one plane. In Figure 5.3 the molecular packing within the unit cell is displayed.

The Na(tta) ligands do not form planar chelate rings with the metal centre as is illustrated by Figure 5.4 (Table 5.3). The average dihedral angle between the planes constructed through the central Zr atom and the coordinated O atoms (O5 and O6 in Figure 5.4) and the ligand backbone atoms (O5—C21—C22—C23—O6) is 16.89˚.

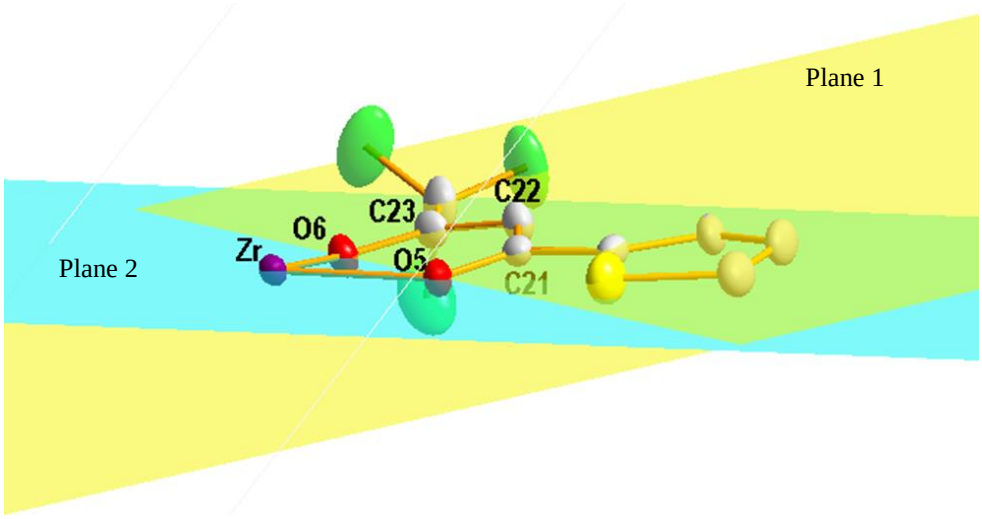

Figure 5.4: Graphical representation of plane 1 through O5—C21—C22—C23—O6 (yellow) and plane 2 through O5—Zr—O6 (turquoise) illustrating the bent nature of the coordinated ligand.

Table 5.3: Selected dihedral angles in $[Zr(tta)_4].H_2O$.

Plane 1	Plane 2	Angle between planes 1 and 2 (˚)
O(1)—Zr—O(2)	O(1)—C(5)—C(6)—C(7)—O(2)	13.4
O(3)—Zr—O(4)	O(3)—C(13)—C(14)—C(15)—O(4)	19.6
O(5)—Zr—O(6)*	O(5)—C(21)—C(22)—C(23)—O(6)	19.2
O(7)—Zr—O(8)	O(7)—C(29)—C(30)—C(31)—O(8)	15.2

***Dihedral angle between the two planes illustrated in Figure 5.3.**

The C—C bonds adjacent to the thenoyl rings are shorter (average bond length of 1.44 Å) than the C—C bonds adjacent to the CF_3 groups (average bond length: 1.53 Å). These observations are consistent with those observed bySoling *et al*.[9]

[9] Soling, H., *Acta Chemica Scandinavica*, **A30**, 163-170, 1976.

The solvent molecule H_2O is situated between S2 and S4 of the neighboring thenoyl groups (Figure 5.5). The hydrogen atoms of the water molecule could not be placed due to the strong interactions with the sulphur atoms. This solvent molecule was not present in the structure reported by Baskin *et al*.[8]

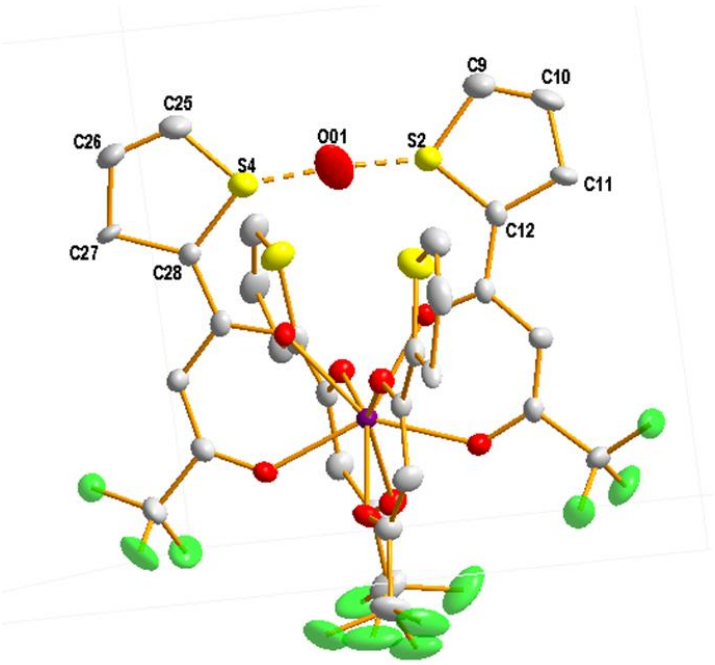

Figure 5.5: Graphical illustration of the water molecule connecting the two thenoyl (S4 and S2) rings within the unit cell of the title compound. Only a portion of the unit cell is shown, hydrogen atoms omitted for clarity, 25% probability displacement ellipsoids.

The structure has no classic hydrogen bonding interactions. However weak C—F…F and C—F…S intramolecular interactions are observed and stabilize the molecule. The interactions are listed in Table 5.4 and are illustrated in Figure 5.6 and Figure 5.7.

Table 5.4: Fluorine-fluorine and fluorine-sulphur interaction geometry (Å, °).

Donor--F…A	D—F Å	D—A Å	DFA(°)
C--F…F [(a)]	1.299	2.719	122.169(20)
C--F…S [(b)]	1.261	3.228	123.695(19)

Symmetry code: (a) x, -1 + y, z, (b) -0.5 + x, 1 – y, z

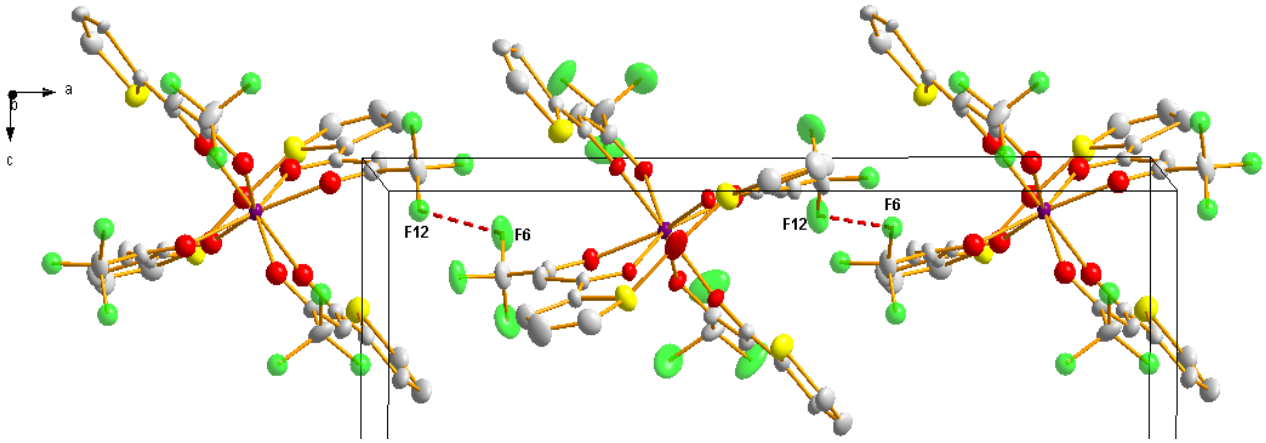

Figure 5.6: Illustration of the fluorine–fluorine interactions viewed along the b-axis. Only a portion of the unit cell is shown, hydrogen atoms omitted for clarity, 25% probability displacement ellipsoids.

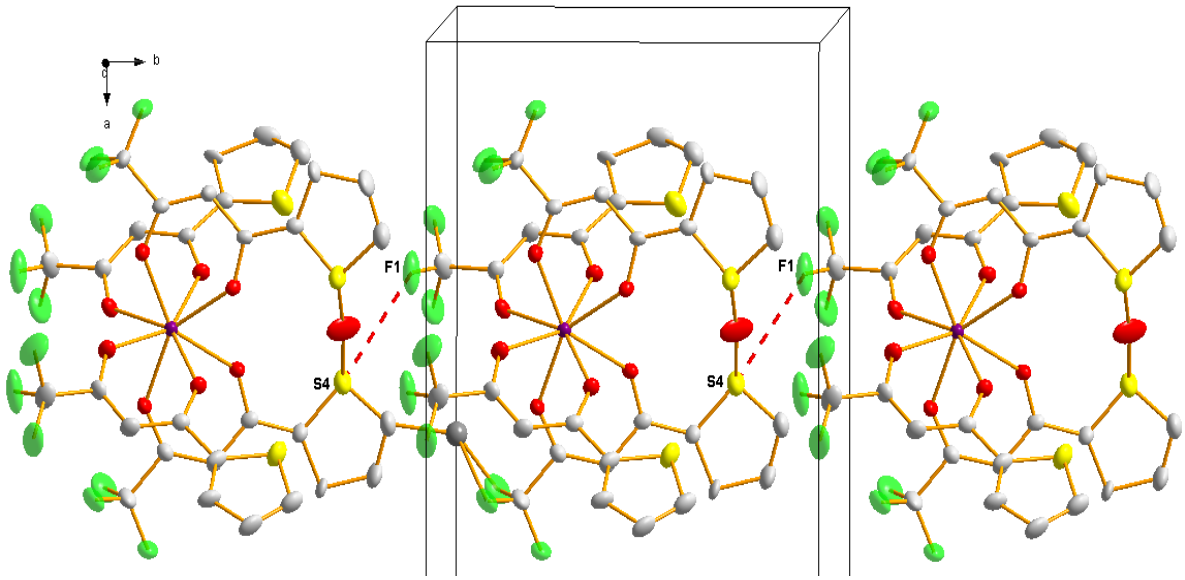

Figure 5.7: Illustration of the sulphur–fluorine interactions viewed along the c-axis. Only a portion of the unit cell is shown, hydrogen atoms omitted for clarity, 25% probability displacement ellipsoids.

Furthermore CF-π stacking is observed and is illustrated in Figure 5.8. The F5 to centroid F10 to centroid distances are reported as 3.580(10) and 3.598(10). The bond distances and angles of these interactions are listed in Table5.5.

Table 5.5: π-Stacking geometry for $[Zr(tta)_4.H_2O$ (Å, °).

Y--X--C	X…Cg (Å)	Y…Cg (°)	Y--X…Cg (°)
C(16)--F(5)…Cg(4) [(a)]	3.580(10)	130.8(8)	4.545(11)
C(32)--F(10)…Cg(2) [(b)]	3.598(10)	127.3(7)	4.565(11)

Symmetry code: (a) -1/2+x,1-y,z, (b) 1/2+x,1-y,z

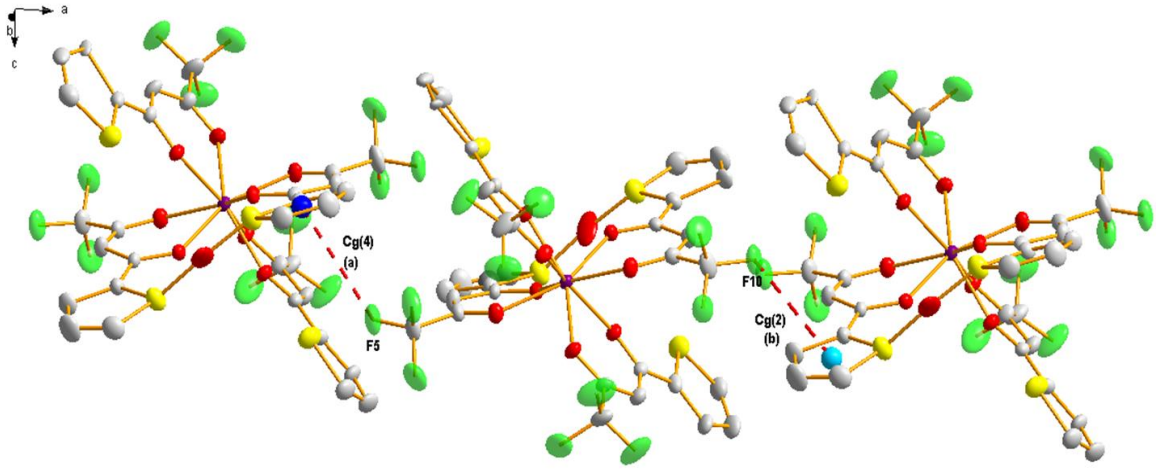

Figure 5.6: Illustration of the π-interaction between F10 and the centroid of the ring S4, C25, C26, C27, C28 and between F5 and the centroid of the C16 ring S2, C9, C10, C11, C12 when viewed along the the c-axis. Only a portion of the unit cell shown, hydrogen atoms omitted for clarity, 25% probability displacement ellipsoids.

It was important to compare the structure that was published by Baskin and the tetrakis(thenoyltrifluoroacetylacetonato)zirconium(IV) monohydrate $[Zr(tta)_4].H_2O$. The comparison of the two structures was tabulated in (Table 5.6). There were no bond distances available for the structure ZrT_4 and the structure was nos reported in the CSD. There were only basic dimensions as well as the d values. A similar structure by Steyn was used for further comparisons tabulated in (Table 5.7).

Table 5.6: Basic dimensions for tetrakis(thenoyltrifluoroacetylacetonato)zirconium(IV) $[ZrT_4]$ compared to tetrakis(thenoyltrifluoroacetylacetonato)zirconium(IV) monohydrate $[Zr_4(tta_4)].H_2O$.[8]

Cell parameters	$[ZrT_4]$	$[Zr(tta)_4]$
a	17.271	20.4(5)
b	20.422	10.7(5)
c	10.779	17.2(5)
Unit cell volume	3801.8	3763(2)
Density	1.76	1.694

Table 5.6: Geometrical data for tetrakis(1,1,1-trifluoroacetylacetonato-κ2-O,O')zirconium(IV) $[Zr(tfa)_4]$[10] toluene solvate compared to tetrakis(thenoyltrifluoroacetylacetonato)zirconium(IV) monohydrate $[Zr(tta)_4].H_2O$.

Bond	Average Bond(Å)	
Zr-O	$[Zr(tta)_4].H_2O$	$[Zr(tfa)_4]$
$Zr-O_1$	2.08(7)	2.16(1)
$Zr-O_2$	2.15(6)	2.19(2)
$Zr-O_3$	2.15(8)	2.16(1)
$Zr-O_4$	2.19(7)	2.20(2)
Average Plane Angles (°)		
Plane1 and Plane2	19.84	19.56
Plane1 and Plane 2	20.23	13.49
Average Bite Angles (°)		
O(1)—Zr—O(2)	75.27	74.14
O(7)—Zr—O(8)	75.41	74.80

Compared to the structure published by Steyn[10] with a similar ligand, the bond distances of the oxygen atoms that form the inner coordination sphere on the side of the CF_3 groups are almost the same. The same similarity is seen between the bond distances of the thenoyl group. There are however differences observed between the dihedral angles between the plane a and how the ligand twists. The angles between the planes reported for $[Zr(tfa)_4]$ are bigger than those observed for $[Zr(tta)_4].H_2O$ The bite angles that were reported for $[Zr(tfa)_4]$ were almost the same as reported for $[Zr(tta)_4].H_2O$.

5.3.3 Conclusion

The crystal structure of tetrakis(thenoyltrifluoroacetylacetonato)zirconium(IV) monohydrate $[Zr(tta).H_2O]$ reported in this chapter is a polymorph of the structure reported by Baskin *et al.*[8] The only difference between the two structures is the solvent H_2O molecule that connects the thenoyl rings through S4 and S2.

[10] Steyn M.,*MSc Diddertation: Speciation And Interconversion Mechanism Of Mixed Halo And O,O- And O,NBidentate Ligand Complexes Of Zirconium.* University of the Free State, UFS 2009.

6 Preliminary Kinetic Study of the Formation of [Zr(tta)$_4$] and [Hf(tta)$_4$] Complexes

6.1 Introduction

This chapter will focus on the preliminary kinetic investigation of the formation of tetrakis(thenoyltrifluoroacetylacetonato)zirconium(IV) that is discussed in Chapter 5 as well as the formation of tetrakis(thenoyltrifluoroacetylacetonato)hafnium(IV). Fluorine-19 nuclear magnetic resonance spectroscopy (^{19}F-NMR) was employed for these experiments and the spectra are obtained in a similar way as ^{1}H-NMR. The advantage of ^{19}F-NMR over ^{1}H-NMR is that the overlapping of signals can be overcome due to the fact that fluorine has 9 electrons compared to hydrogen that possesses just 1 electron. More importantly, since there are usually fewer fluorine nuclei in the target molecule, it often simplifies the spectrum. For biological studies, ^{19}F-NMR kinetics has also gained popularity since it provides detailed information about the coordination of the ligand to the metal center and detailed structural information without overlapping hindrances. For these reasons ^{19}F-NMR was chosen to be the primary tool for the preliminary kinetic investigation undertaken in this study since the ligand, Thenoyltrifluoroacetone (ttaH), contain a CF_3 group that could easily be identified and followed by ^{19}F-NMR.

This preliminary kinetic investigation will include the characterization of the ligand, formation kinetics for the zirconium and hafnium complexes and competition studies *via* NMR, the results and the discussion. Scheme 6.1 illustrates the setup of these experiments.

Step 1. Recording of the external reference probe's (KF) NMR spectrum.

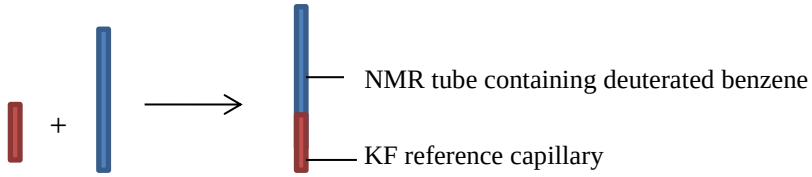

Step 2. Addition of the ligand to the contents of step 1 and recording the spectrum thereof.

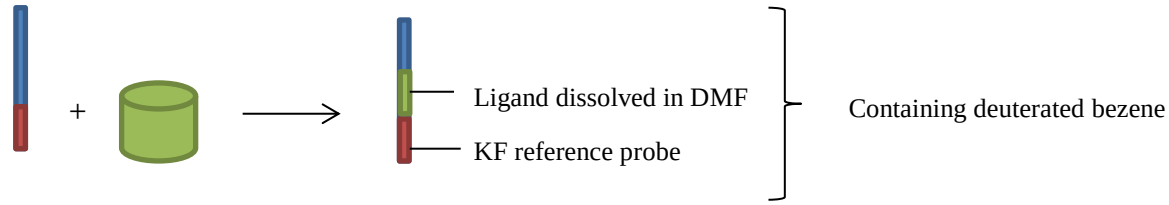

Step 3. Addition of the dissolved metal salt to the contents of step 2 and initiating the kinetic run using the timetime interval indicated in Par. 6.2.

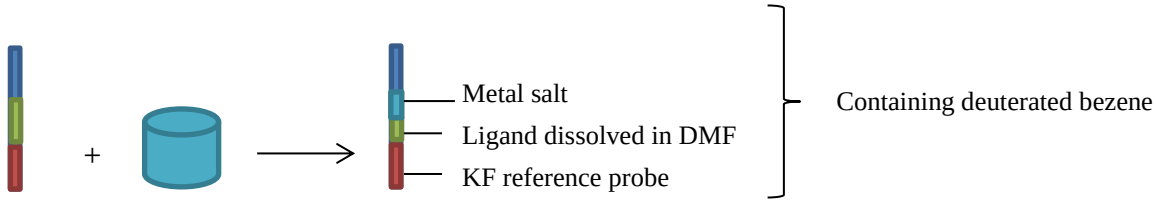

Scheme 6.1: Schematic representation of the experimental order and setup of the kinetic runs.

6.2 Experimental

The reagents and chemicals that were utilized during this investigation were of analytical grade. Zirconium tetrachloride [$ZrCl_4$], hafnium tetrachloride [$HfCl_4$], sodium hydroxide, NaOH and thenoyltrifluoroacetylacetone (ttaH) were used as received from Sigma Aldrich. Kinetic measurements were perfomed by locking on the deuterated benzene and using the potassium fluoride (peak -119.0 ppm) as a reference peak on both the Bruker 300 MHz and the Bruker 600 MHz nuclear magnetic resonance spectrometers.

To reduce the formation of HCl during these experiments, the ttaH was neutralized by the addition of one equivalent NaOH, to ensure that Na(tta), thus sodium thenoyltrifluoroacetylacetonate, is the entering ligand in all kinetic runs.

The samples were prepared as follows:

- The metal salt was dissolved in DMF and stirred until a homogeneous colourless mixture was obtained,

- NaOH and ttaH were dissolved separately in DMF (NaOH does not readily dissolve in DMF)
- The ttaH solution was slowly added to the NaOH solution and the mixture was stirred at 50 ˚C until the NaOH was dissolved.

Each ^{19}F-NMR kinetic experiment was performed as follows:

- A NMR tube containing all the reagents, the deuterated benzene, ligand, metal and the reference probe (external reference probe containing KF dissolved in water) was inserted into the NMR magnet and the magnet was shimmed;
- After shimming, the external reference probe was inserted in a NMR tube containing only deuterated benzene (600 µl) and a reference spectrum was recorded,
- A second spectrum containing the reference probe and (deprotonated thenoyltrifluoroacetone) Na(tta) (600 µl in DMF) was recorded (total volume 1200 µl). This spectrum is then an indication of the free ligand;
- Kinetic runs were initiated by adding the respective metal salt (600 µl in DMF) to the ligand solution, bringing the total volume to 1800 µl;
- The kinetic runs consisted of 30 individual runs that spanned over a 9 h time period.

All the kinetic data was fitted to the following first-order equation:

$$h_\infty = h_\infty - (h_\infty - h_\mathrm{o})e^{-k_{obs}t} \qquad \textbf{…eqn 6.1}$$

This total time period for every set of spectra in the figures which follow was divided into four segments:

- The first segment consisted of 15 spectra recorded back-to-back with each recording lasting for 303 s;
- The second segment consisted of five spectra with 603 s intervals between each recording;
- The third segment consisted of five spectra with 1803 s between each recording;
- The final segment consisted of five spectra with 3303 s intervals between each recording.

Several experiments employing different ratios of metal : ligand were undertaken. Table 6.1 a and b lists the different experiments that were performed.

The basis of conducting these experiments in this manner was with the foresight that the ligand would react with the metal center to finally form a higher coordinated, i.e. tetrakis complex as

seen from the solid state crystallographic evaluations (see Chapter 5). Therefore experiments have been designed to follow the stepwise formation of the complexes.

Competition experiments wherein mixtures of zirconium(IV) and hafnium(IV) could be evaluated, were also conducted.

Table 6.1a: List of masses weighed and concentrations used for the preliminary kinetic studies of the formation of tetrakis(thenoyltrifluoroacetylacetonato)zirconium(IV) and tetrakis(thenoyltrifluoroacetylacetonato)hafnium(IV). (b) for the competition studies of ([$ZrCl_4$] + [$HfCl_4$]) *vs* Na(tta).

Experiment (a)		Mass Weighed			Concentrations		
Entry No	NMR	$ZrCl_4$ (mg)	$HfCl_4$ (mg)	Na(tta) (mg)	[Metal] (M)	[Na(tta)] (M)	[Metal] : [Na(tta)]
1	^{19}F	49.8	-	192	0.118	0.481	1 : 4
2	^{19}F	50.1	-	238	0.119	0.596	1 : 5
3	^{1}H	40.0	-	152	0.095	0.382	1 : 4
4	^{19}F	-	50.1	139	0.0869	0.347	1 : 4
5	^{19}F	-	49.3	174	0.0855	0.435	1 : 5

Experiment (b)		Mass Weighed			Concentrations M		
Entry No	NMR	$ZrCl_4$ (mg)	$HfCl_4$ (mg)	Na(tta) (mg)	[$ZrCl_4$]:[$HfCl_4$] [Metal] (M)	[Na(tta)] M	[Metal]:[Na(tta)]
1	^{19}F	18.5	25.0	70	0.0441 : 0.0434	0.175	0.5: 0.5 : 2
2	^{19}F	18.2	25.0	140	0.0433 : 0.0434	0.350	0.5: 0.5 : 4
3	^{19}F	18.1	25.0	156	0.0431 : 0.0434	0.390	0.5: 0.5 : 4.5
4	^{19}F	18.4	24.8	174	0.0438 : 0.0431	0.435	0.5: 0.5 : 5

*The total volume of the sample for each of the chemical kinetic experiments was 1800 microliters: 600 µl deuterated benzene, 600 µl DMF was used to dissolve the metal chloride and a further 600 µl DMF was used to dissolve the ligand.

6.3 Characterization Studies

By identifying the different coordination numbers as specified above in the various experiments the starting material has been characterized systematically and is reported and illustrated below.

6.3.1 Characterization of ttaH (thenoyltrifluoroacetylacetone), Na(tta) (sodium thenoyltrifluoroacetylacetonate), [Zr(tta)$_4$] and [Hf(tta)$_4$]

The following compounds, ttaH, Na(tta), [Zr(tta)$_4$] and [Hf(tta)$_4$], as synthesized according to the procedure reported in Chapter 4, were characterized by ^{19}F and ^{1}H-NMR. Figure 6.1a and Figure 6.1b illustrate the ^{1}H-NMR spectra of these starting materials and will be used to characterize and serve as reference for the kinetic experiments throughout the chapter.

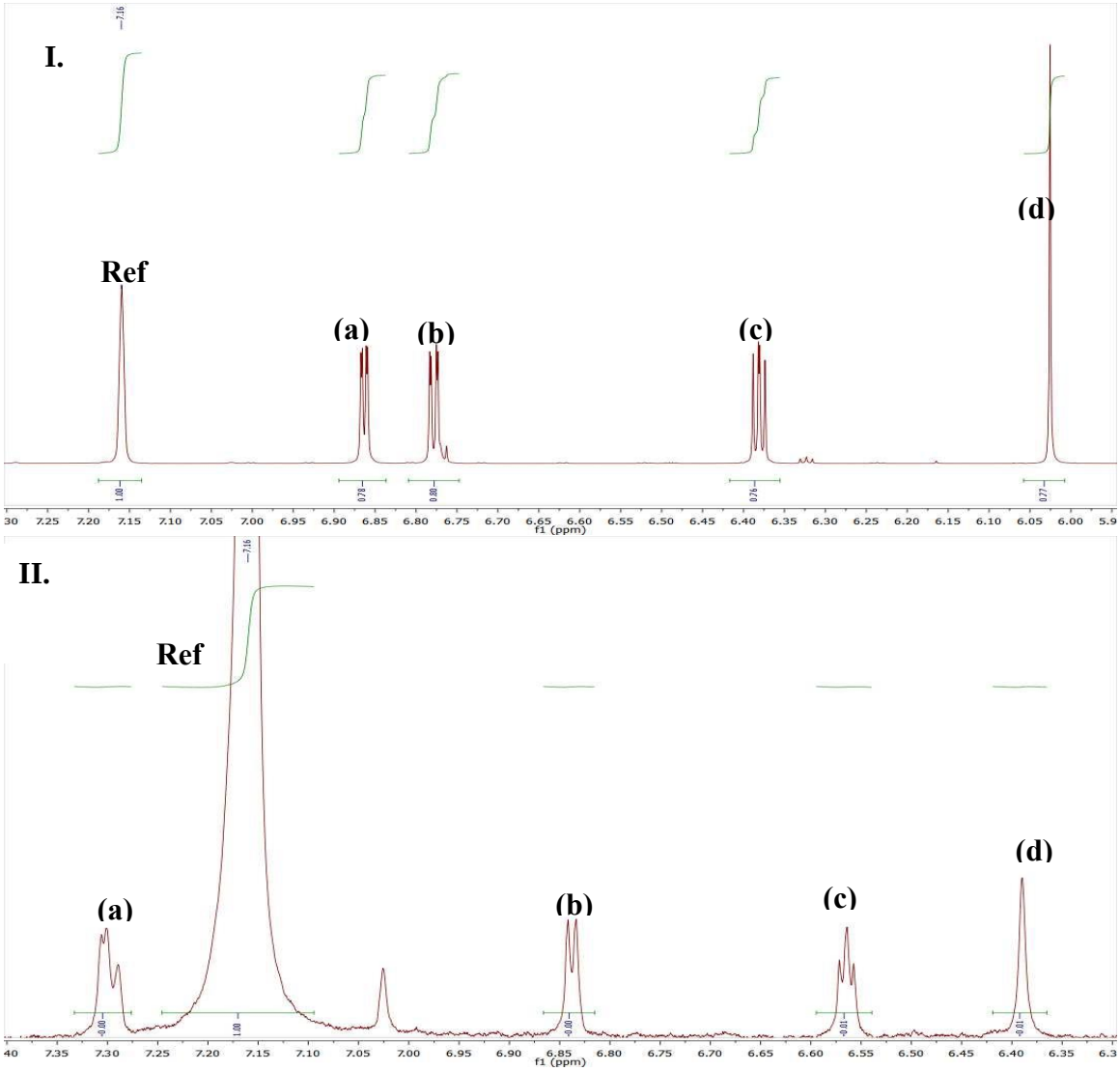

Figure 6.1a: ^{1}H-NMR spectra of [ttaH] = 0.047 M (I) and Na(tta) = 0.046 M (II). (a)-(c) are the thenoyl proton peaks, (d) the methyne proton peak and the benzene reference peak at 7.16 ppm at 20.0°C.

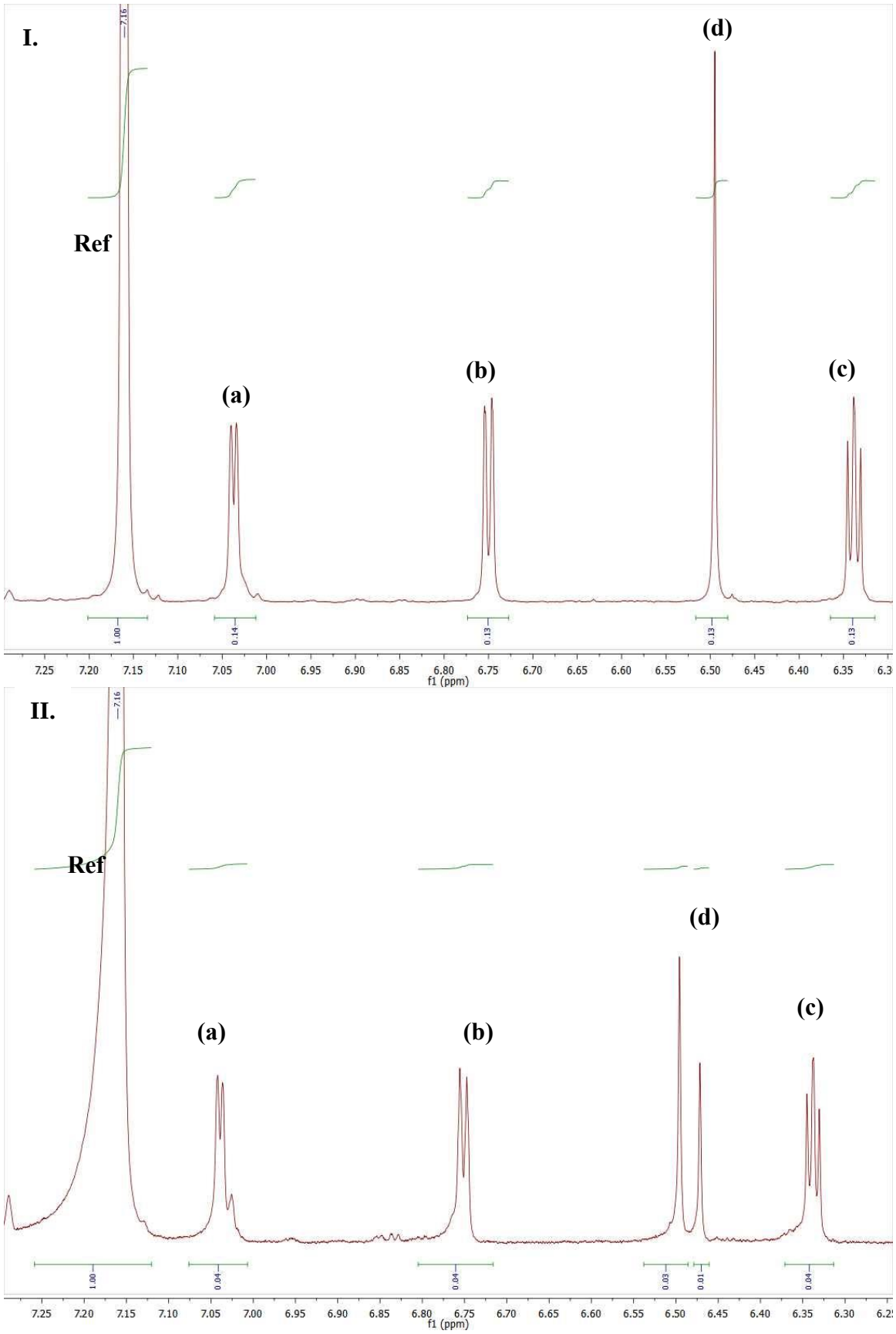

Figure 6.1b: ^{1}H-NMR spectra of [Zr(tta)$_4$] = 0.178 M (I) and [Hf(tta)$_4$] = 0.129 M (II). (a)-(c) are the thenoyl proton peaks, (d) the methyne proton peak and the benzene reference peak at 7.16 ppm at 20.0°C.

6.3.2 Characterization of [Zr(tta)$_4$] and [Hf(tta)$_4$] - benchtop synthesized complexes

Figure 6.2 a illustrates the ^{19}F-NMR spectra of ttaH (I) and Na(tta) (II). The ^{19}F-NMR spectra in Figure 6.2b illustrates the characterization spectra of [Zr(tta)$_4$] and [Hf(tta)$_4$] that were prepared on benchtop in the procedure reported in Chapter 4, for referencing purposes of the various kinetic investigations performed. Although the kinetic runs, reported later on, assumes the formation of the tetrakis complexes, it refers to the second slower reaction. The first, fast reactions represent most probably lower coordinated Zr(IV) and Hf(IV) species, although not characterised formally. The peaks and chemical shifts reported in Table 6.2 represent the final, tetrakis complexes as characterised by XRD.

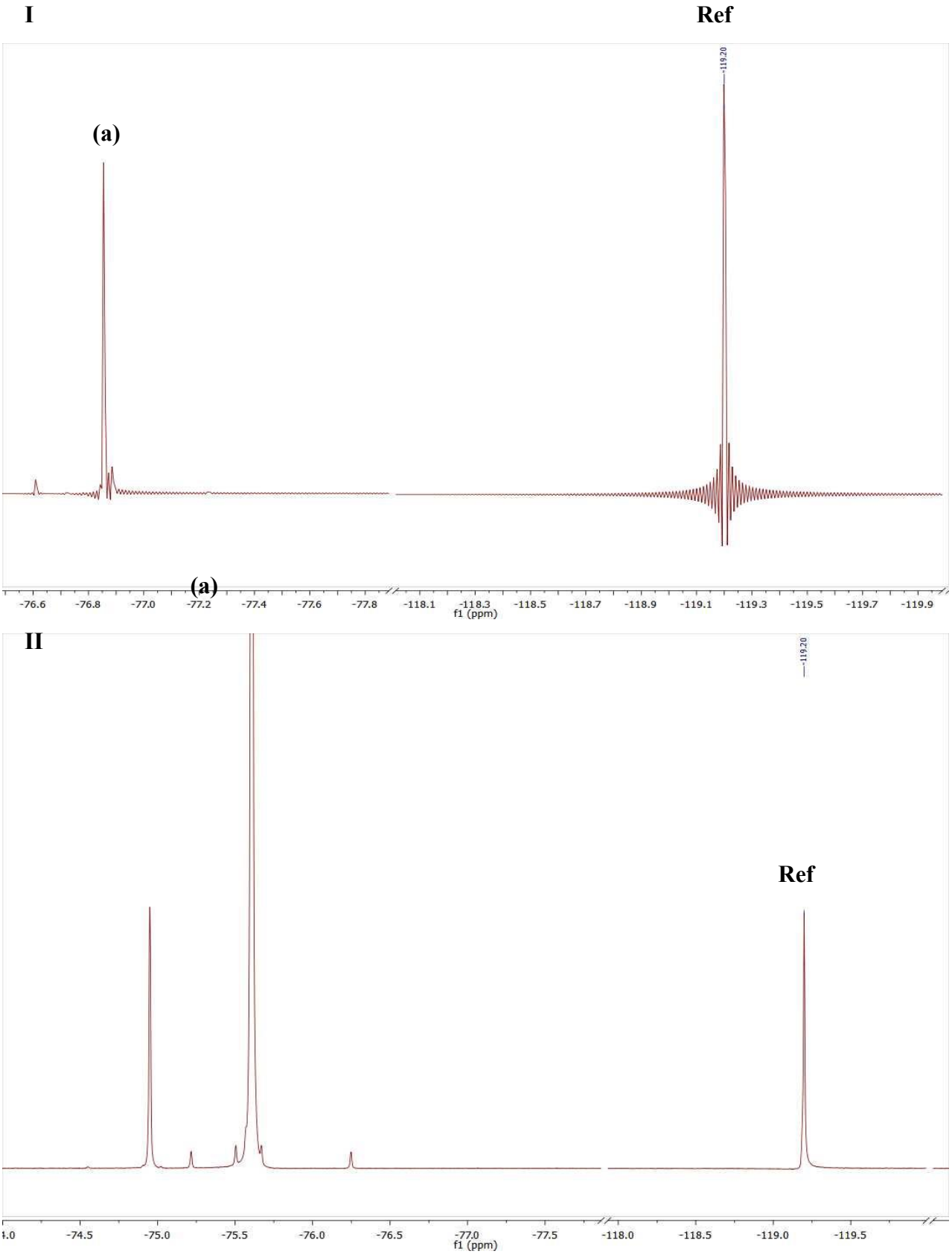

Figure 6.2a: ^{19}F-NMR spectra of [ttaH] = 0.047 M (I) and [Na(tta)] = 0.046 M (II). The reference peak (KF) is observed at -119 ppm at 20.0 ˚C.

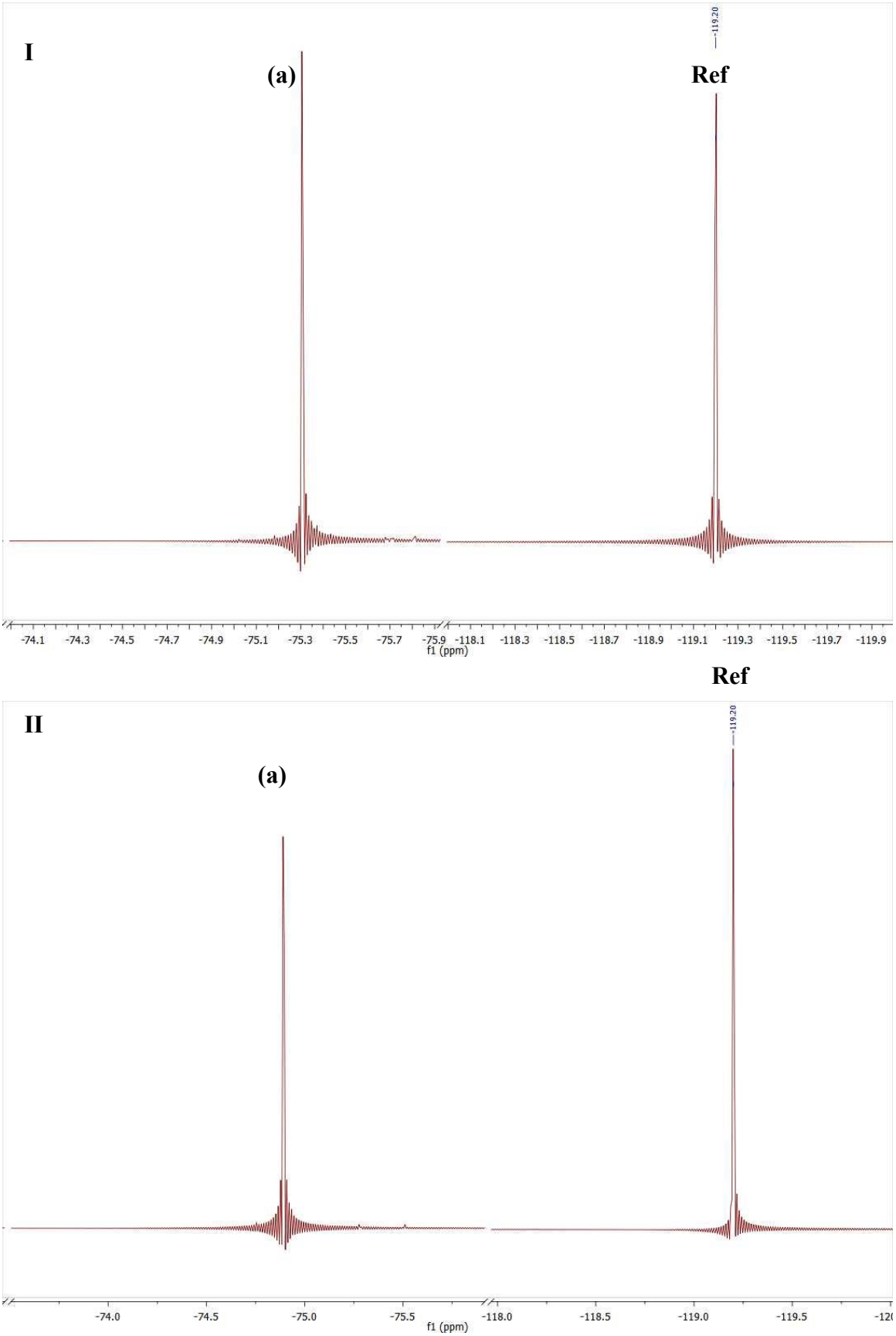

Figure 6.2b: ^{19}F-NMR spectra of [Zr(tta)$_4$] = 0.178 M (I) and [Hf(tta)$_4$] = 0.129 M(II) where (a) is the [Zr(tta)$_4$] and [Hf(tta)$_4$] peak respectively and the reference peak (KF) is observed at -119 ppm at 20.0˚C.

6.3.3 Summary of the chemical shifts of all the characterized compounds

The chemical shifts and multiplicity from Figure 6.1a, b and 6.2 a, b have been summarized in Table 6.2 below.

Table 6.2: Summary of the chemical shifts of the characterized compounds.

Compound	^{1}H (ppm)	^{19}F (ppm)
ttaH	6.86 (dd), 6.77 (dd), 6.38 (t)	-76.86 (s)
Na(tta)	7.63 (s), 7.04, 6.76 (dd), 6.50 (s), 6.47 (s), 6.34 (t)	-75.63 (s)
[Hf(tta)$_4$]	7.04 (d), 6.74 (d), 6.49 (s), 6.34 (t)	-74.89 (s)
[Zr(tta)$_4$]	7.31 (d), 7.02 (s), 6.84 (d), 6.56 (t),6.39 (s)	-75.30 (s)

6.4 Preliminary Kinetic Study of the formation of [Zr(tta)$_4$] and [Hf(tta)$_4$]

The ligand ttaH has been employed as an effective chelating reagent for many metallic systems. This fluorinated β-diketone along with other similar ligands has been reported to have applications in supercritical fluid extraction of transition metals, lanthanides and actinides.[1] They have also been reported to provide 'clean technology' for metal extraction. Clean technology is a major advantage since most separation methods discussed in Chapter 2 were reported to be either expensive or producing harmful side products to the environment. Therefore it was favorable for this study to evaluate Na(tta) as ligand in an attempt to develop a separation method for zirconium and hafnium. The following subsections will focus on the NMR reaction kinetics of tta$^-$ as a chelating agent for zirconium(IV) and hafnium(IV) and competition studies of the combined metal's affinity for tta$^-$. In the following subsections, various NMR spectra plots and kinetic plots (Micromath Scientist), illustrating the decrease of tta$^-$ and formation of the zirconium or hafnium complex with the ligand are illustrated. Table 6.2 contains the summary of the chemical shifts and spin multiplicities of the NMR spectra illustrated throughout the various subsections.

Individual investigations based on how the respective metal would behave in the presence of tta$^-$ were performed and are discussed in the following subsections. These initial kinetic runs of the

[1] Jone, R. D. G., *Acta Cryst*., **B32,** 1224-1227, 1976.

individual metals were performed at varying metal to ligand ratios (1:4 and 1:5). These were performed in efforts to get an indication of the intimate relative rates of the reactions and thus the reaction mechanism of the coordination of the ligand to the respective metals. Keeping in mind that only tetra-coordinated metal-bidentate ligand complexes were observed in solid state, several experiments utilizing varying metal : ligand ratios were designed to see if intermediate species could be identified. The purpose was to assist in the identification of possible subtle differences in the behaviour of Zr(IV) opposed to Hf(IV). This was done with the foresight of performing competition studies between the zirconium(IV) and hafnium(IV).

6.4.1 Preliminary Kinetic Study of the formation of $[Zr(tta)_4]$

The formation reaction of $[Zr(tta)_4]$ was followed by a variety of ^{19}F-NMR and ^{1}H-NMR experiments. Two reactions namely a fast first reaction followed by a slower, second reaction were observed. The NMR stacked plot of each reaction is accompanied by kinetic plots of the peak integration values *versus* time.

The succeeding subsections will follow the chronological order described by the entries tabulated in Table 6.1a.

6.4.1.1. ^{19}F-NMR Kinetic Investigation of the formation of $[Zr(tta)_4]$ ([Zr]:[Natta]=1:4, first fast reaction)

The formation reaction of $[Zr(tta)_4]$ was monitored by ^{19}F-NMR (repetitive scans illustrated in plot Figure 6.3). The figure is a graphical representation of the first rapid reaction that took place in the 1 : 4 reaction. A typical kinetic data plot was fitted to eqn 6.1 as illustrated in Figure 6.4 (I) ligand consumption and (II) product formation in order to determine the observed rate constant, k_{obs}.

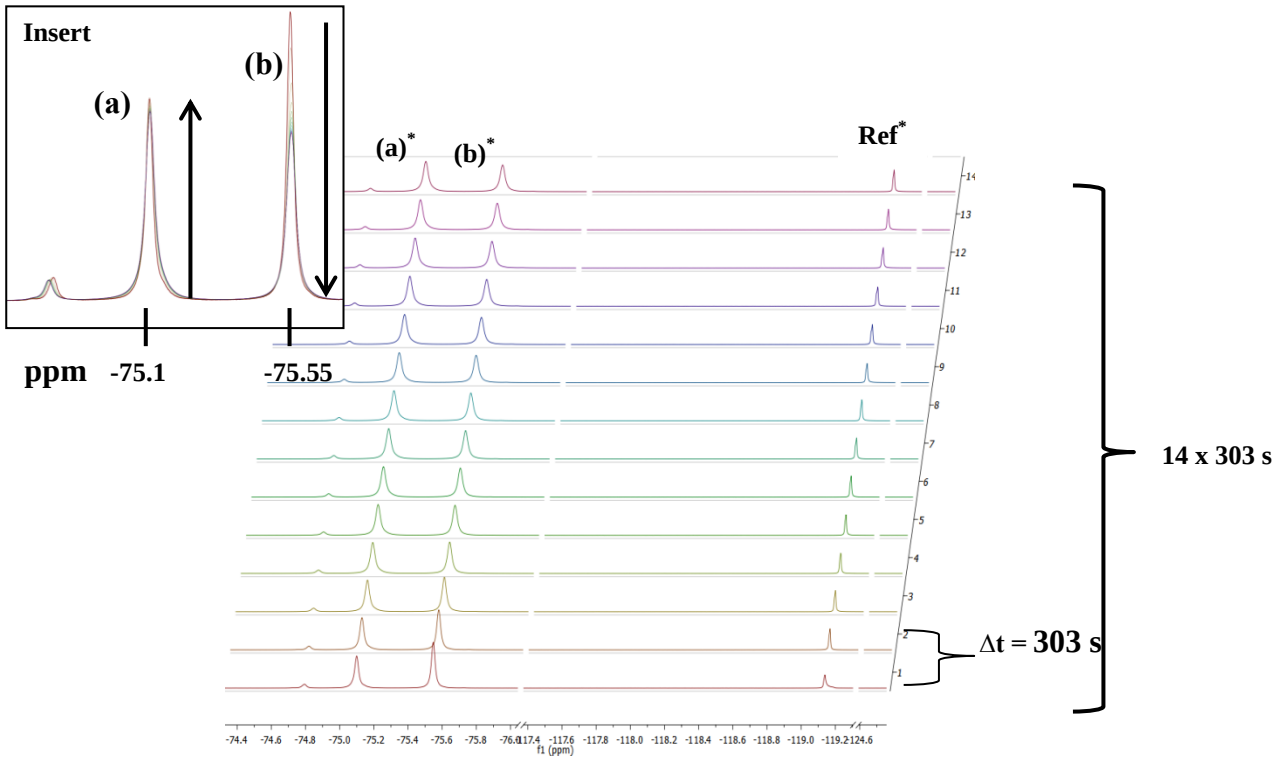

Figure 6.3: Observed stacked ^{19}F-NMR spectra illustrating the progression of the first fast reaction, Entry No. 1 (Table 6.1 (a)) [Zr] : [Na(tta)] = 1 : 4. [Zr(tta)$_4$] formation at -75.1 ppm, Na(tta) consumption at -75.5 ppm. [ZrCl$_4$] = 0.118 M, [Na(tta)] = 0.481 M, Temp = 20.0 ˚C, ligand and metal dissolved in DMF and spectra collected in deuterated benzene (C$_6$D$_6$), total time of the first fast reaction = 4242 s, Δt indicates the time between successive spectra.
Insert: Superimposed ^{19}F-NMR spectra illustrating (a) formation of product [Zr(tta)$_4$] and (b) disappearance of ligand (Na(tta)).
***(a) Product formation. *(b) Ligand disappearance. *Ref = KF reference probe signal.**

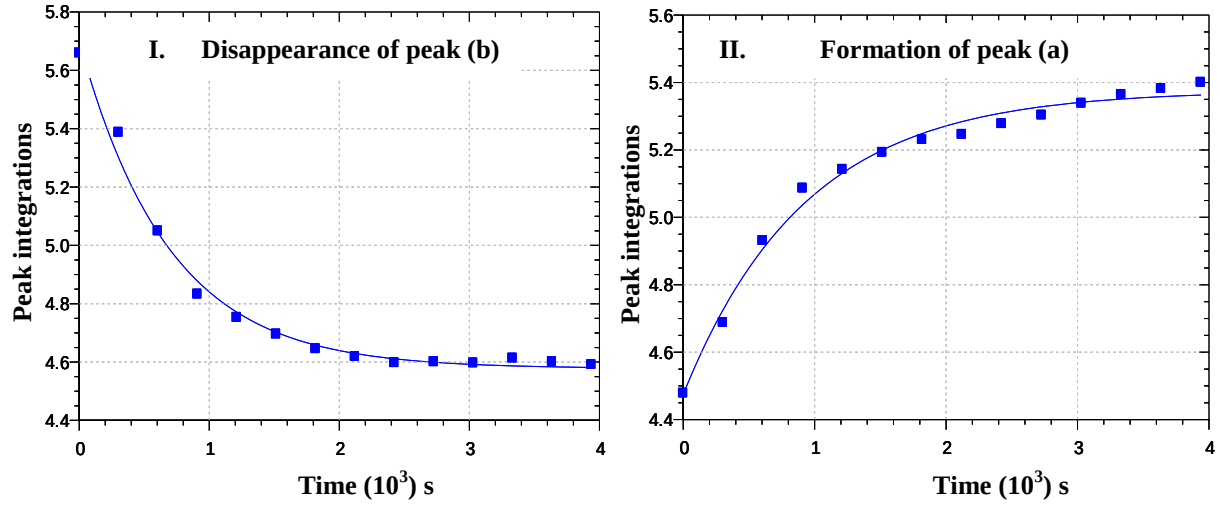

Figure 6.4: (I) ^{19}F-NMR peak integration *vs* time data for ligand consumption of the first fast reaction. [ZrCl$_4$] = 0.118 M, [Na(tta)] = 0.481 M k_{obs}=1.08(9) x 10^{-3} s^{-1}. (II) ^{19}F-NMR peak intensity *vs* time data for the product formation [Zr(tta)$_4$] of the first fast reaction, k_{obs} = 1.50(9) x 10^{-3} s^{-1}, ligand and metal salt dissolved in DMF and spectra collected in deuterated benzene (C$_6$D$_6$) at 20.0 ºC. Total time represented on Micromath Scientist plot is of the combined first fast reaction and the second slow reaction.

6.4.1.2 ^{19}F-NMR Kinetic Investigation of the formation of [Zr(tta)$_4$] ([Zr]:[Na(tta)] = 1:4, second slow reaction)

The formation reaction of [Zr(tta)$_4$] was monitored by ^{19}F-NMR (repetitive scans illustrated in Figure 6.5). The figure is a graphical representation of the second slow reaction that took place in the (metal : ligand) 1 : 4 ratio reaction. A typical kinetic data plot was fitted to eqn 6.1 as illustrated in Figure 6.6 for ligand consumption (I) and product formation (II) in order to determine the observed rate constant, k_{obs}.

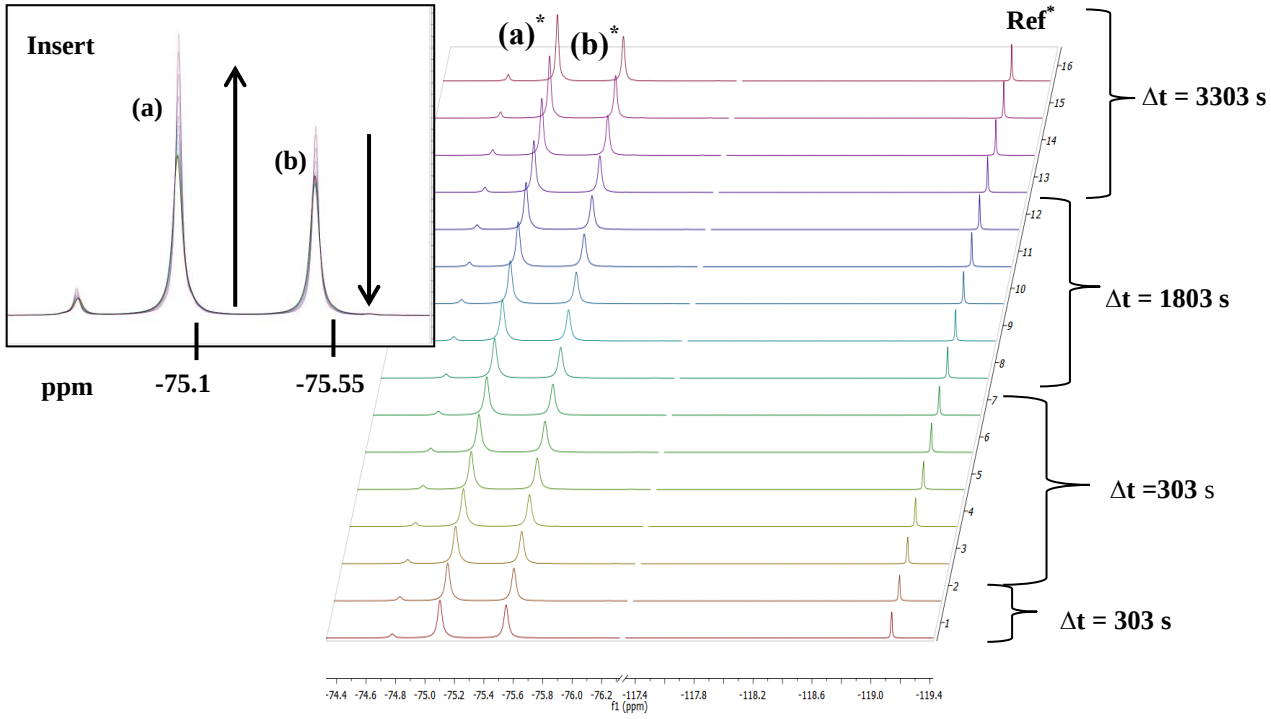

Figure 6.5: Observed stacked ^{19}F-NMR spectra illustrating the progression of the second slow reaction, Entry No. 1 (Table 6.1 (a)) [Zr] : [Na(tta)] = 1 : 4, [Zr(tta)$_4$] formation at -75.1 ppm, Na(tta) consumption at -75.5 ppm. [ZrCl$_4$] = 0.118 M, [Na(tta)] = 0.481 M, Temp = 20.0 ˚C, ligand and metal dissolved in DMF and spectra collected in deuterated benzene (C_6D_6), total time of the second slow reaction = 24606 s, Δt indicates the time between successive spectra.
Insert: Superimposed ^{19}F-NMR spectra illustrating (a) formation of product [Zr(tta)$_4$] and (b) disappearance of ligand (Na(tta)).
***(a) Product formation. *(b) Ligand disappearance. *Ref = KF reference probe signal.**

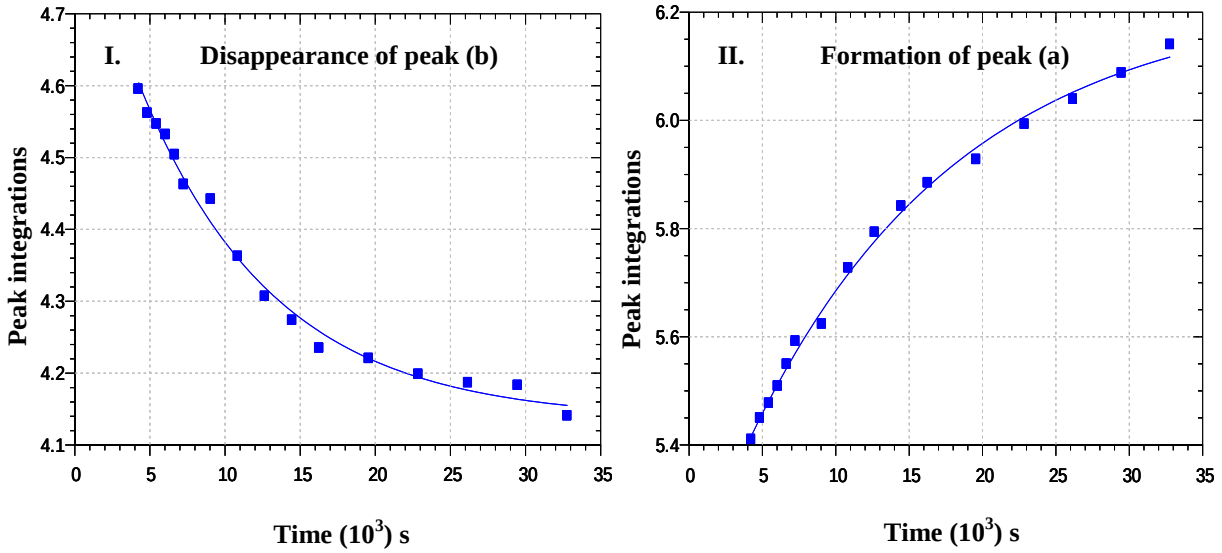

Figure 6.6: (I) ^{19}F-NMR peak integration *vs* time data for ligand consumption of the second slow reaction, [$ZrCl_4$] = 0.118 M, [Na(tta)] = 0.481 M, k_{obs}=1.90(6) x 10^{-4} s^{-1}. (II) ^{19}F-NMR peak intensity *vs* time data for product formation [$Zr(tta)_4$] of the second slow reaction, k_{obs} = 2.94(6) x 10^{-4} s^{-1}, ligand and metal salt dissolved in DMF and spectra collected in deuterated benzene (C_6D_6) at 20.0 °C. Total time represented on Micromath Scientist plot is of the combined first fast reaction and the second slow reaction.

Figure 6.7 shows a plot of the combined reactions, the first fast reaction graph (I) product formation (blue plot), ligand consumption (red plot) and the second slow reaction graph (II) product formation (red plot) ligand consumption (blue plot) can also be constructed on the peak integrations *vs* time. The plots for both the fast and slow reactions are shown. As indicated above, the second slow reaction is assumed to the tetrakis complex, while the first fast reaction represents a lower coordinated complex.

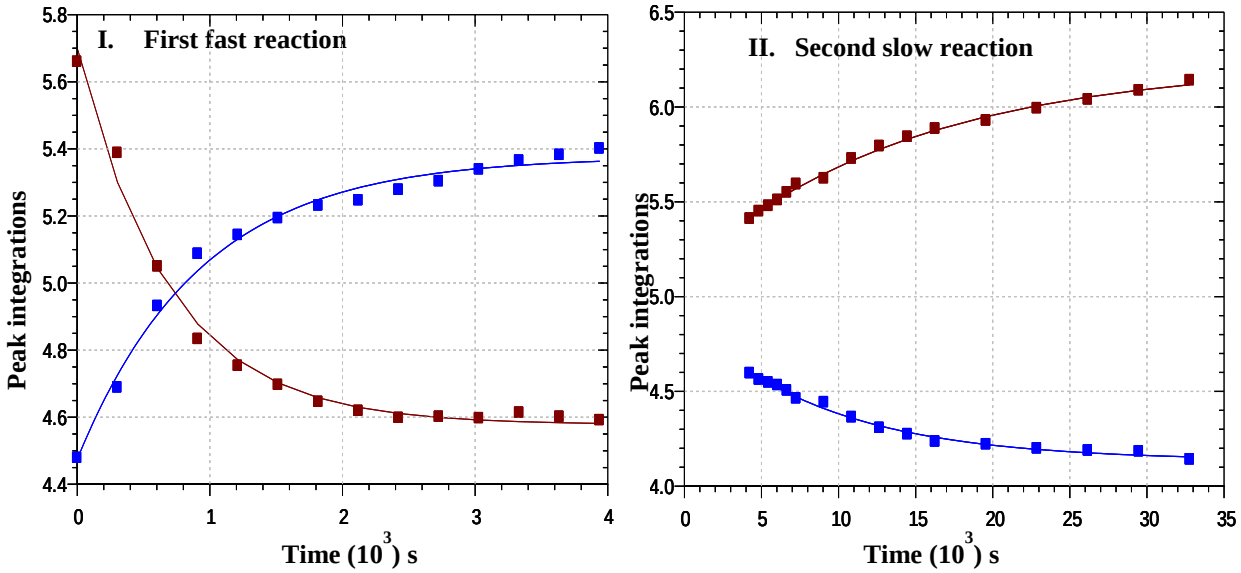

Figure 6.7: Micromath Scientist plots of combined reactions formation of complex and consumption of ligand, I (first fast reaction) and II (second slow reaction), [Zr]:[Na(tta)] = 1:4; Entry 1, Table 6.1(a)

6.4.1.3 ^{19}F-NMR Kinetic Investigation of the formation [Zr(tta)$_4$] ([Zr]:[Na(tta)] = 1 : 5, first fast reaction)

The formation reaction of [Zr(tta)$_4$] was followed by ^{19}F-NMR (repetitive scans illustrated in the stacked plot in Figure 6.8). This figure is a graphical representation of the first rapid reaction that took place in the 1 : 5 ratio reaction. A typical kinetic data plot was fitted to eqn 6.1 as illustrated by Figure 6.9 for ligand consumption (I) and product formation (II) in order to determine the observed rate constant, k_{obs}.

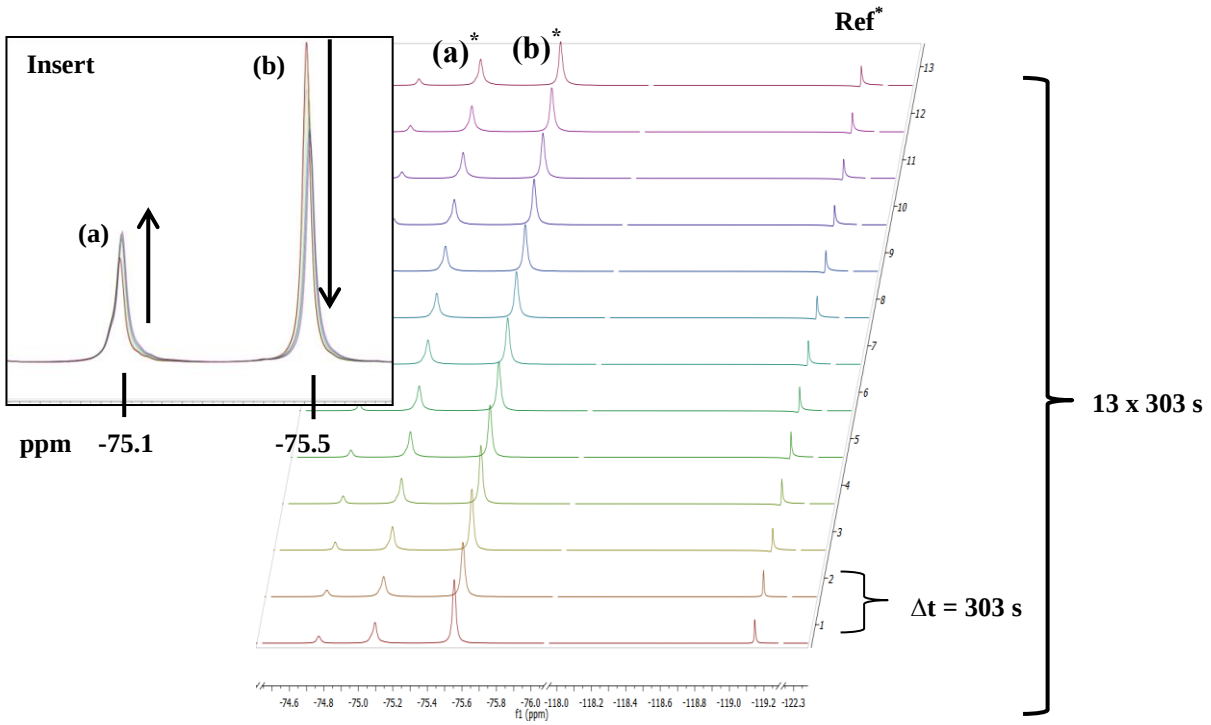

Figure 6.8: Observed stacked ^{19}F-NMR spectra illustrating the progression of the first fast reaction, Entry 2 Table 6.1(a) [Zr] : [Na(tta)] = 1 : 5. [Zr(tta)$_4$] formation at -75.1 ppm, Na(tta) consumption at -75.5 ppm. [ZrCl$_4$]= 0.119 M, [Na(tta)] = 0.596 M, Temp = 20.0 ˚C, ligand and metal dissolved in DMF and spectra collected in deuterated benzene (C_6D_6), total time of the first fast reaction = 3939 s, Δt indicates the time between successive spectra.Insert: Superimposed ^{19}F-NMR spectra illustrating (a) formation of product [Zr(tta)$_4$] and (b) disappearance of ligand (Na(tta)).
***(a) Product formation. *(b) Ligand disappearance. *Ref = KF reference probe signal.**

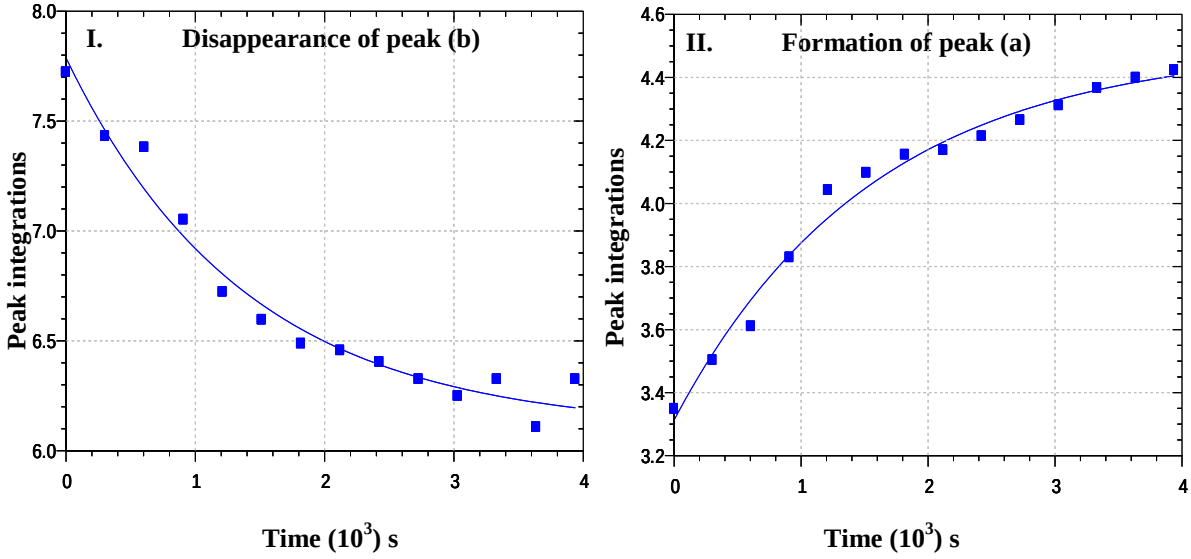

Figure 6.9:(I) ^{19}F-NMR peak integration *vs* time data for ligand consumption of the first fast reaction, [$ZrCl_4$]= 0.119 M, [Na(tta)] = 0.596 M, k_{obs}= 7.196(6) x 10^{-4} s^{-1}. (II) ^{19}F-NMR peak intensity *vs* time data for the product formation [$Zr(tta)_4$] of the first fast reaction k_{obs} = 6.41(6) x 10^{-4} s^{-1}, ligand and metal dissolved in DMF and spectra collected in deuterated benzene (C_6D_6) at 20.0 ºC. The total time for the fast and slow reaction represented on the Micromath Scientist plots = 28848 s. Total time represented on micromath scientist plot is of the combined first fast reaction and the second slow reaction.

6.4.1.4 ^{19}F-NMR Kinetic Investigation of the formation of [$Zr(tta)_4$] ([Zr]:[Na(tta)] = 1 : 5, second slow reaction)

The formation reaction of [$Zr(tta)_4$] was followed by ^{19}F-NMR (repetitive scans illustrated in the stacked plot in Figure 6.10). This figure is a graphical representation of the second slow reaction that took place in the 1 : 5 ratio reaction. A typical kinetic data plot was fitted to eqn 6.1 (illustrated by Figure 6.11) for ligand consumption (I) and product formation (II) in order to determine the observed rate constant, k_{obs}.

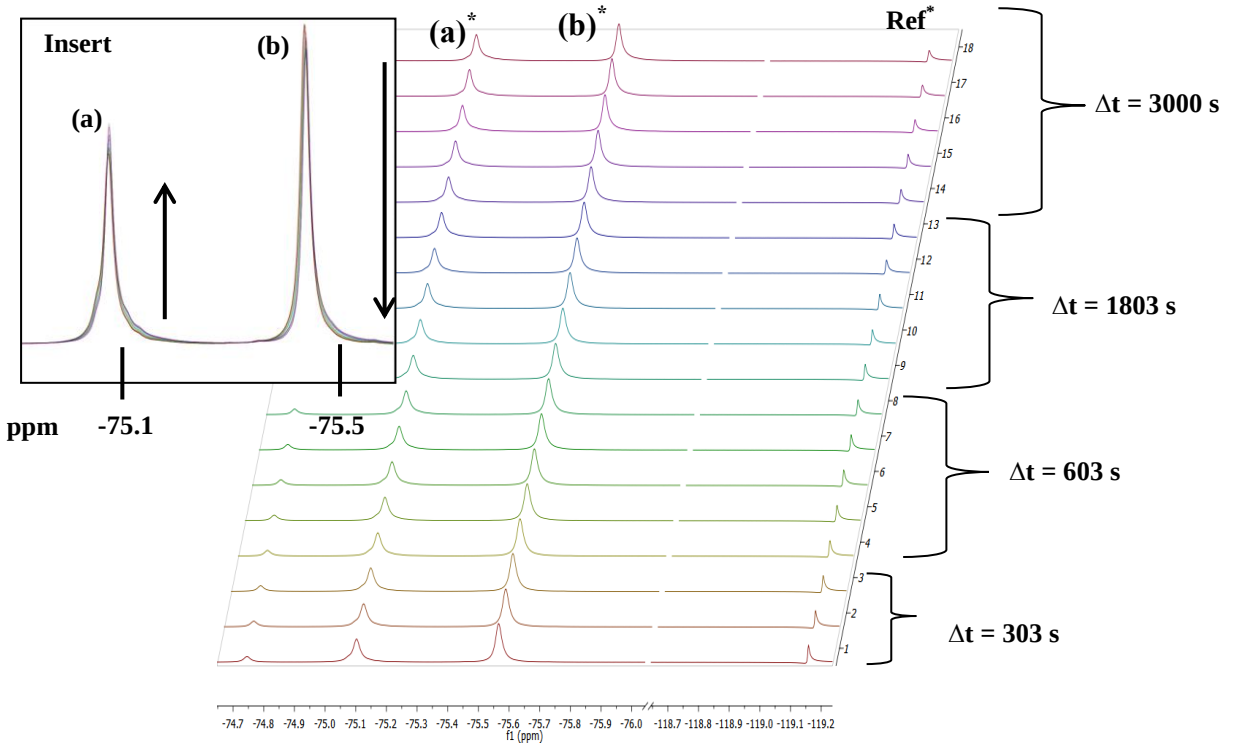

Figure 6.10: Observed stacked ^{19}F-NMR spectra illustrating the progression of the slow reaction. Entry 2, (Table 6.1 (a)) [Zr] : [Na(tta)] = 1 : 5. [Zr(tta)$_4$] formation at -75.1 ppm, Na(tta) consumption at -75.5 ppm. [ZrCl$_4$]= 0.119 M, [Na(tta)] = 0.596 M, Temp = 20.0 ˚C, ligand and metal dissolved in DMF and spectra collected in deuterated benzene (C_6D_6), total time of the second slow reaction = 29454 s, Δt indicates the time between successive spectra. Insert: Superimposed ^{19}F-NMR spectra illustrating (a) formation of product [Zr(tta)$_4$] and (b) disappearance of ligand (Na(tta)).
***(a) Product formation. *(b) Ligand disappearance. *Ref = KF reference probe signal.**

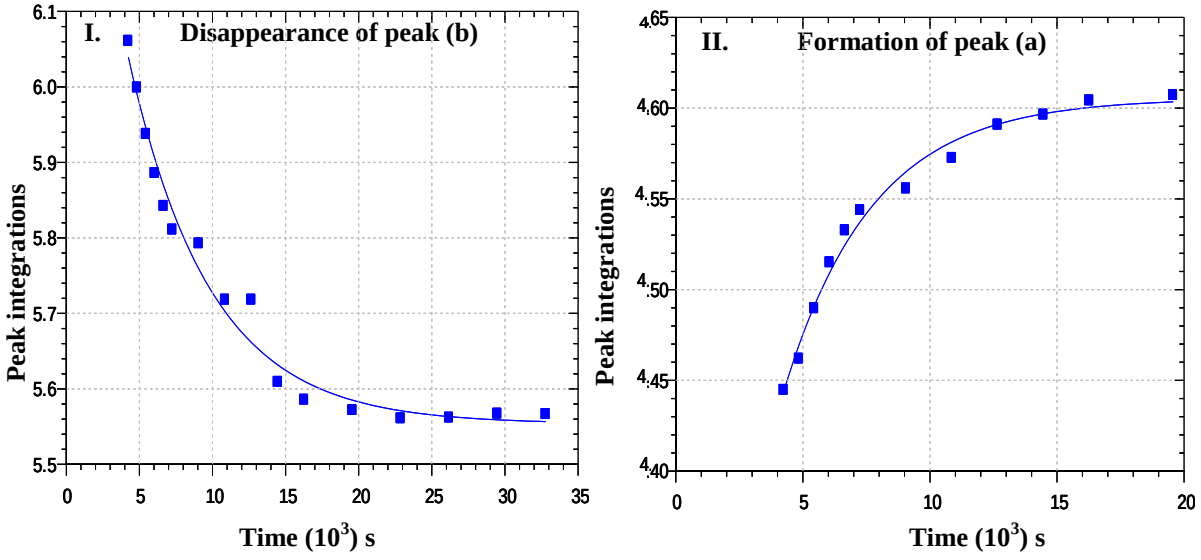

Figure 6.11: (I) ^{19}F-NMR peak integration *vs* time data for ligand consumption of the second reaction, [ZrCl$_4$]= 0.119 M, [Na(tta)] = 0.596 M, k_{obs}= 1.79(2) x 10^{-4} s^{-1}. (II) ^{19}F-NMR peak intensity *vs* time data for product formation [Zr(tta)$_4$] of the second slow reaction k_{obs} = 2.88(3) x 10^{-4} s^{-1}, ligand and metal dissolved in DMF and spectra collected in deuterated benzene (C_6D_6) at 20.0 ºC. Total time represented on Micromath Scientist plot is for the combined first fast reaction and the second slow reaction.

A plot of the combined reactions, the first fast reaction graph (I) product formation (blue plot) and ligand consumption (red plot) and the second slow reaction graph (II) product formation (blue plot) and ligand consumption (red plot) (Figure 6.12) was constructed of the peak integrations *vs* time. The plots for both the fast and slow reactions are shown.

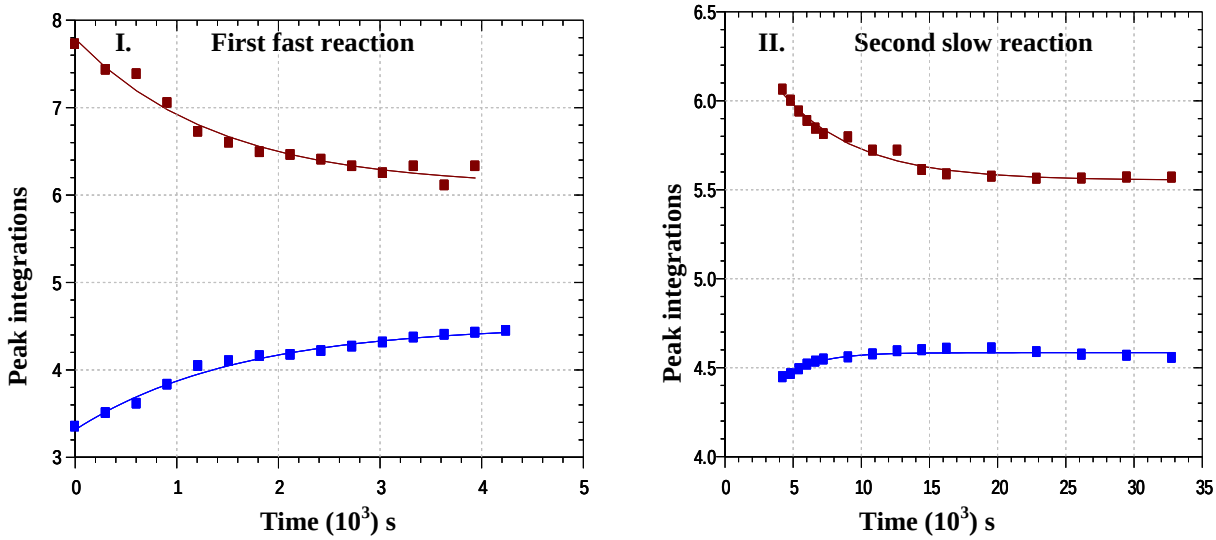

Figure 6.12: Micromath Scientist plots of combined reaction formation of complex and consumption of ligand, (I) illustrates the first fast reaction and (II) illustrates the second slow reaction [Zr] : [Na(tta)] = 1 : 5 Entry 2, (Table 6.1 (a)).

6.4.1.5 ^{1}H-NMR Kinetic Investigation of the formation reaction of [Zr(tta)$_4$] ([Zr]:[Na(tta)] = 1 : 4, first fast reaction)

The formation reaction of [Zr(tta)$_4$] was followed by ^{1}H-NMR (repetitive scans illustrated in the stacked plot in Figure 6.13). This figure is a graphical representation of the first rapid reaction that took place in the 1 : 4 ratio reaction. A typical kinetic data plot was fitted to eqn 6.1 as illustrated by Figure 6.14 for ligand consuption (I) and product formation (II) in order to determine the observed rate constant, k_{obs}.

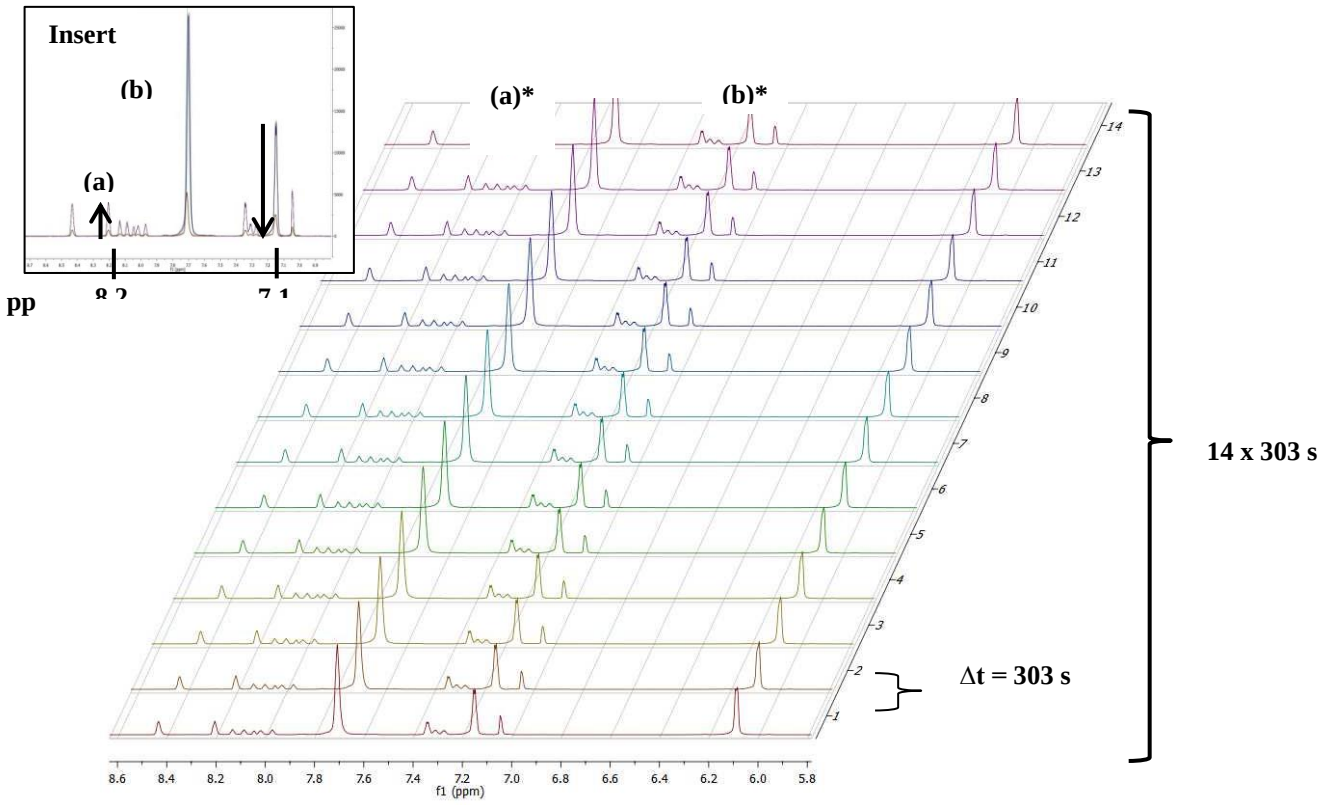

Figure 6.13: Observed stacked ^{1}H-NMR spectra illustrating the progression of the first fast reaction, Entry No. 3, (Table 6.1 (a)) [Zr] : [Na(tta)] = 1 : 4. [Zr(tta)$_4$] formation at 8.2 ppm, Na(tta) consumption at 7.1 ppm. [ZrCl$_4$] = 0.095 M, [Na(tta)]=0.382 M, Temp = 20.0 ˚C, ligand and metal dissolved in deutrated DMF and spectra collected in deuterated DMF (C_3D_7NO), total time of the first fast reaction = 4242 s, Δt indicates the time between successive spectra. Insert: Superimposed ^{1}H-NMR spectra illustrating (a) formation of product [Zr(tta)$_4$] and (b) disappearance of ligand (Na(tta)).
***(a) Product formation. *(b) Ligand disappearance.**

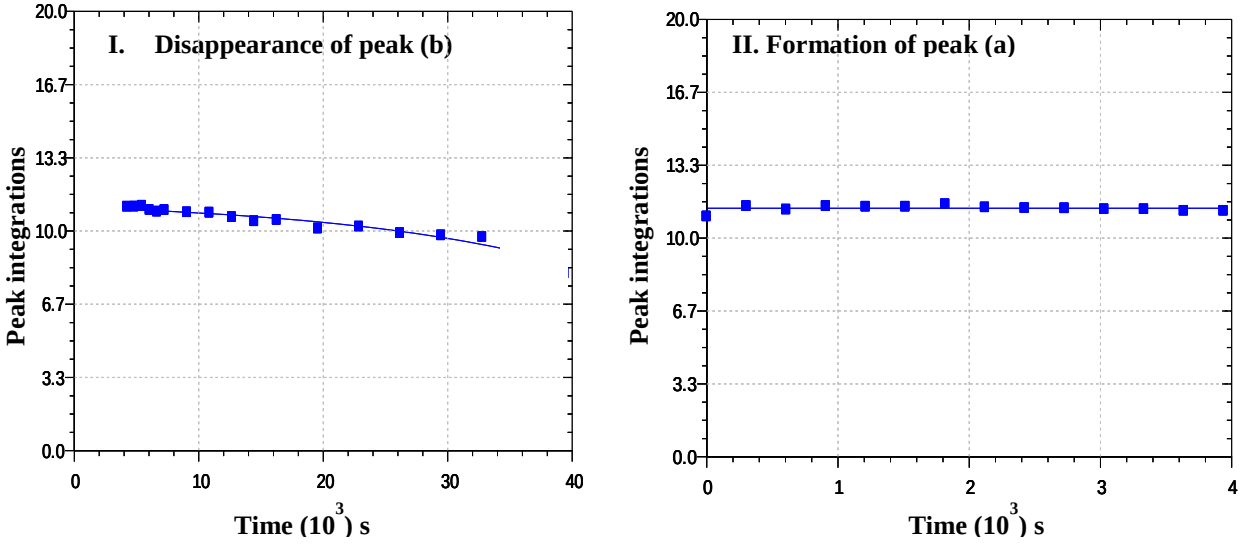

Figure 6.14: (I) ^{1}H-NMR peak integration *vs* time data for ligand consumption of the first fast reaction [ZrCl$_4$] = 0.095 M, [Na(tta)]=0.382 M, k_{obs}= 1.79(2) x 10^{-4} s^{-1}. (II) ^{19}F-NMR peak intensity *vs* time data for product formation [Zr(tta)$_4$]of the first fast reaction, k_{obs} = 2.88(3) x 10^{-4} s^{-1}, ligand and metal dissolved in DMF and spectra collected in deuterated DMF (C_3D_7NO) at 20.0 ºC. Total time represented on Micromath Scientist plot is of the combined first fast reaction and the second slow reaction.

6.4.1.6 ^{1}H-NMR Kinetic Investigation of [Zr(tta)$_4$] 1 : 4, second slow reaction)

The formation reaction of [Zr(tta)$_4$] was followed by ^{1}H-NMR (repetitive scans illustrated in the stacked plot Figure 6.15). This figure is a graphical representation of the second slower reaction that took place in the 1 : 4 ratio reaction. A typical kinetic data plot was fitted to eqn 6.1 as illustrated by Figure 6.16 for ligand consumption (I) and product formation (II) in order to obtain the observed rate constant, k_{obs}.

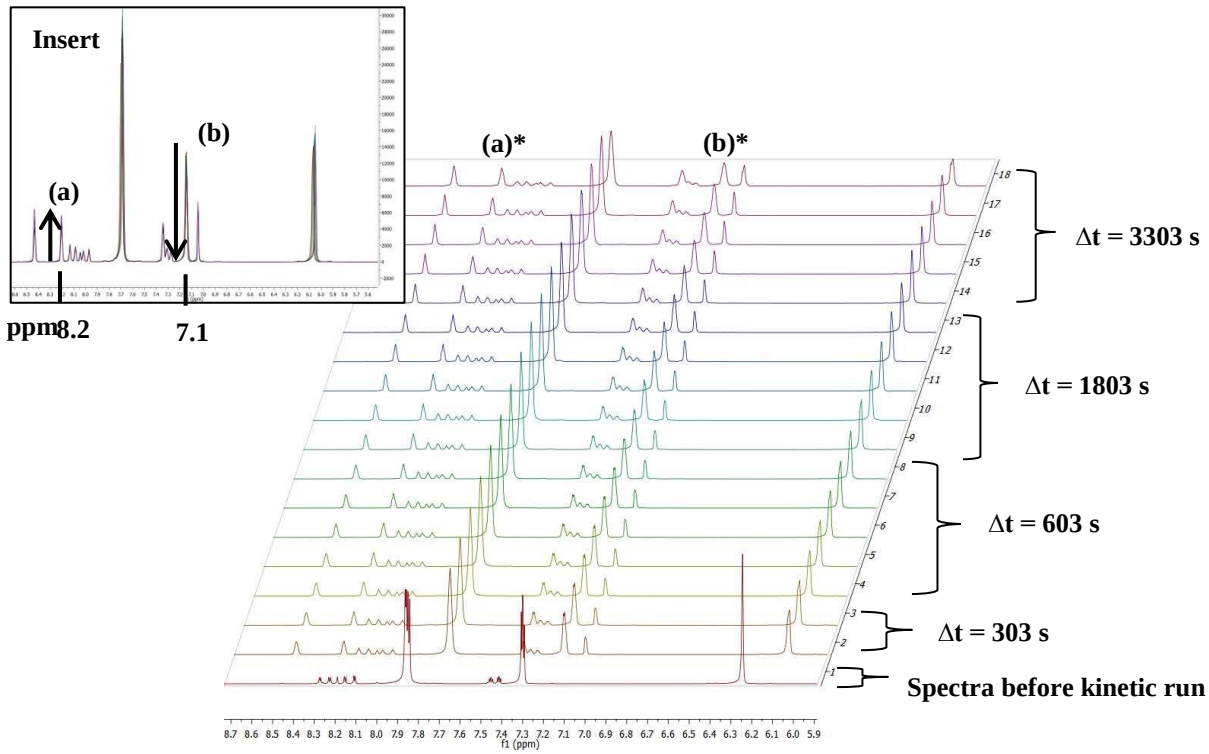

Figure 6.15: Observed stacked ^{1}H-NMR spectra illustrating the progression of the slow reaction. Entry No.3, (Table 6.1 (a)) [Zr] : [Na(tta)] = 1 : 5. [Zr(tta)$_4$] formation at 8.2 ppm, Na(tta) consumption at 7.1 ppm. [ZrCl$_4$] = 0.095 M, [Na(tta)]=0.382 M, Temp = 20.0 ˚C, ligand and metal dissolved in DMF and spectra collected in deuterated DMF (C_3D_7NO), total time of the second slow reaction = 29454 s, Δt indicates the time between successive spectra. Insert: Superimposed ^{1}H-NMR spectra illustrating (a) formation of product [Zr(tta)$_4$] and (b) disappearance of ligand (Na(tta)).
***(a) Product formation. *(b) Ligand disappearance.**

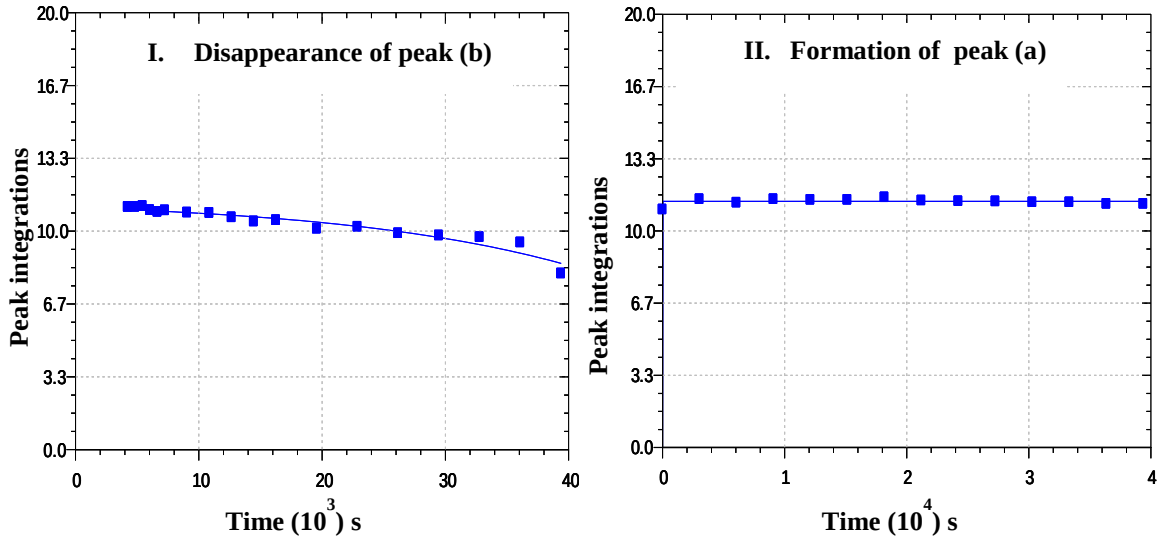

Figure 6.16: (I) ^{1}H-NMR peak integration *vs* time data for ligand consumption of the second reaction, [$ZrCl_4$] = 0.095 M, [Na(tta)]=0.382 M, k_{obs}= 1.79(2) x 10^{-4} s^{-1}. (II) ^{1}H-NMR peak intensity *vs* time data for product formation [$Zr(tta)_4$], second slow reaction k_{obs} = 2.88(3) x 10^{-4} s^{-1}, ligand and metal dissolved in DMF and spectra collected in deuterated DMF (C_3D_7NO), at 20.0 ºC. Total time represented for the Mircomath Scientist plot is for the combined first fast reaction and the second slow reaction. Total time represented on micromath scientist plot is of the combined first fast reaction and the second slow reaction.

6.4.2 Preliminary Kinetic Study of the formation of Tetrakis(thenoyltrifluoroacetylacetonato)Hafnium(IV) [$Hf(tta)_4$]

Similar to the formation reaction observed between [$ZrCl_4$] and Na(tta), the number of peaks observed on the spectra of the reaction between [$HfCl_4$] and Na(tta) is consistent with that of Zr(IV) and Na(tta). The product formation peak shifts significantly to allow for differentiation between [$Zr(tta)_4$] and [$Hf(tta)_4$] product formation peaks. This is the first distinctive difference between zirconium(IV) and hafnium(IV) observed in this study. This difference will further be exploited in competition studies where the affinity for the ligand will be investigated. The reference peak (KF) and the ligand (Na(tta)) peak appeared at -119 ppm and at -75.5 ppm respectively. The measurements were recorded on a 300MHz NMR instrument. As expected the hafnium(IV) reaction also proceeded in two steps: a first fast reaction: followed by a second slow reaction. Each reaction's stacked NMR plot is accompanied by two graphical representations of ligand consumption (I) and product formation (II). Again, two reactions were observed, the first corresponding to a lower coordinated metal species, while the econd represents the formation of the tetrakis species of which the chemical shifts correspond to those given in Table 6.2 as characterized by XRD.

6.4.2.1 ^{19}F-NMR Kinetic Investigation of the formation of [Hf(tta)$_4$]([Hf]:[Na(tta) = 1 : 4, first fast reaction)

The formation reaction of [Hf(tta)$_4$], was followed by ^{19}F-NMR (repetitive scans are illustrated in the stacked plot, Figure 6.17). Figure 6.17 is a graphical representation of the first rapid reaction that took place in the 1 : 4 ratio reaction. A typical kinetic data plot was fitted to eqn 6.1 as illustrated by (Figure 6.18) for ligand consumption (I) and product formation (II) in order to determine the observed rate constant, k_{obs}.

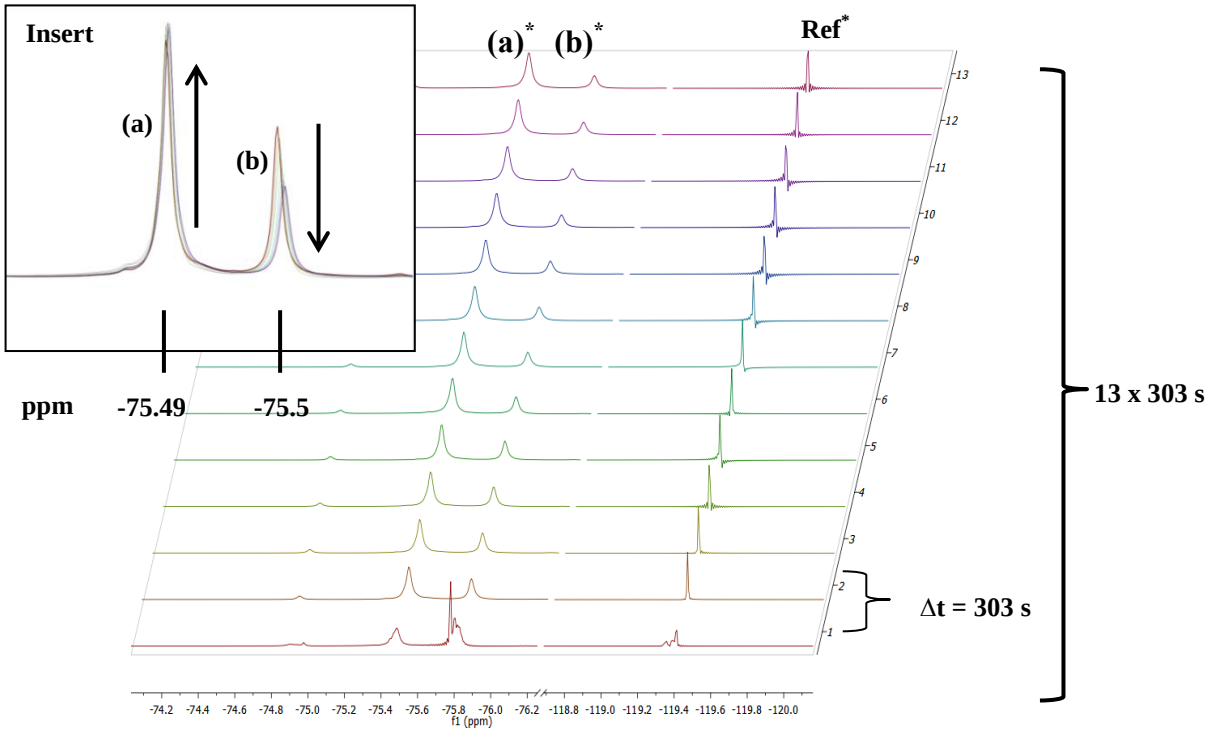

Figure 6.17: Observed stacked ^{19}F-NMR spectra illustrating the progression of the first fast reaction, Entry No. 4, (Table 6.1(a)) [Hf] : [Na(tta)] = 1 : 4. [Hf(tta)$_4$] formation at -75.49 ppm, Na(tta) consumption at -75.5 ppm. [HfCl$_4$] = 0.087 M, [Na(tta)]= 0.347 M, Temp = 20.0 ˚C, ligand and metal dissolved in DMF and spectra collected in deuterated benzene (C$_6$D$_6$), total time of the first fast reaction = 3939 s, Δt indicates the time between successive spectra. Insert: Superimposed ^{19}F-NMR spectra illustrating (a) formation of the product [Hf(tta)$_4$] and (b) disappearance of the ligand (Na(tta)).
***(a) Product formation. *(b) Ligand disappearance. *Ref = KF reference probe signal.**

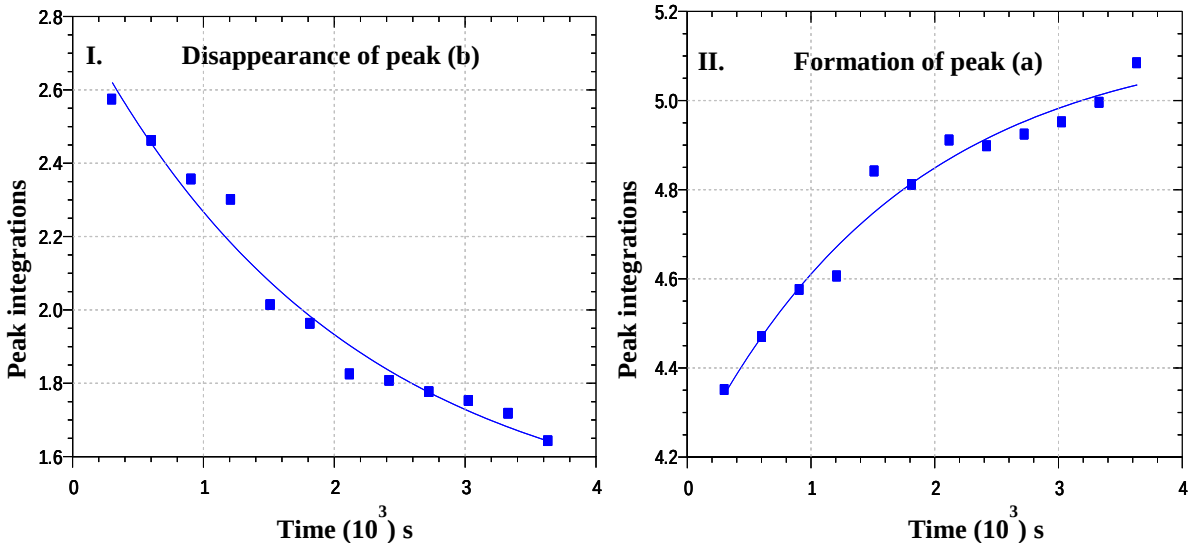

Figure 6.18: (I) ^{19}F-NMR peak integration *vs* time data for ligand consumption of the first reaction, [$HfCl_4$] = 0.087 M, [Na(tta)]= 0.347 M, k_{obs}= 3.24 (2) x 10^{-3} s^{-1}. (II) ^{19}F-NMR peak intensity *vs* time data for product formation [$Hf(tta)_4$], first fast reaction k_{obs} = 3.78(8) x 10^{-3} s^{-1}, ligand and metal salt dissolved in DMF and spectra collected in deuterated benzene (C_6D_6) at 20.0 ºC. Total time represented on Micromath Scientist plot is of the combined first fast reaction and the second slow reaction.

6.4.2.2 ^{19}F-NMR Kinetic Investigation of ([$Hf(tta)_4$] 1 : 4, second slow reaction)

The formation reaction of [$Hf(tta)_4$] was followed by ^{19}F-NMR (repetitive scans illustrated in the stacked plot, Figure 6.19). The figure is a graphical representation of the second slow reaction that took place in the 1 : 4 reaction. A typical kinetic data plot was fitted to eqn 6.1 as illustrated by Figure 6.20 for ligand consumption (I) and product (II) in order to determine the observed rate constant, k_{obs}.

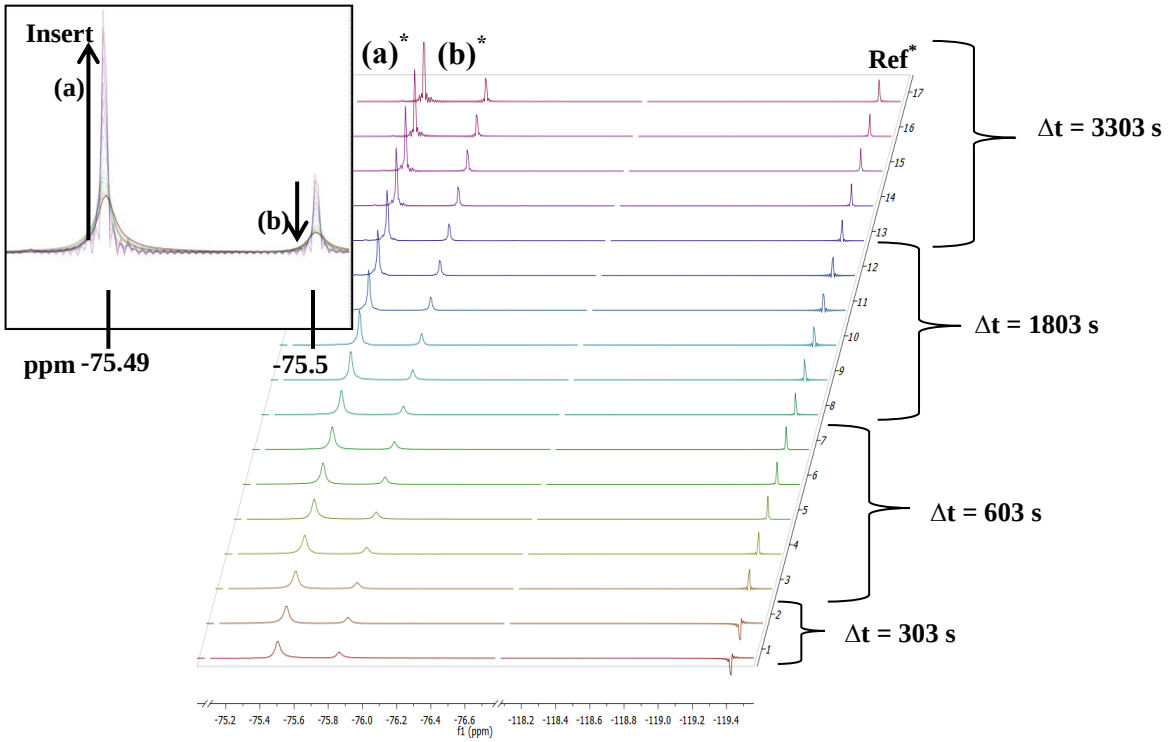

Figure 6.19: Observed stacked ^{19}F-NMR spectra illustrating the progression of the slow reaction, Entry No. 4, (Table 6.1 (a))[Hf] : [Na(tta)] = 1 : 4, [Hf(tta)$_4$] formation at -75.49 ppm, Na(tta) consumption at -75.5 ppm. [HfCl$_4$] = 0.087 M, [Na(tta)]= 0.347 M, Temp = 20.0 ˚C, ligand and metal dissolved in DMF and spectra collected in deuterated Benzene (C_6D_6), total time of the second slow reaction = 29151 s. , Δt indicates the time between successive spectra. Insert: Superimposed ^{19}F-NMR spectra illustrating (a) formation of the product [Hf(tta)$_4$] and (b) disappearance of the ligand (Na(tta)).
***(a) Product formation. *(b) Ligand disappearance. *Ref = KF reference probe signal.**

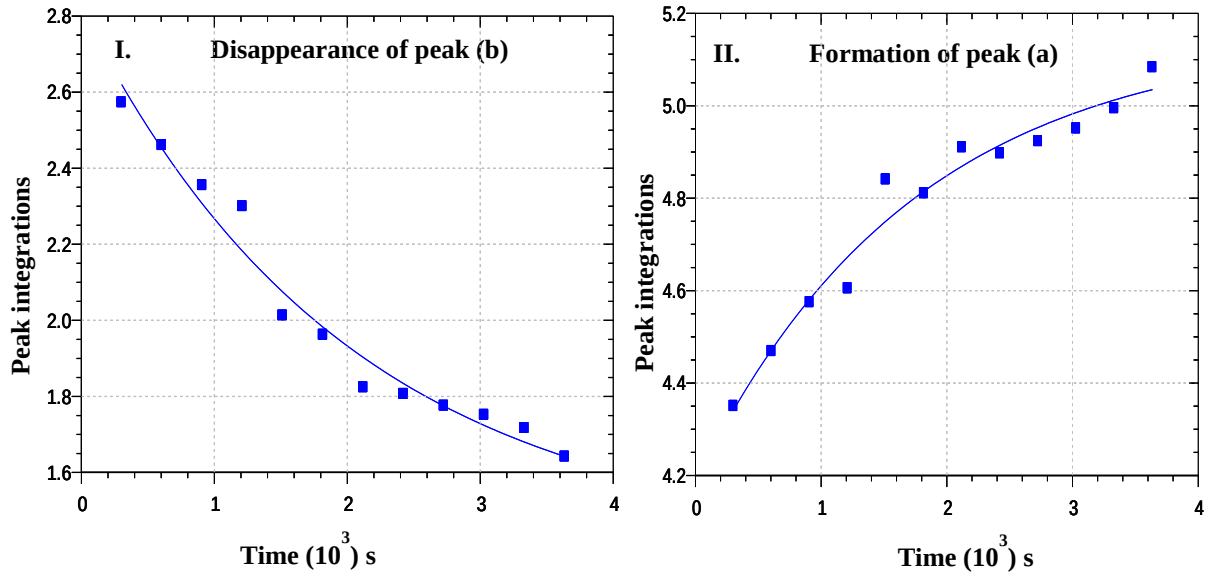

Figure 6.20: (I) ^{19}F-NMR peak integration *vs* time data for the ligand consumption of the second reaction, [HfCl$_4$] = 0.087 M, [Na(tta)]= 0.347 M, k_{obs}= 2.02(1) x 10^{-3} s^{-1}. (II) ^{19}F-NMR peak intensity *vs* time data for product formation [Hf(tta)$_4$] of the first fast reaction k_{obs} = 2.94(1) x 10^{-3} s^{-1}, ligand and metal dissolved in DMF and spectra collected in deuterated benzene (C_6D_6) at 20.0 ºC. Total time represented on Micromath Scientist plot is of the combined first fast reaction and the second slow reaction.

A plot of the combined reactions, product formation (blue plot) and ligand consumption (red plot) (Figure 6.21) can also be constructed of the peak integrations *vs* time. The plots for both the fast and slow reactions are shown.

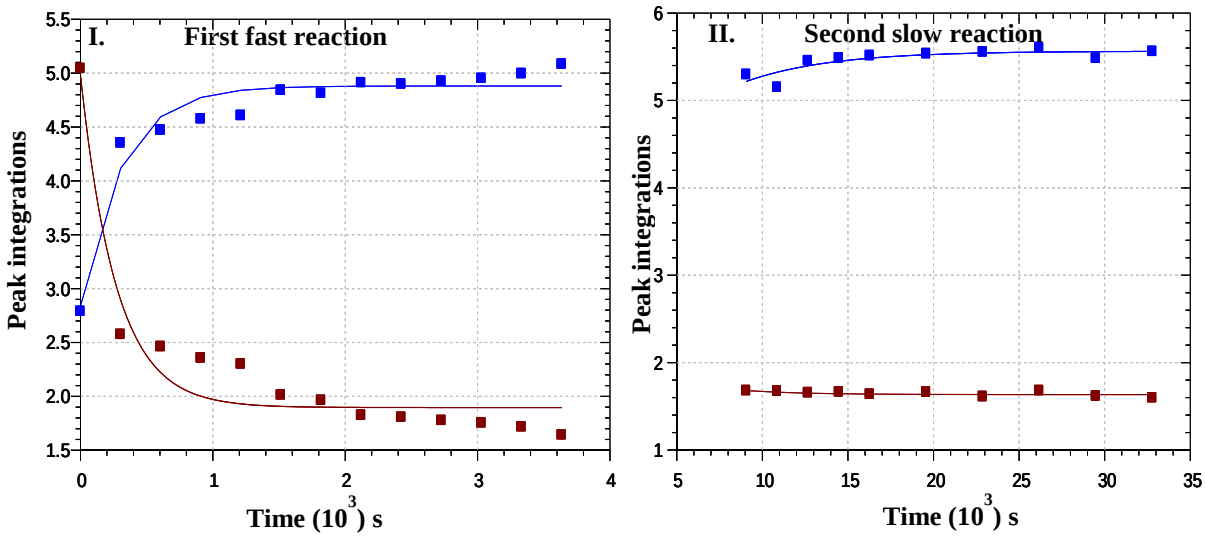

Figure 6.21: Micromath Scientist plots of combined formation of the complex (blue) and consumption of the ligand (red), (I) illustrates the first fast reaction and (II) illustrates the second slow reaction.
[Hf] : [Na(tta)] = 1 : 4, Entry No. 4, (Table 6.1 (a)).

6.4.2.3 ^{19}F-NMR Kinetic Investigation of the formation of [Hf(tta)$_4$] of ([Hf]:[Na(tta)] = 1 : 5, first fast reaction)

The formation reaction of [Hf(tta)$_4$] was followed by ^{19}F-NMR (repetitive scans illustrated in the stacked plot Figure 6.22). The figure is a graphical representation of the first rapid reaction that took place in the 1 : 5 reaction. A typical kinetic data plot was fitted to eqn 6.1 as illustrated by Figure 6.23 for ligand consumption (I) and product formation (II) in order to determine the observed rate constant, $k_{obs.}$

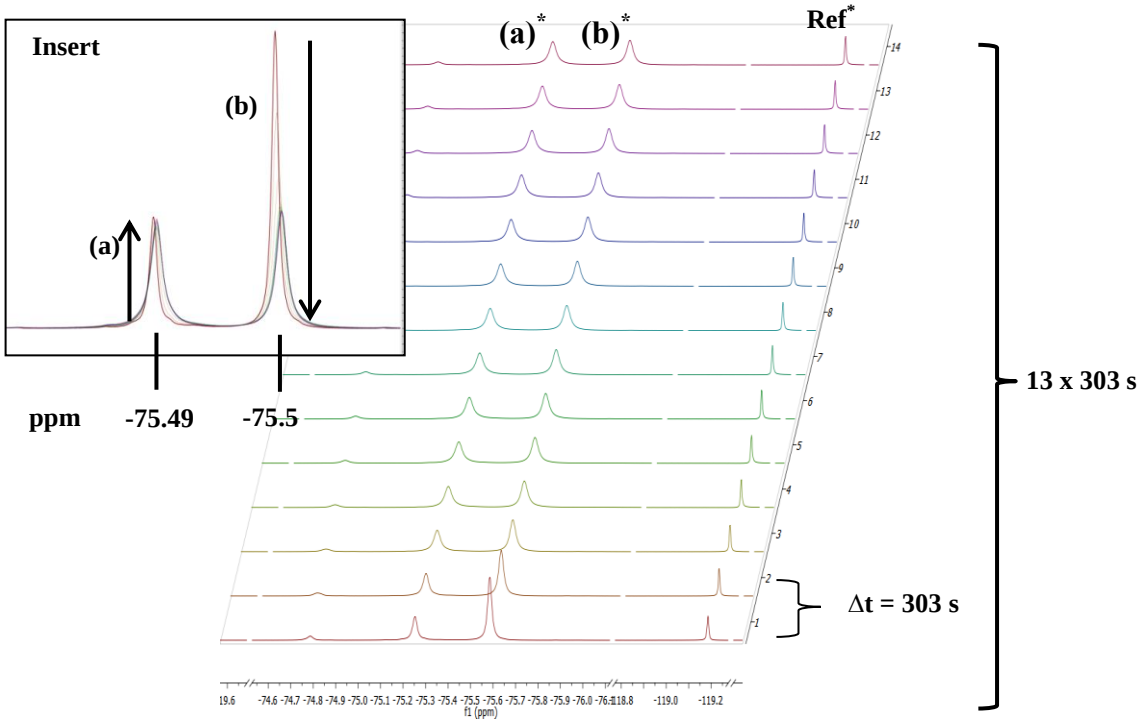

Figure 6.22: Observed stacked ^{19}F-NMR spectra illustrating the progression of the first fast reaction, Entry No. 5, (Table 6.1(a)), [Hf] : [Na(tta)] = 1 : 5. [Hf(tta)$_4$] formation at -75.49 ppm, Na(tta) consumption at -75.5 ppm. [HfCl$_4$] = 0.08 M, [Na(tta)]= 0.435 M, Temp = 20.0 ˚C, ligand and metal dissolved in DMF and spectra collected in deuterated bezene (C$_6$D$_6$), total time of the first fast reaction = 4242 s. Δt indicates the time between successive spectra. Insert: Superimposed ^{19}F-NMR spectra illustrating (a) formation of product [Hf(tta)$_4$] and (b) disappearance of ligand (Na(tta)).
***(a) Product formation. *(b) Ligand disappearance. *Ref = KF reference probe signal.**

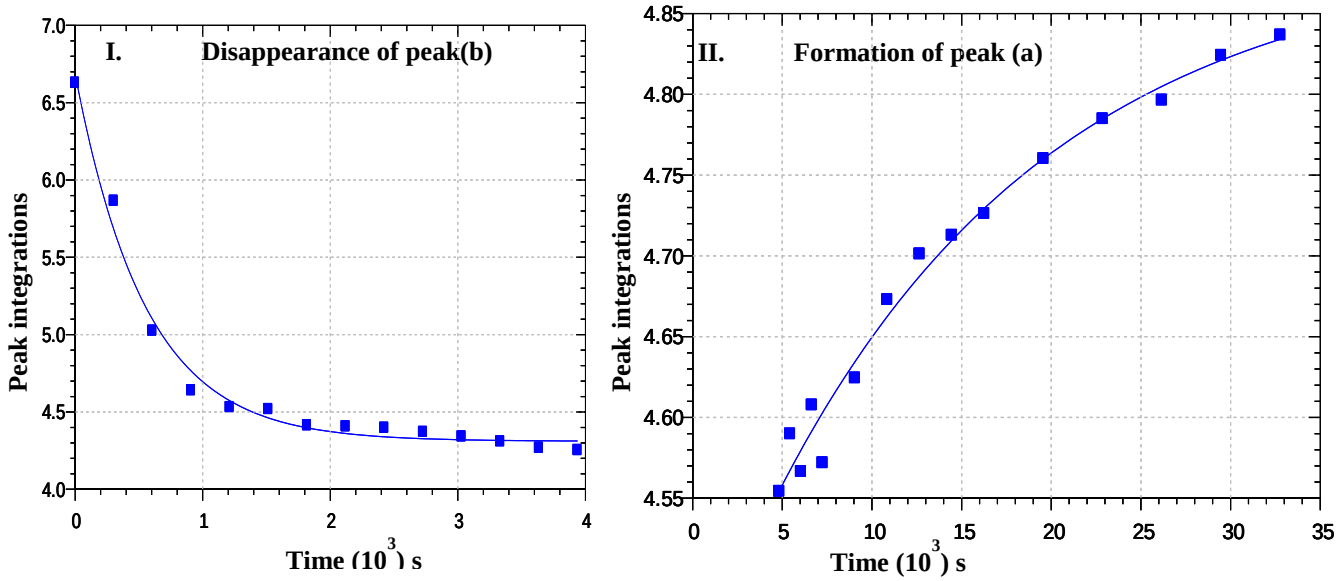

Figure 6.23: (I) ^{19}F-NMR peak intensity *vs* time data for the ligand consumption of the first reaction, [[HfCl$_4$] = 0.08 M, [Na(tta)]= 0.435 M, M in benzene at 20.0ºC, k_{obs}=1.82(1) x 10^{-3} s$^{-1,}$ (II) ^{19}F-NMR peak intensity *vs* time data for the product formation [Hf(tta)$_4$], first reaction k_{obs} = 1.45(1) x 10^{-3} s^{-1}. Total time represented on Micromath Scientist plot is of the combined first fast reaction and the second slow reaction.

6.4.2.4 ^{19}F-NMR Kinetic Investigation of the formation of [Hf(tta)$_4$] of ([Hf]:[Na(tta)] = 1 : 5, second slow reaction)

The formation reaction of [Hf(tta)$_4$] was followed by ^{19}F-NMR (repetitive scans illustrated in the stacked plot Figure 6.24). The figure is a graphical representation of the second slow reaction that took place in the 1 : 5 reaction. A typical kinetic data plot was fitted to eqn 6.1 as illustrated in Figure 6.25 for ligand consuption (I) and product formation (II) in order to determine the observed rate constant, k_{obs}.

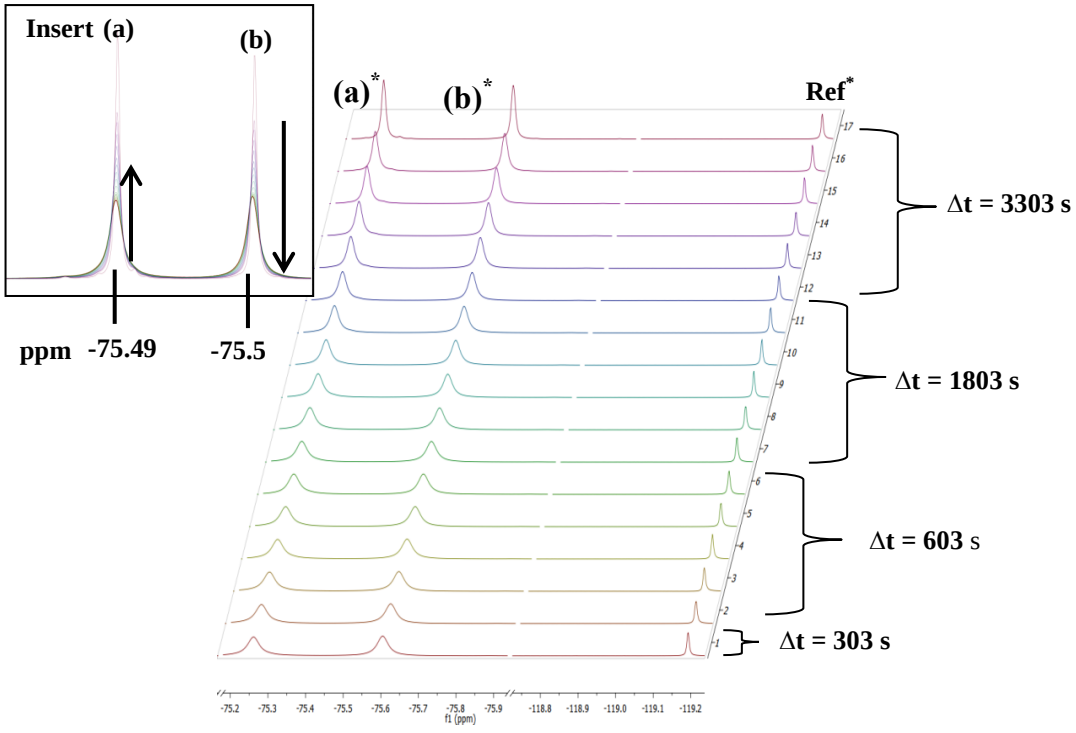

Figure 6.24: Observed stacked ^{19}F-NMR spectra illustrating the progression of the slow reaction, Entry No. 5 (Table 6.1 (a)) [Hf] : [Na(tta)] = 1 : 5. [Hf(tta)$_4$] formation at -75.49 ppm, Na(tta) consumption at -75.5 ppm. [HfCl$_4$] = 0.08 M, [Na(tta)]= 0.435 M, Temp = 20.0 ˚C, ligand and metal dissolved in DMF and spectra collected in deuterated benzene (C_6D_6), total time of the second slow reaction = 28848 s Δt indicates the time between successive spectra. Insert: Superimposed ^{19}F-NMR spectra illustrating (a) formation of product [Hf(tta)$_4$] and (b) disappearance of ligand (Na(tta)).
***(a) Product formation. *(b) Ligand disappearance. *Ref = KF reference probe signal.**

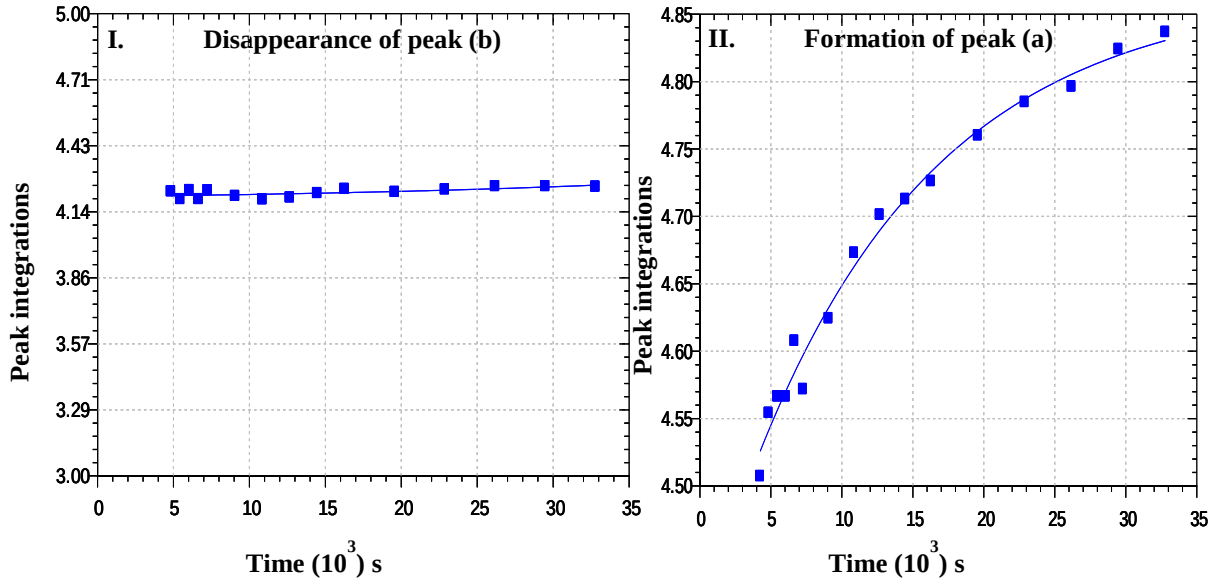

Figure 6.25: (I)^{19}F-NMR peak intensity *vs* time data for ligand consumption of the second reaction [$HfCl_4$] = 0.08 M, [Na(tta)]= 0.435 M, in deuterated benzene (C_6D_6) at 20.0°C k_{obs}=3.8(1) x 10^{-3} s^{-1} (II)^{19}F-NMR peak intensity *vs* time data for product formation [$Hf(tta)_4$] of the second reaction, k_{obs} = 7.7(1) x 10^{-3} s^{-1}. Total time represented on Micromath Scientist plot is of the combined first fast reaction and the second slow reaction.

A plot of the reactions of the combined reactions, product formation (blue plot) and ligand consumption (red plot) (Figure 6.26) can also be constructed of the peak integrations *vs* time. The plots for both the fast and slow reactions are shown.

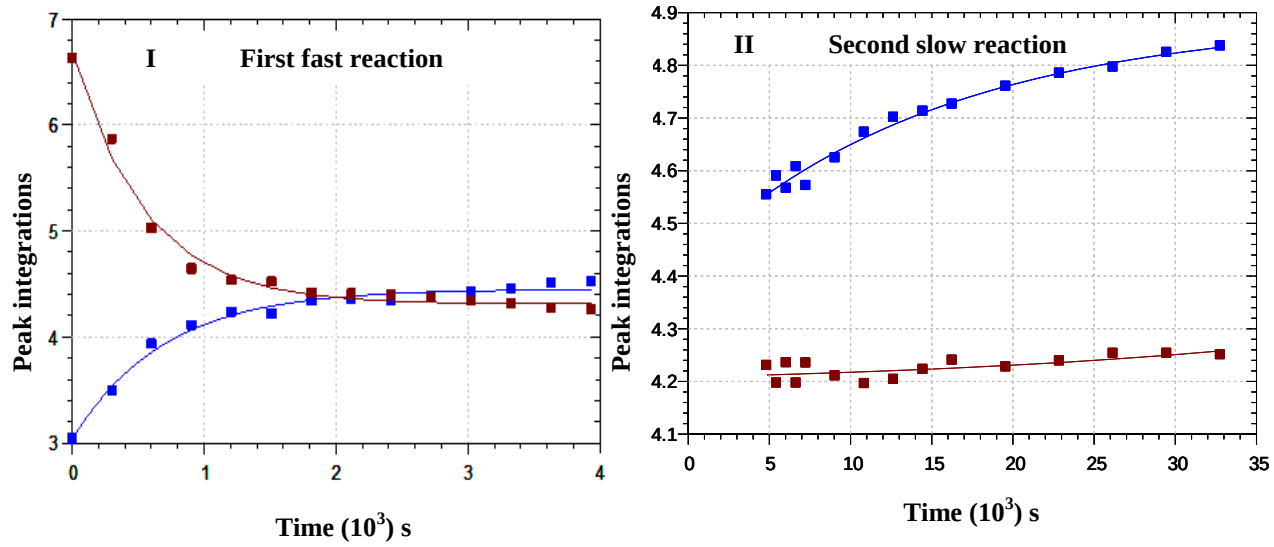

Figure 6.26: Micromath Scientist plots of combined formation of complex (blue) and consumption of ligand (red), (I) illustrates the first fast reaction and (II) illustrates the second slow reaction.
[Hf] : [Na(tta)] = 1 : 5, Entry 5, Table 6.1(a).

6.5 Competition Studies of ([$ZrCl_4$] : [$HfCl_4$]) *vs* [Na(tta)]

The outer electron configuration arrangement of zirconium(IV) and hafnium(IV) is identical ([Kr]$4d^2 5s^2$ for zirconium(IV) and [Xe]$4d^2 6s^2$ for hafnium(IV)).[2] This results in these two metals exhibiting identical chemical behavior[2] and it makes it difficult to develop efficient separation methods to produce hafnium-free zirconium or zirconium-free hafnium that is necessary for the application in nuclear reactors.

In a similar study by Pinnavaia *et al.*[3] trifluoroacetylacetone (tfacac) was utilized in a kinetic investigation and the ^{19}F-NMR spectra showed the hafnium(IV) and zirconium(IV) compounds investigated gave identical ^{19}F-NMR spectra (See Chapter 2 Paragraph 2.6.).

The following competition studies were performed with molar equivalent amounts of zirconium tetrachloride and hafnium tetrachloride, combined and dissolved in DMF and reacted with Na(tta) at varying ratios. The reactions were performed in order to investigate the affinity of the respective zirconium(IV) and hafnium(IV) towards the ligand.

6.5.1 ^{19}F-NMR Kinetic Investigation of ([$ZrCl_4$] : [$HfCl_4$]) *vs* [Na(tta)] ([Zr]:[Hf]:[Na(tta)] = 0.5 : 0.5 : 2) (first fast reaction)

The formation reaction of [$Hf(tta)_4$] and [$Zr(tta)_4$] for the competition study was followed by ^{19}F-NMR (repetitive scans illustrated in the stacked plot Figure 6.27). Figure 6.27 is a graphical representation of the first rapid reaction that took place in the 1 : 2 reaction. A typical kinetic data plot was fitted as illustrated in Figure 6.28 and Figure 2.29 in order to determine the observed rate constant k_{obs}. Figure 6.28 illustrates the (I) product formation of [$Zr(tta)_4$] and (II) illustrates the product formation of [$Hf(tta)_4$], while Figure 6.29 illustrates the ligand consumption for the first fast reaction.

[2] Brown, T. E., LeMay, E. H., Bursten B. E., Murphy, C., Woodward, P., *Chemistry The Central Science 13th Ed, Prentice Hall*, 2014.
[3] Pinnavaia, T. J., Fay, R. C., *Inorg. Chem.* **5**, 233-239, 1966.

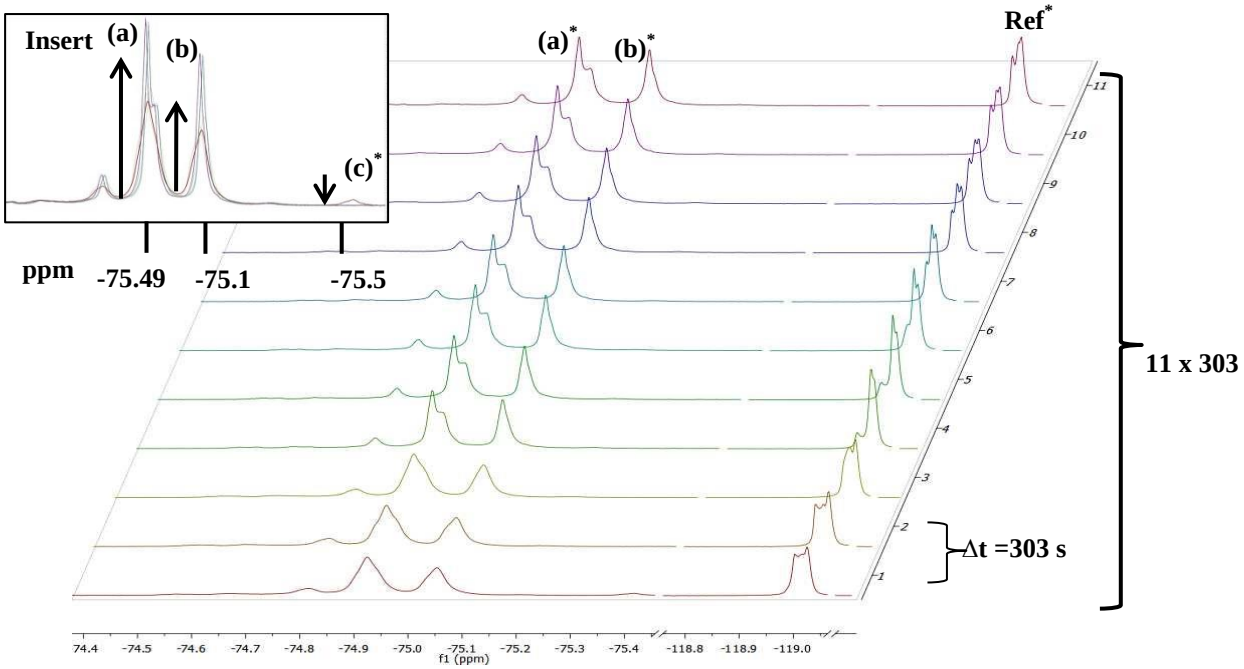

Figure 6.27: Observed stacked ^{19}F-NMR spectra illustrating the progression of the first fast reaction, Entry No. 1 (Table 6.1 (b)) [Zr] : [Hf] : [Na(tta)] = 1 : 2. [Zr(tta)$_4$] formation peak (b) at -75.1 ppm, [Hf(tta)$_4$] formation peak (a) at -75.49 ppm and Na(tta) consumption at -75.5 ppm. [HfCl$_4$]= 0.043 M, [ZrCl$_4$] = 0.044 M, [Na(tta)] = 0.175 M, Temp = 20.0 ˚C, ligand and metal dissolved in DMF and spectra collected in deuterated benzene (C$_6$D$_6$), total time of the first fast reaction = 3333 s Δt indicates the time between successive spectra. Insert: Superimposed ^{19}F-NMR spectra illustrating (a) formation of product [Hf(tta)$_4$], (b)[Zr(tta)$_4$] and (c) disappearance of ligand (Na(tta)).
***(a) Product formation for the hafnium(IV) species . *(b) Product formation for the zirconium(IV) species. *(c) Ligand consumption peak for the Na(tta). *Ref = KF reference probe signal.**

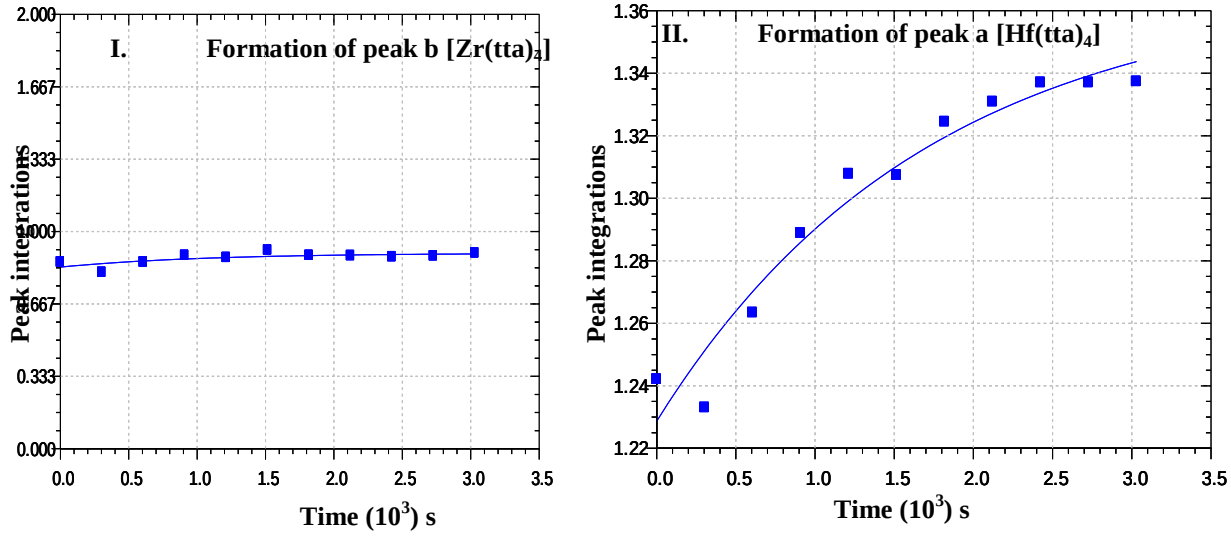

Figure 6.28: (I) ^{19}F-NMR peak intensity *vs* time data for the product formation of [Zr(tta)$_4$] first fast reaction [HfCl$_4$]= 0.043 M, [ZrCl$_4$] = 0.044 M, [Na(tta)] = 0.175 M, k_{obs} = 4.82(4) x 10^{-3} s^{-1}. (II) ^{19}F-NMR peak intensity *vs* time data for the product formation [Hf(tta)$_4$], first fast reaction k_{obs} = 4.9(4) x 10^{-3} s^{-1}. Total time represented on micromath scientist plot is of the combined first fast reaction and the second slow reaction.

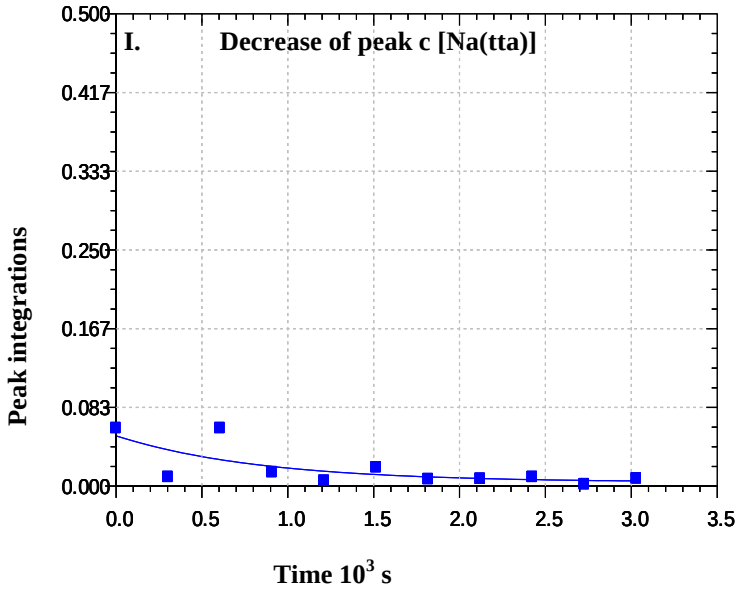

Figure 6.29: (I) ^{19}F-NMR peak intensity *vs* time data for the first fast reaction, ligand consumption, [Na(tta)] = 0.197 M, k_{obs} = 6.27(4) x 10^{-4} s^{-1}. Total time represented on micromath scientist plot is of the combined first fast reaction and the second slow reaction.

6.5.2 ^{19}F-NMR Kinetic Investigation of ([$ZrCl_4$] : [$HfCl_4$]) *vs* [Na(tta)] ([Zr]:[Hf]:[Na(tta)] = 0.5 : 0.5 : 2, second slow reaction)

The formation reaction of [$Hf(tta)_4$] and [$Zr(tta)_4$] in the competition reaction was followed by ^{19}F-NMR (repetitive scans illustrated in the stacked plot Figure 6.30). Figure 6.30 is a graphical representation of the second slow reaction that took place in the 1 : 2 reaction. A typical kinetic data plot was fitted as illustrated in Figure 6.31 for the product formation of (I) [$Zr(tta)_4$] peak (b) and (II) the product formation of [$Hf(tta)_4$] peak (a) in order to determine the observed rate constant, k_{obs}. Figure 6.32 illustrate the ligand consumption during the second slow reaction.

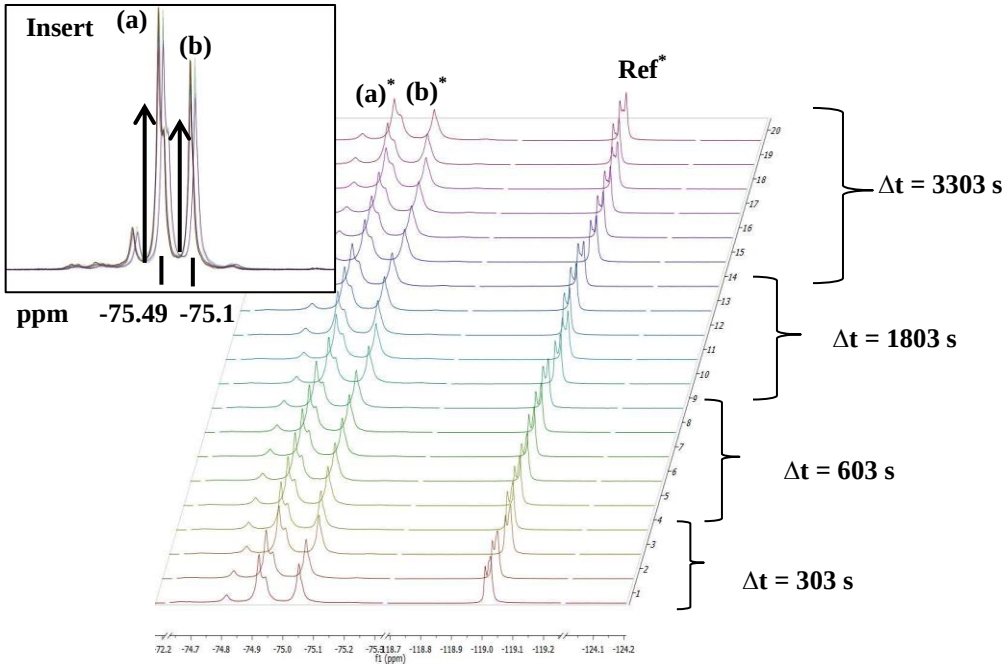

Figure 6.30: Observed stacked ^{19}F-NMR spectra illustrating the progression of the second slow reaction. Entry No. 1 (Table 6.1 (b))[Hf] : [Zr] : [Na(tta)] = 0.5 : 0.5 : 2, [Hf(tta)$_4$] formation peak (a) at -75.49 ppm, [Zr(tta)$_4$] formation peak (b) at -75.1 ppm and [Na(tta)] consumption peak (c) at -75.5 ppm. [HfCl$_4$] = 0.0496 M, [HfCl$_4$]= 0.043 M, [ZrCl$_4$] = 0.044 M, [Na(tta)] = 0.175 M, Temp = 20.0 ˚C, ligand and metal salt dissolved in DMF and spectra collected in deuterated benzene (C$_6$D$_6$), total time of the second slow reaction of the second slow reaction = 31575 s Δt indicates the time between successive spectra. Insert: Superimposed ^{19}F-NMR spectra illustrating (a) formation of product [Hf(tta)$_4$], (b) formation of product [Zr(tta)$_4$]. *(a) Product formation for the hafnium(IV) species . *(b) Product formation for the zirconium(IV) species. *Ref = KF reference probe signal.

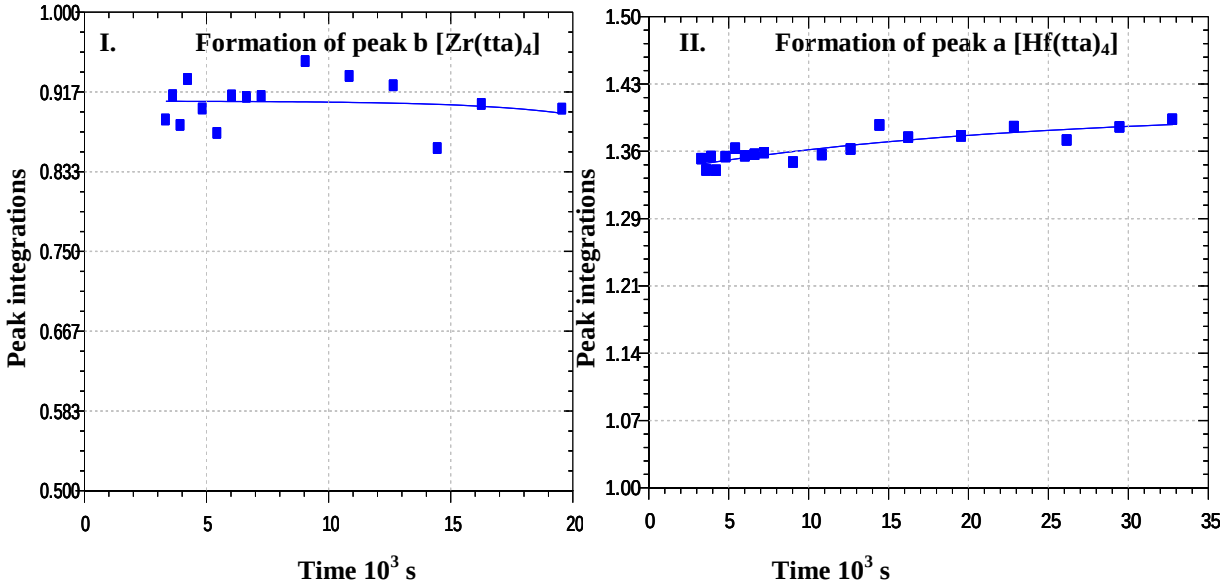

Figure 6.31: (I) ^{19}F-NMR peak intensity *vs* time data for the product formation [Zr(tta)$_4$] (b) second slow reaction [HfCl$_4$]= 0.043 M, [ZrCl$_4$] = 0.044 M, [Na(tta)] = 0.175 M k_{obs} = 9.3(2) x 10^{-5} s^{-1}.(II)^{19}F-NMR peak intensity *vs* time data for the product formation [Hf(tta)$_4$] (a) second reaction k_{obs} = 1.56(2) x 10^{-5} s^{-1}. Total time represented on Micromath Scientist plot is of the combined first fast reaction and the second slow

reaction. Total time represented on micromath scientist plot is of the combined first fast reaction and the second slow reaction.

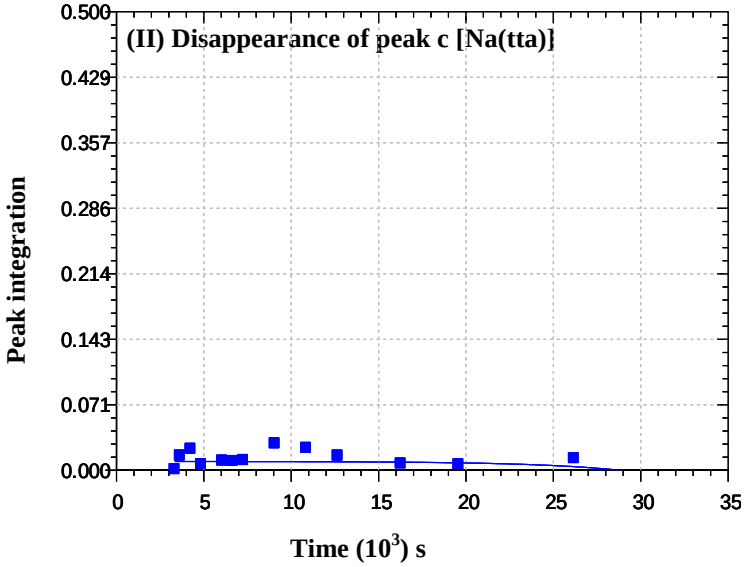

Figure 32. (II) ^{19}F-NMR peak intensity *vs* time data for second slow reaction, ligand consumption [$HfCl_4$]= 0.043 M, [$ZrCl_4$] = 0.044 M, [Na(tta)] = 0.175 M M k_{obs} = 2.25(3)x 10^{-4} s^{-1}. Total time represented on Micromath Scientist plot is of the combined first fast reaction and the second slow reaction. Total time represented on micromath scientist plot is of the combined first fast reaction and the second slow reaction.

A plot of the combined reactions, product formation of [$Zr(tta)_4$] peak (b) (blue block plot), [$Hf(tta)_4$] peak (a) (orange cross plot) and ligand consumption peak (c) (red block plot) was constructed of the peak integrations *vs* time data (Figure 6.33) of the second slow reaction.

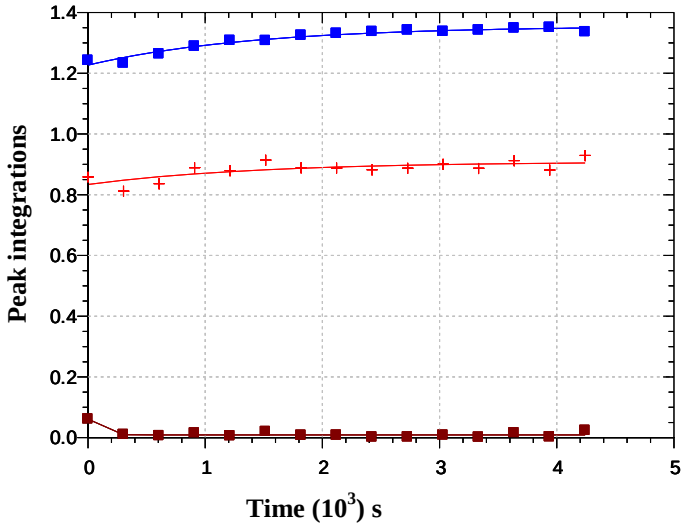

Figure 6.33: Combined scientist plots of ligand consumption and complex formation plots of the second slow reaction. [Zr] : [Na(tta)] = 0.5 : 0.5 : 2, Entry No. 1 (Table 6.1 (b)).

6.5.3 ^{19}F-NMR Kinetic Investigation of ([$ZrCl_4$] : [$HfCl_4$]) *vs* [Na(tta)] ([Zr]:[Hf]:[Na(tta)] = 0.5 : 0.5 : 4, first fast reaction)

The formation reaction of [$Hf(tta)_4$] and [$Zr(tta)_4$] in the competition study was followed by ^{19}F-NMR (repetitive scans illustrated in the stacked plot Figure 6.34). The figure is a graphical representation of the first rapid reaction that took place in the 1 : 4 reaction. A typical kinetic data plot was fitted as illustrated in Figure 6.35, (I) illustrates the product formation [$Zr(tta)_4$] and (II) illustrates the product formation of [$Hf(tta)_4$]. Figure 6.36 illustrates the ligand consumption of Na(tta) for the first rapid reaction. All of these plots were fitted in order to determine the observed rate constants, k_{obs}.

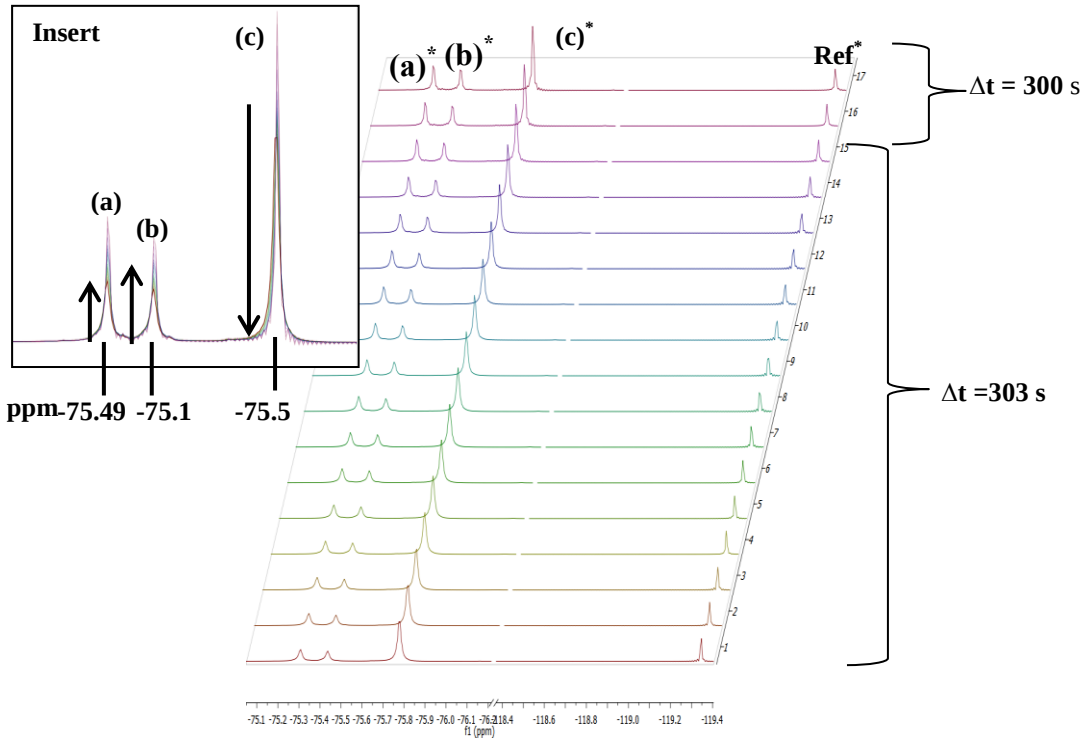

Figure 6.34: Observed stacked ^{19}F-NMR spectra illustrating the progression of the first fast reaction. Entry No. 2 (Table 6.1(b)) [Hf : Zr] : [Na(tta)] = 1 : 4, [$Hf(tta)_4$] formation peak (a) at -75.49 ppm, [$Zr(tta)_4$] formation peak (b) at -75.1 ppm and Na(tta) consumption at -75.5 ppm. [$HfCl_4$]= 0.043 M, [$ZrCl_4$]= 0.043 M, [Na(tta)] = 0.350 M, Temp = 20.0 ˚C, ligand and metal dissolved in DMF and spectra collected in deuterated Benzene (C_6D_6), total time of the first fast reaction = 5751 s Δt indicates the time between successive spectra. Insert: Superimposed ^{19}F-NMR spectra illustrating (a) formation of product [$Hf(tta)_4$], (b) formation of product [$Zr(tta)_4$] and (c) disappearance of ligand (Na(tta)).

***(a) Product formation for the hafnium(IV) species.**

***(b) Product formation for the zirconium(IV) species. *(c) Ligand consumption peak for the Na(tta).**

***Ref = KF reference probe signal.**

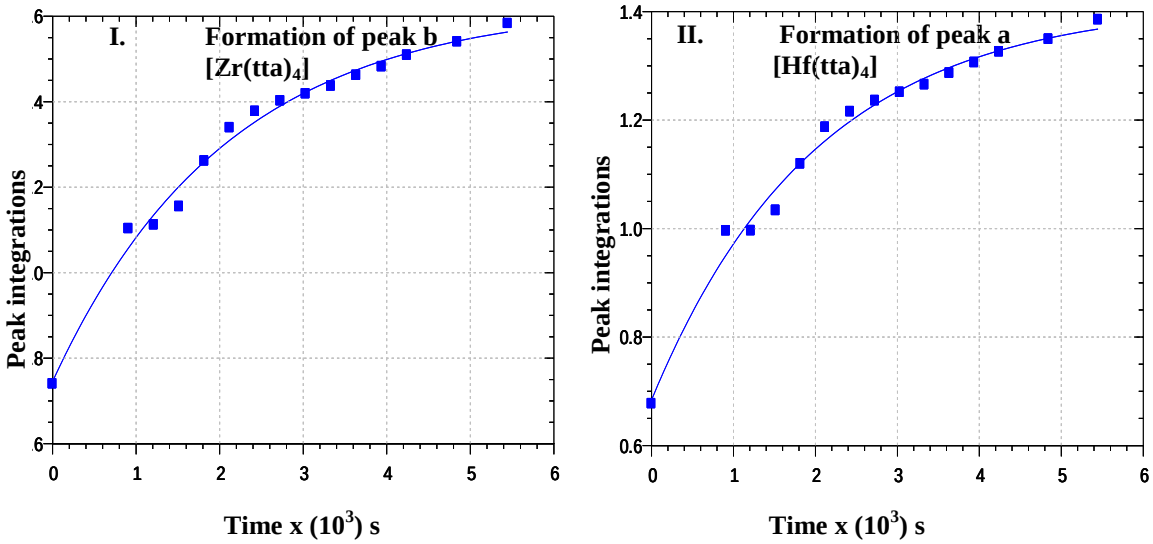

Figure 6.35: (I) ^{19}F-NMR peak intensity *vs* time data for the product formation [Zr(tta)$_4$] first fast reaction [HfCl$_4$]= 0.043 M, [ZrCl$_4$]= 0.043 M, [Na(tta)] = 0.350 M k_{obs} = 7.8(4) x (10^{-4}) s^{-1}. (II) ^{19}F-NMR peak intensity *vs* time data for the product formation [Hf(tta)$_4$] first reaction k_{obs} = 7.07(3) x (10^{-4}) s^{-1}. Total time represented on Micromath Scientist plot is of the combined first fast reaction and the second slow reaction.

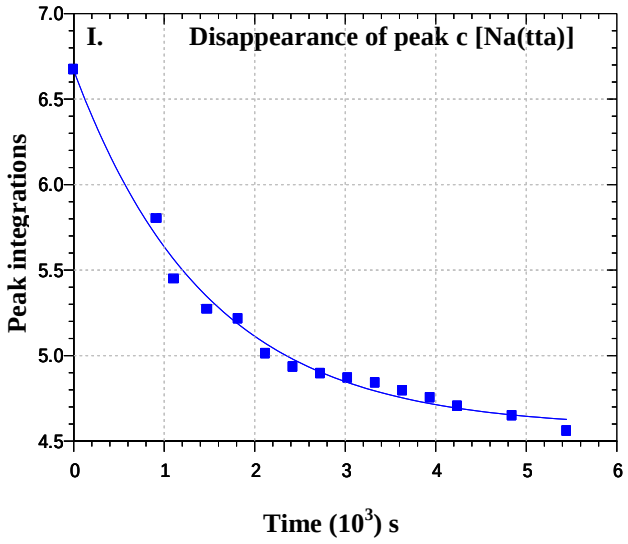

Figure 6.36: (I) ^{19}F-NMR peak intensity *vs* time data for ligand consumption of the first fast reaction, [HfCl$_4$]= 0.043 M, [ZrCl$_4$]= 0.043 M, [Na(tta)] = 0.350 M in benzene at 20.0°C k_{obs}= 6.27(4) x 10^{-4} s^{-1}. Total time represented on Micromath Scientist plot is of the combined first fast reaction and the second slow reaction.

6.5.4 ^{19}F-NMR Kinetic Investigation of ([$ZrCl_4$] + [$HfCl_4$]) *vs* [Na(tta)] ([Zr]:[Hf]:[Na(tta)] = 0.5 : 0.5 : 4, second slow reaction)

The formation reaction of [$Hf(tta)_4$] and [$Zr(tta)_4$] in the competition reaction was followed by ^{19}F-NMR (repetitive scans illustrated in the stacked plot Figure 6.37) Figure 3.7 is a graphical representation of the second slow reaction that took place in the 1 : 4 reaction. A typical kinetic data plot was fitted as illustrated by Figure 6.38 for (I) product formation of [$Zr(tta)_4$] and (II) product formation of [$Hf(tta)_4$] in order to determine the observed rate constant, k_{obs}. Figure 6.39 illustrates the ligand consumption of Na(tta) for the second reaction.

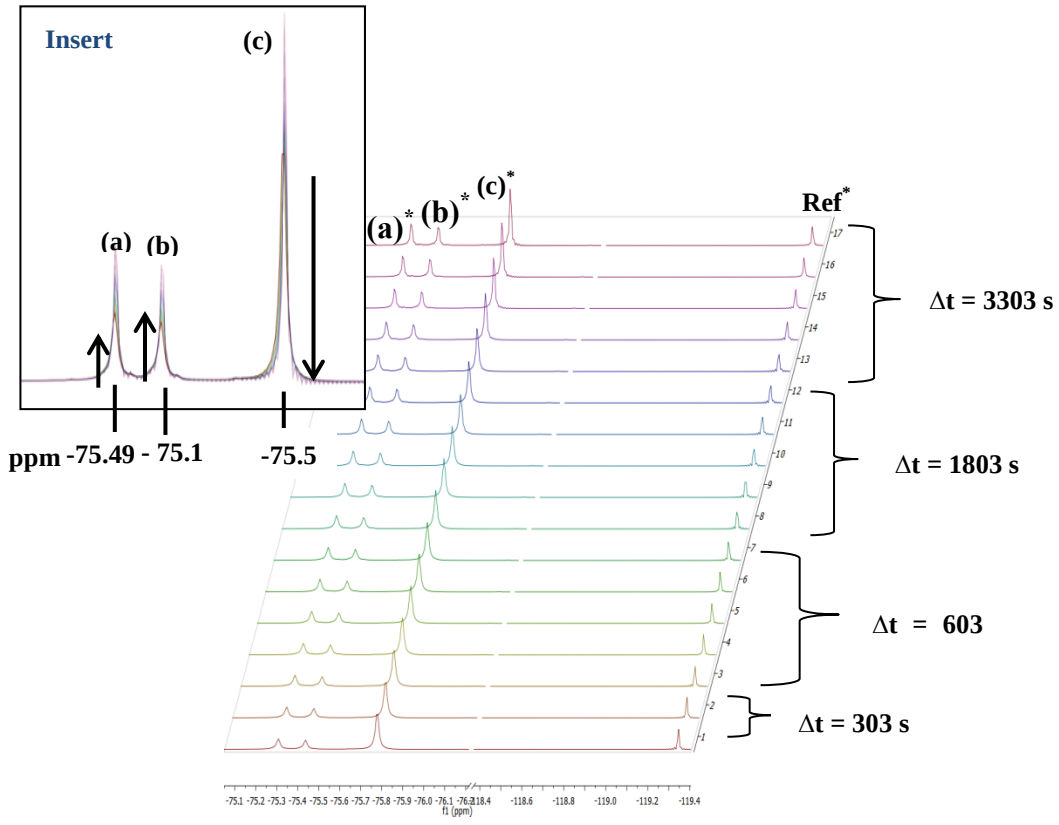

Figure 6.37: Observed stacked ^{19}F-NMR spectra illustrating the progression of the second slow reaction. Entry No. 2 (Table 6.1 (b)) [Hf : Zr] : [Na(tta)] = 1 : 4, [$Hf(tta)_4$] formation peak (a) at -75.49 ppm, [$Zr(tta)_4$] formation peak (b) at -75.1 ppm and Na(tta) consumption peak (c) at -75.5 ppm. [$HfCl_4$]= 0.043 M, [$ZrCl_4$]= 0.043 M, [Na(tta)] = 0.350, Temp = 20.0 ˚C, ligand and metal dissolved in DMF and spectra collected in deuterated benzene (C_6D_6), total time of the second slow reaction = 27039 s Δt indicates the time between successive spectra. Insert: Superimposed ^{19}F-NMR spectra illustrating (a) formation of product [$Hf(tta)_4$], (b) formation of product [$Zr(tta)_4$] and (c) disappearance of ligand (Na(tta)).
***(a) Product formation for the hafnium(IV) species . *(b) Product formation for the zirconium(IV) species. *(c) Ligand consumption peak for the Na(tta). *Ref = KF reference probe signal.**

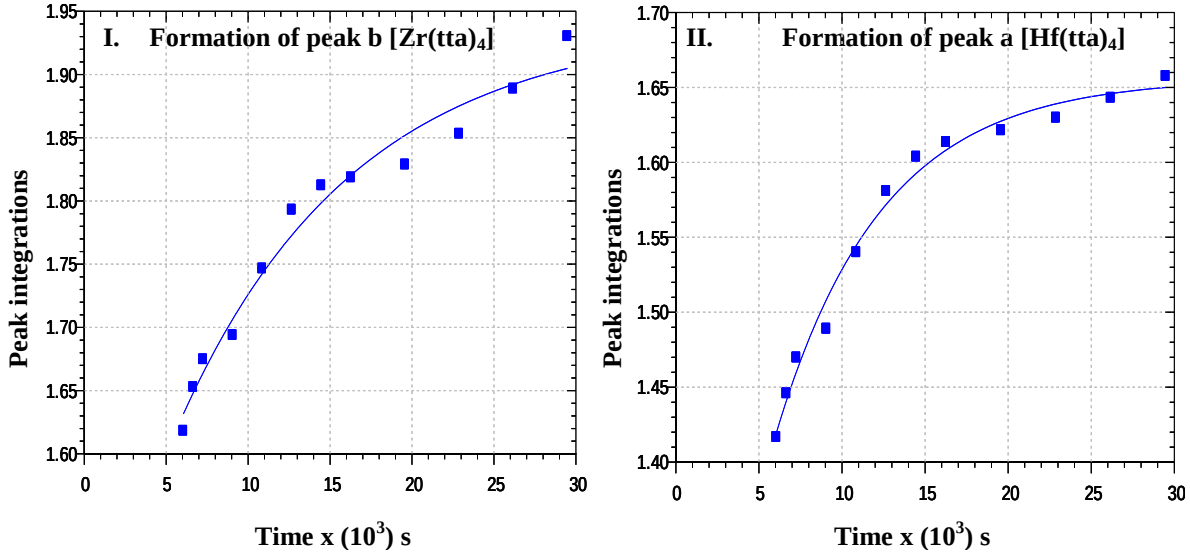

Figure 6.38: (I) ^{19}F-NMR peak intensity *vs* time data for the product formation of [Zr(tta)$_4$]second slow reaction [HfCl$_4$]= 0.043 M, [ZrCl$_4$]= 0.043 M, [Na(tta)] = 0.350k_{obs} = 2.4(4) x 10^{-3} s^{-1}.(II)^{19}F-NMR peak intensity *vs* time data for the product formation [Hf(tta)$_4$] second reaction k_{obs} = 2.85(4) x 10^{-3} s^{-1}. Total time represented on Micromath Scientist plot is of the combined first fast reaction and the second slow reaction

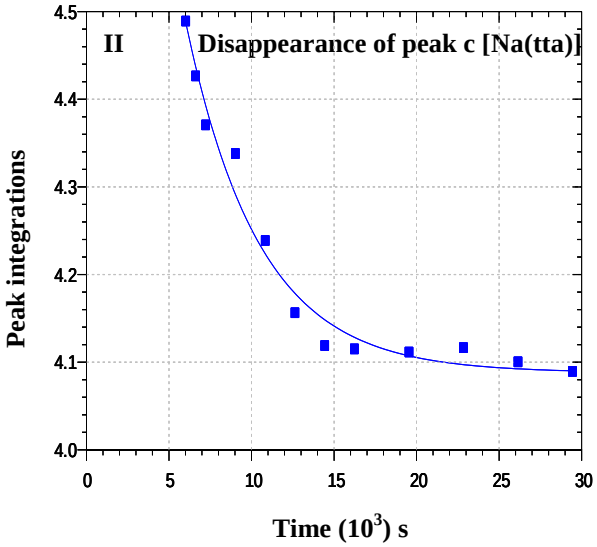

Figure 6.39: (II) ^{19}F-NMR peak intensity vs time data for second slow reaction ligand [HfCl$_4$]= 0.043 M, [ZrCl$_4$]= 0.043 M, [Na(tta)] = 0.350 k_{obs}= 1.01(3) x 10^{-3} s^{-1}. Total time represented on micromath scientist plot is of the combined first fast reaction and the second slow reaction

A plot of the combined reactions, product formation [Zr(tta)$_4$] (dark blue block plot), [Hf(tta)$_4$] (light blue circles plot) and ligand consumption (red block plot) (Figure 6.40) was constructed of the peak integrations *vs* time.

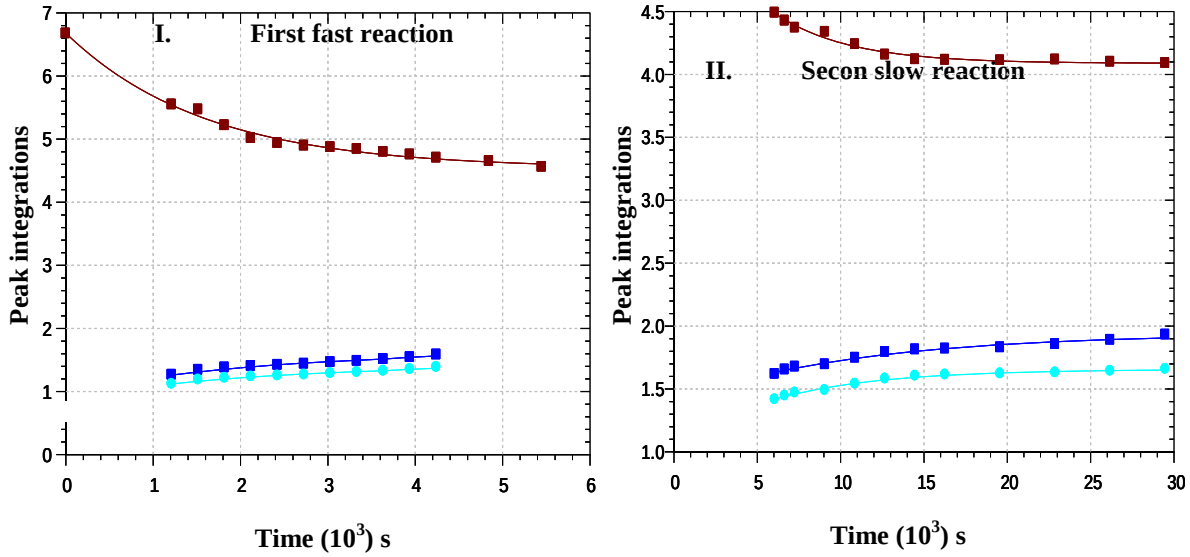

Figure 6.40: Combined scientist plots of ligand consumption and complex formation plots of (I) first fast reaction and (II) second slow reaction. [Zr(tta)4] (dark blue block plot), [Hf(tta)4] (light blue circles plot) and ligand consumption (red block plot).

6.5.5 ^{19}F-NMR Kinetic Investigation of ([$ZrCl_4$] + [$HfCl_4$]) *vs* [Na(tta)] ([Zr]:[Hf]:[Na(tta)] = 0.5 : 0.5 : 4.5, first fast reaction)

The formation reaction of [Hf(tta)$_4$] and [Zr(tta)$_4$] in the competition study was followed by ^{19}F-NMR (repetitive scans illustrated in the stacked plot Figure 6.41). Figure 6.41 is a graphical representation of the first rapid reaction that took place in the 1 : 4.5 reaction. A typical kinetic data plot was fitted as illustrated by (Figure 6.42 and Figure 43 for (I) product formation of [Zr(tta)$_4$] and (II) product formation of [Hf(tta)$_4$] and Figure 6.43 for the ligand consumption in order to determine the observed rate constant, k_{obs}.

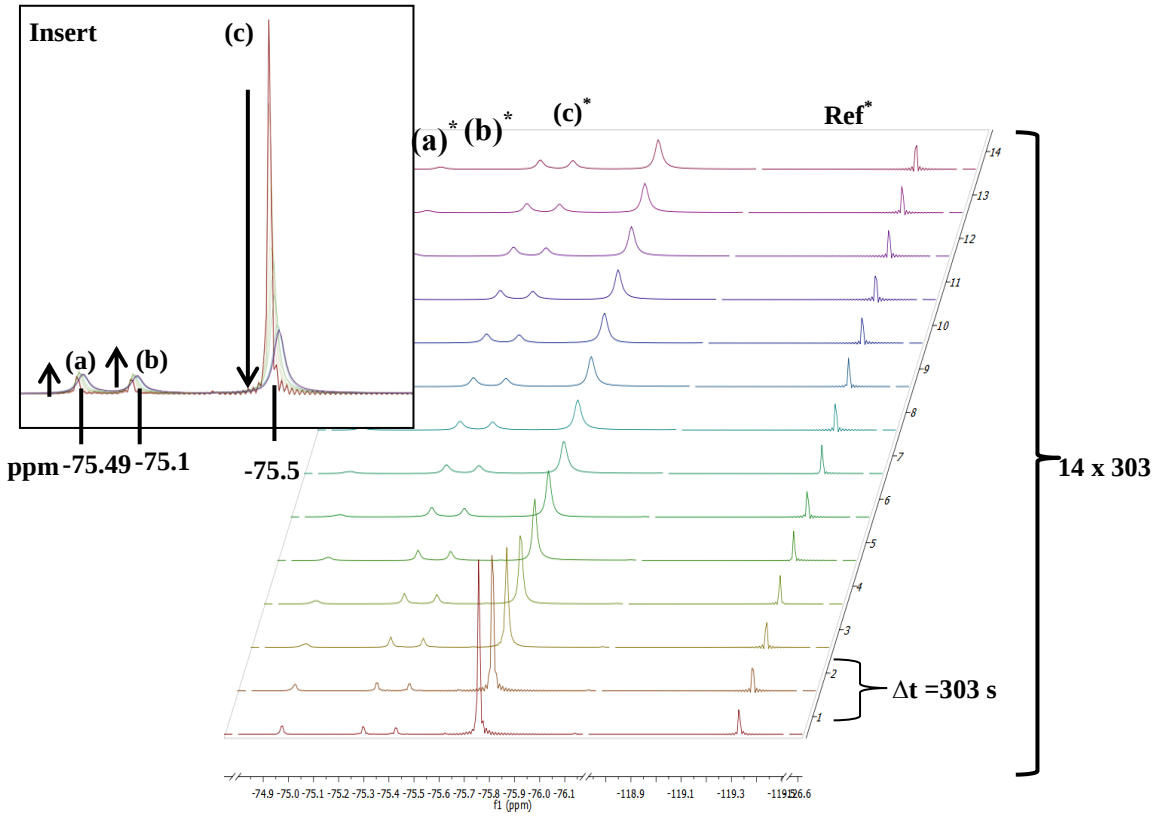

Figure 6.40: Observed stacked ^{19}F-NMR spectra illustrating the progression of the first fast reaction. Entry 3, (Table 6.1(b)) [Hf : Zr] : [Na(tta)] = 0.5 : 0.5 : 4.5, [Hf(tta)$_4$] formation at peak (a) -75.49 ppm, [Zr(tta)$_4$] formation peak (b) at -75.1 ppm and Na(tta) consumption peak (c) at -75.5 ppm. [HfCl$_4$]= 0.043 M, [ZrCl$_4$] = 0.043 M, [Na(tta)] = 0.390 M, Temp = 20.0 ˚C, ligand and metal dissolved in DMF and spectra collected in deuterated bezene (C_6D_6), total time of the first fast reaction = 4242 s Δt indicates the time between successive spectra. Insert: Superimposed ^{19}F-NMR spectra illustrating (a) formation of product [Hf(tta)$_4$], formation of product [Zr(tta)$_4$] and (c) disappearance of ligand (Na(tta)).
***(a) Product formation for the hafnium(IV) species . *(b) Product formation for the zirconium(IV) species.**
***(c) Ligand consumption peak for the Na(tta). *Ref = KF reference probe signal.**

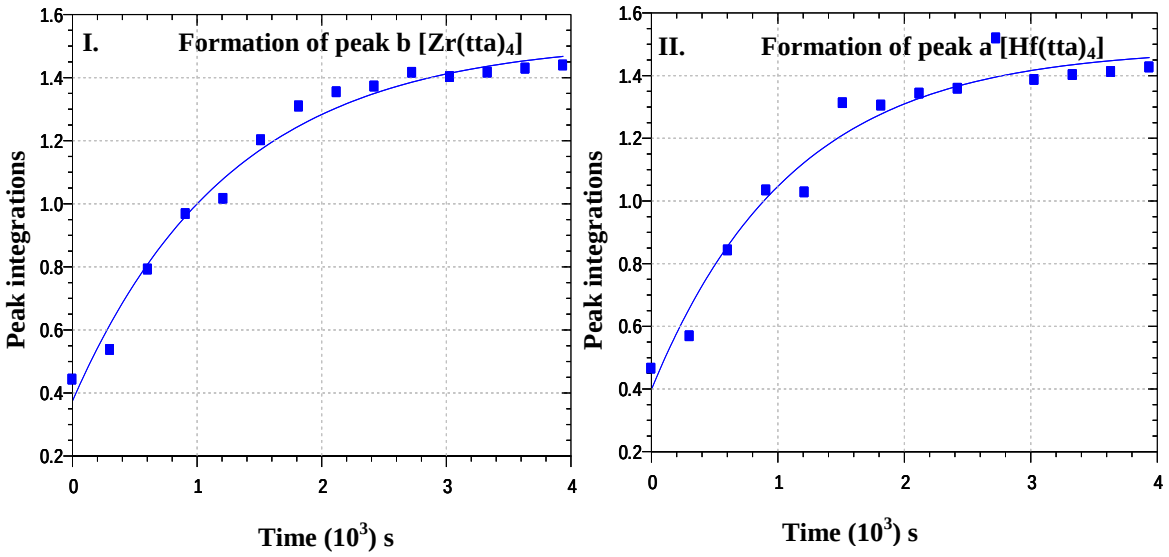

Figure 6.42: (I) ^{19}F-NMR peak intensity *vs* time data for product formation of [Zr(tta)$_4$], first fast reaction [HfCl$_4$]= 0.043 M, [ZrCl$_4$] = 0.043 M, [Na(tta)] = 0.390 M, k_{obs} = 7.9(4) x 10^{-3} s^{-1}.(II)^{19}F-NMR peak intensity *vs* time data for product formation of [Hf(tta)$_4$], first fast reaction k_{obs} = 9.04(4) x 10^{-3}s^{-1}. Total time represented on Micromath Scientist plot is of the combined first fast reaction and the second slow reaction.

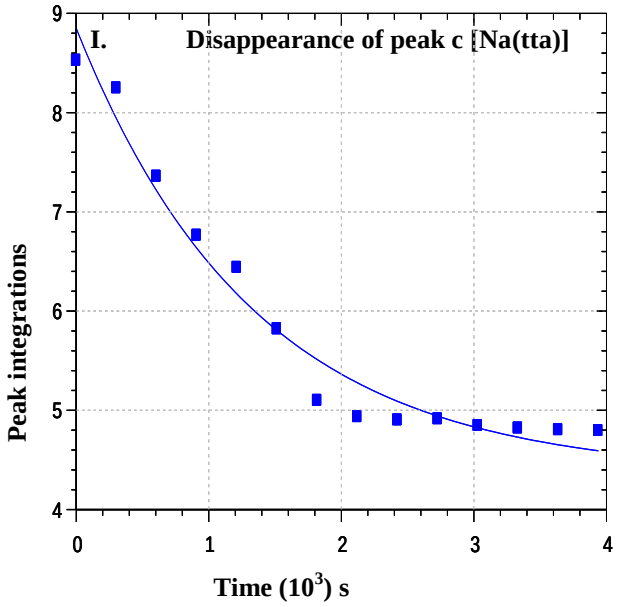

Figure 6.43: I.^{19}F-NMR peak intensity *vs* time data for the ligand consumption [Na(tta)] of the first fast reaction, [$HfCl_4$]= 0.043 M, [$ZrCl_4$] = 0.043 M, [Na(tta)] = 0.390 M k_{obs} = 7.74(4) x 10^{-3} s^{-1}. Total time represented on micromath scientist plot is of the combined first fast reaction and the second slow reaction

6.5.6 ^{19}F-NMR Kinetic Investigation of ([$ZrCl_4$] : [$HfCl_4$]) *vs* [Na(tta)]) ([Zr]:[Hf]:[Na(tta)] = 0.5 : 0.5 : 4.5, second slow reaction)

The formation reaction of [$Hf(tta)_4$] and [$Zr(tta)_4$] in the competition study was followed by ^{19}F-NMR (repetitive scans illustrated in the stacked plot Figure 6.44). Figure 6.44 is a graphical representation of the second slow reaction that took place in the 1 : 4.5 reaction. A typical kinetic data plot was fitted as illustrated by Figure 6.45 for (I) product formation of [$Zr(tta)_4$] and (II) product formation of [$Hf(tta)_4$] in order to determine the observed rate constant, $k_{obs.}$

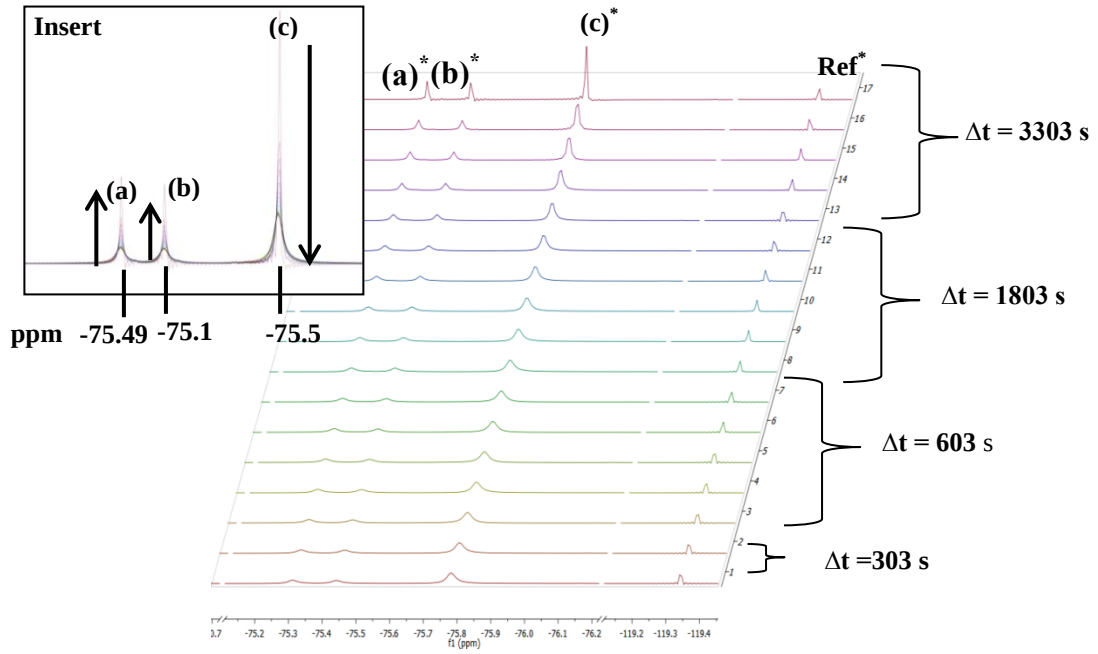

.

Figure 6.44: Observed stacked ^{19}F-NMR spectra illustrating the progression of the second slow reaction. Entry 3, Table 6.1(b) [Hf : Zr] : [Na(tta)] = 0.5: 0.5 : 4.5, [Hf(tta)$_4$] formation peak (a) at -75.49 ppm, [Zr(tta)$_4$] formation peak (b) at -75.1 ppm and Na(tta) consumption peak (c) at -75.5 ppm. [HfCl$_4$]= 0.043 M, [ZrCl$_4$] = 0.043 M, [Na(tta)] = 0.390 M, Temp = 20.0 ˚C, ligand and metal salt dissolved in DMF and spectra collected in deuterated benzene (C$_6$ D$_6$), total time of the second reaction = 29757 s Δt indicates the time between successive spectra. Insert: Superimposed ^{19}F-NMR spectra illustrating (a) formation product [Hf(tta)$_4$], formation of product [Zr(tta)$_4$] and (c) disappearance of ligand (Na(tta)).
***(a) Product formation for the hafnium(IV) species . *(b) Product formation for the zirconium(IV) species. *(c) Ligand consumption peak for the Na(tta). *Ref = KF reference probe signal**

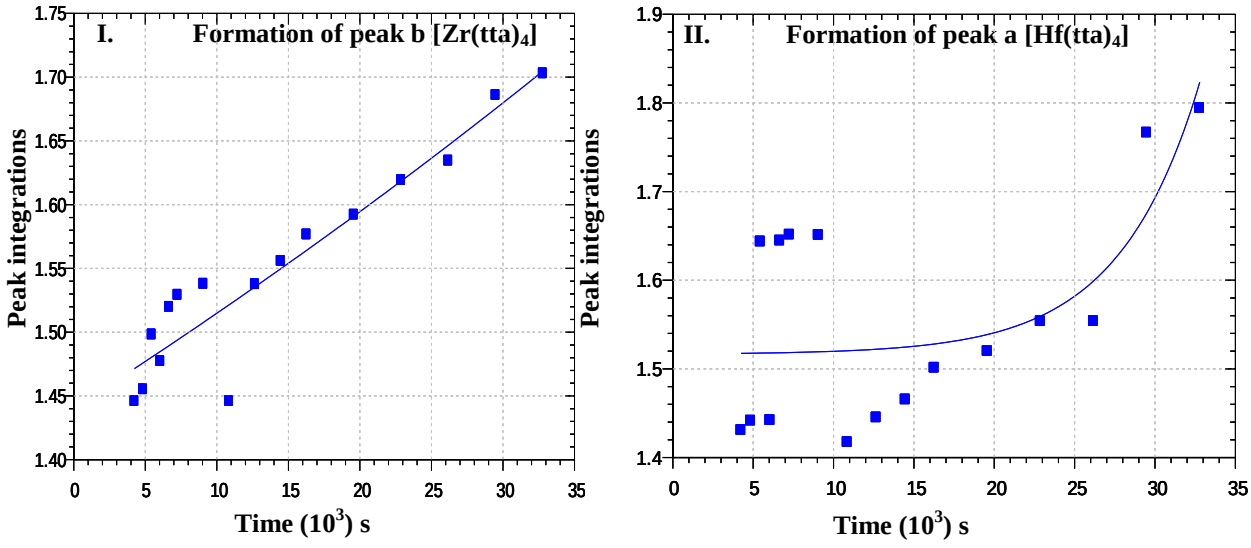

Figure 6.45: (I) ^{19}F-NMR peak intensity *vs* time data for product formation [Zr(tta)$_4$] second slow reaction [HfCl$_4$]= 0.043 M, [ZrCl$_4$] = 0.043 M, [Na(tta)] = 0.390 M k_{obs} = 4.82(4) x 10^{-3} s^{-1}. (II) ^{19}F-NMR peak intensity *vs* time data for product formation [Hf(tta)$_4$] second reaction, k_{obs} = 4.9(4) x 10^{-3} s^{-1}. Total time represented on Micromath Scientist plot is of the combined first fast reaction and the second slow reaction.

A plot of the combined reactions, product formation of [Zr(tta)$_4$] (blue block plot), [Hf(tta)$_4$] (orange cross plot) and ligand consumption (red circles in plot I. and red block in plot II.) (Figure 6.46) has been constructed of the peak integrations *vs* time.

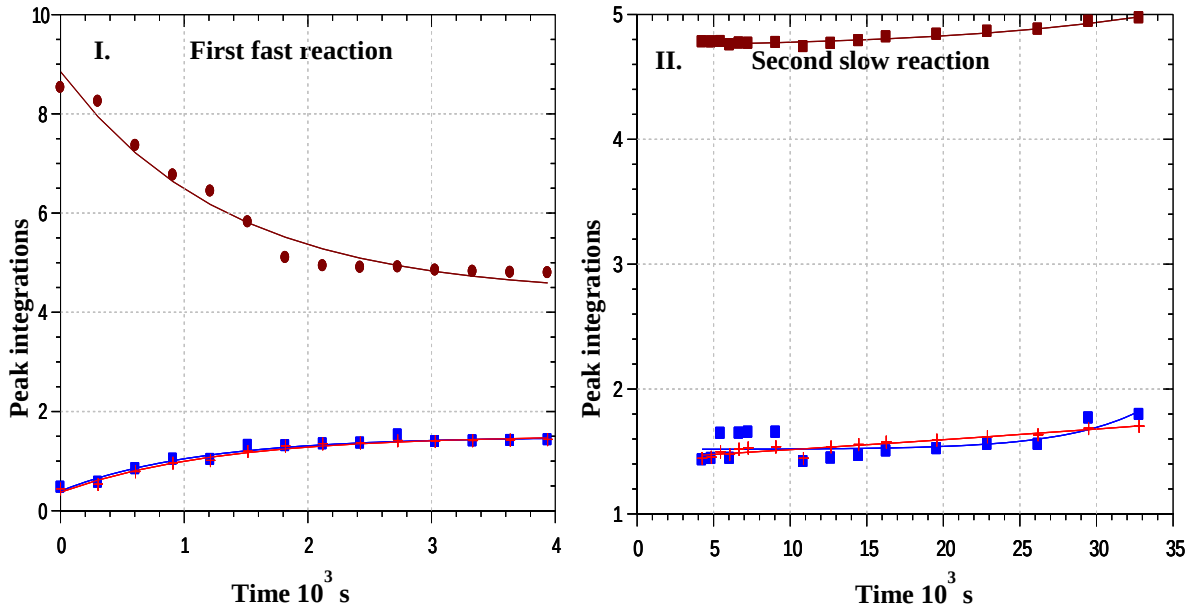

Figure 6.46: ^{19}F-NMR peak intensity *vs* time data for product formation of [Zr(tta)$_4$] and [Hf(tta)$_4$] and ligand consumption for the first fast reaction (I) and the second slow reaction (II). [Hf : Zr] : [Na(tta)] = 0.5: 0.5 : 4.5Entry 3, Table 6.1(b)

6.5.7 ^{19}F-NMR Kinetic Investigation of ([ZrCl$_4$] + [HfCl$_4$]) *vs* [Na(tta)] ([Zr]:[Hf]:[Na(tta)] = 0.5 : 0.5 : 5, first fast reaction)

The formation reaction of [Hf(tta)$_4$] and [Zr(tta)$_4$] in the competition study, was followed by ^{19}F-NMR (repetitive scans illustrated in the stacked plot Figure 6.47) Figure 6.47 is a graphical representation of the first rapid reaction that took place in the 1 : 5 reaction. A typical kinetic data plot was fitted as illustrated in Figure 6.48 for (I) product formation [Zr(tta)$_4$] and (II) the product formation of [Hf(tta)$_4$] and Figure 6.49 for ligand consumption of the first rapid reaction, in order to determine the observed rate constant, k_{obs}.

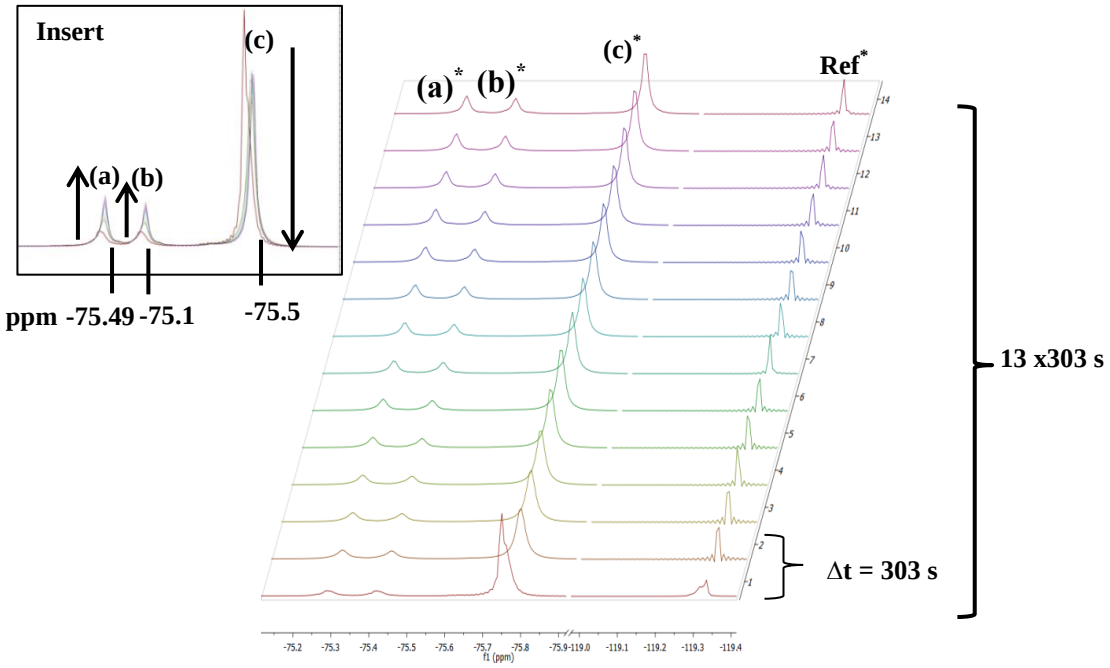

Figure 6.47: Observed stacked ^{19}F-NMR spectra illustrating the progression of the fast reaction. Entry 4 (Table 6.1(b)) [Hf : Zr] : [Na(tta)] = 0.5: 0.5 : 2, [Hf(tta)$_4$] formation peak (a) at -75.49 ppm, [Zr(tta)$_4$] formation peak (b) at -75.1 ppm and Na(tta) consumption peak (c) at -75.5 ppm. [HfCl$_4$]= 0.043 M, [ZrCl$_4$]= 0.044 M, [Na(tta)] = 0.435 M, Temp = 20.0 ˚C, ligand and metal dissolved in DMF and spectra collected in deuterated benzene (C_6D_6), total time of the first reaction = 3939 s Δt indicates the time between successive spectra.Insert: Superimposed ^{19}F-NMR spectra illustrating (a) formation of product [Hf(tta)$_4$], (b) formation of product [Zr(tta)$_4$] and (c) disappearance of ligand (Na(tta)).
***(a) Product formation for the hafnium(IV) species . *(b) Product formation for the zirconium(IV) species.**
***(c) Ligand consumption peak for the Na(tta). *Ref = KF reference probe signal.**

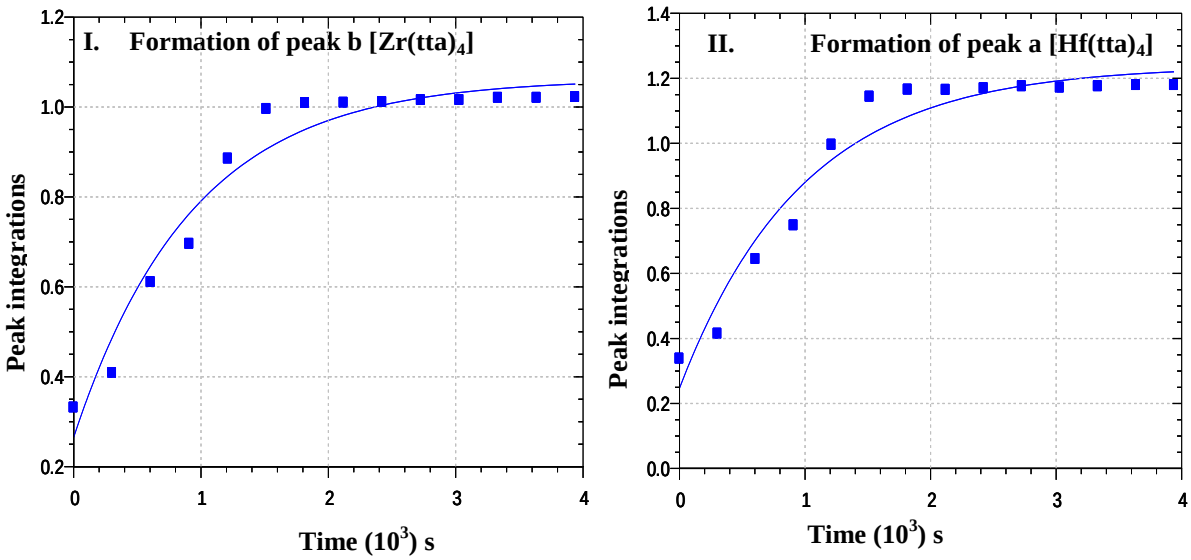

Figure 6.48: (I) ^{19}F-NMR peak intensity *vs* time data for product formation of [Zr(tta)$_4$] first fast reaction [HfCl$_4$]= 0.043 M, [ZrCl$_4$]= 0.044 M, [Na(tta)] = 0.435 M k_{obs} = 4.82(4) x 10^{-3} s^{-1}. II.^{19}F-NMR peak intensity *vs* time data for product formation of [Hf(tta)$_4$] for the first reaction, k_{obs}= 4.9(4) x 10^{-3} s^{-1}. Total time represented on Micromath Scientist plot is of the combined first fast reaction and the second slow reaction.

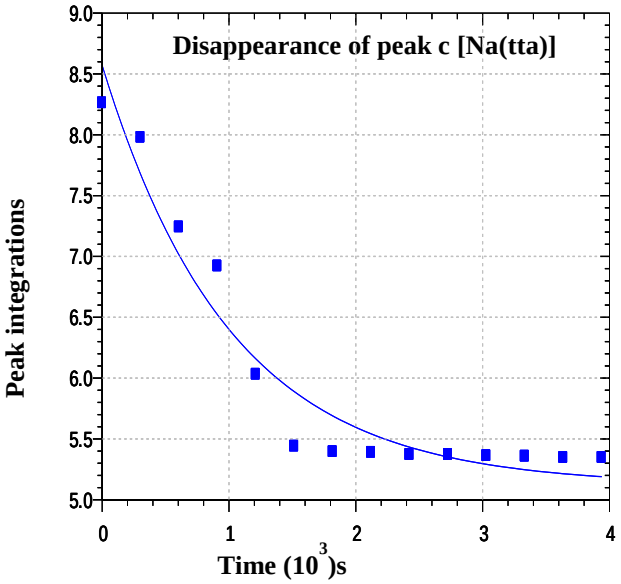

Figure 6.49: ^{19}F-NMR peak intensity *vs* time data for ligand consumption of the first fast reaction, [$HfCl_4$]= 0.043 M, [$ZrCl_4$]= 0.044 M, [Na(tta)] = 0.435 M in benzene at 20°C, k_{obs}= 7.47(1) x 10^{-5}. Total time represented on micromath scientist plot is of the combined first fast reaction and the second slow reaction

6.5.8 ^{19}F-NMR Kinetic Investigation of ([$ZrCl_4$] : [$HfCl_4$]) *vs* [Na(tta)] ([Zr]:[Hf]:[Na(tta)] = 0.5 : 0.5 : 5) (second slow reaction)

The formation reaction of [$Hf(tta)_4$] and [$Zr(tta)_4$] in the competition was followed by ^{19}F-NMR (repetitive scans illustrated in the stacked plot Figure 6.50) Figure 6.50 is a graphical representation of the second slow reaction that took place in the 1 : 5 reaction. A typical kinetic data plot was fitted as illustrated in Figure 6.51 for (I) the product formation of [$Zr(tta)_4$] and (II) the product formation of [$Hf(tta)_4$] in order to determine the observed rate constant, k_{obs}.

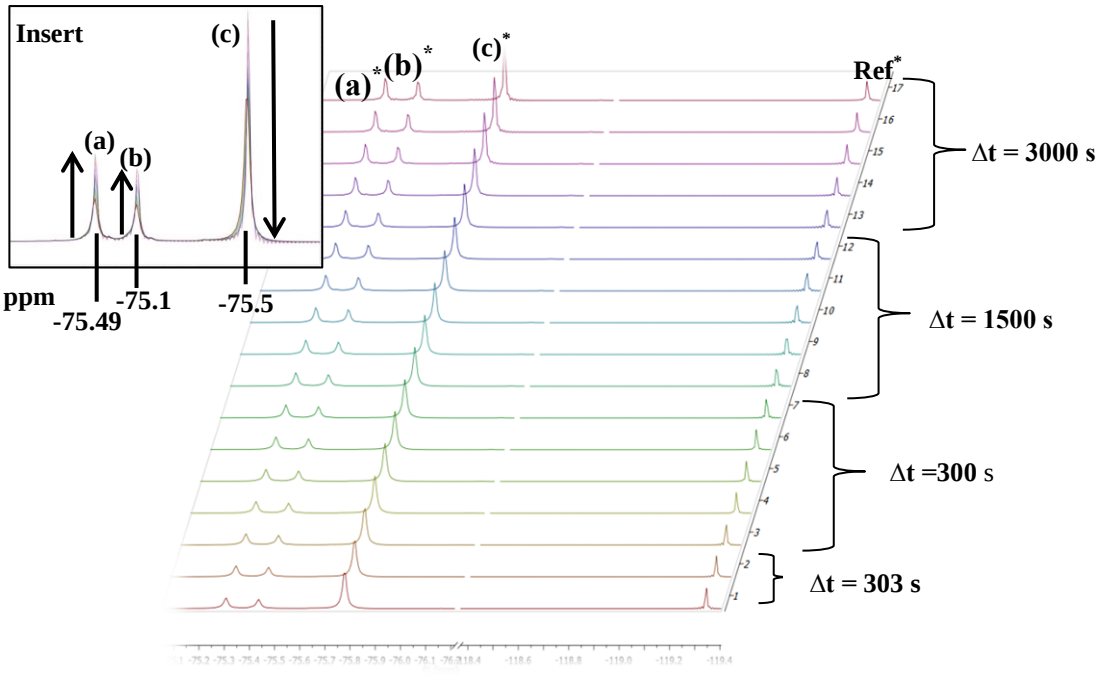

Figure 6.50: Observed stacked ^{19}F-NMR spectra illustrating the progression of the second slow reaction. Entry No. 4 (Table 6.1 (b))[Hf : Zr] : [Na(tta)] = 0.5: 0.5 : 5, [Hf(tta)$_4$] formation peak (a) at -75.49 ppm, [Zr(tta)$_4$] formation peak (b) at -75.1 ppm and Na(tta) consumption -75.5 ppm. [HfCl$_4$]= 0.043 M, [ZrCl$_4$]= 0.044 M, [Na(tta)] = 0.435. Temp = 20.0 ˚C, ligand and metal dissolved in DMF and spectra collected in deuterated benzene (C$_6$D$_6$), total time of the second slow reaction = 30363 s, Δt indicates the time between successive spectra. Insert Superimposed ^{19}F-NMR spectra illustrating (a) formation product [Hf(tta)$_4$], (b) formation of product [Zr(tta)$_4$] and (c) disappearance of ligand (Na(tta)).
***(a) Product formation for the hafnium(IV) species . *(b) Product formation for the zirconium(IV) species.**
***(c) Ligand consumption peak for the Na(tta). *Ref = KF reference probe signal.**

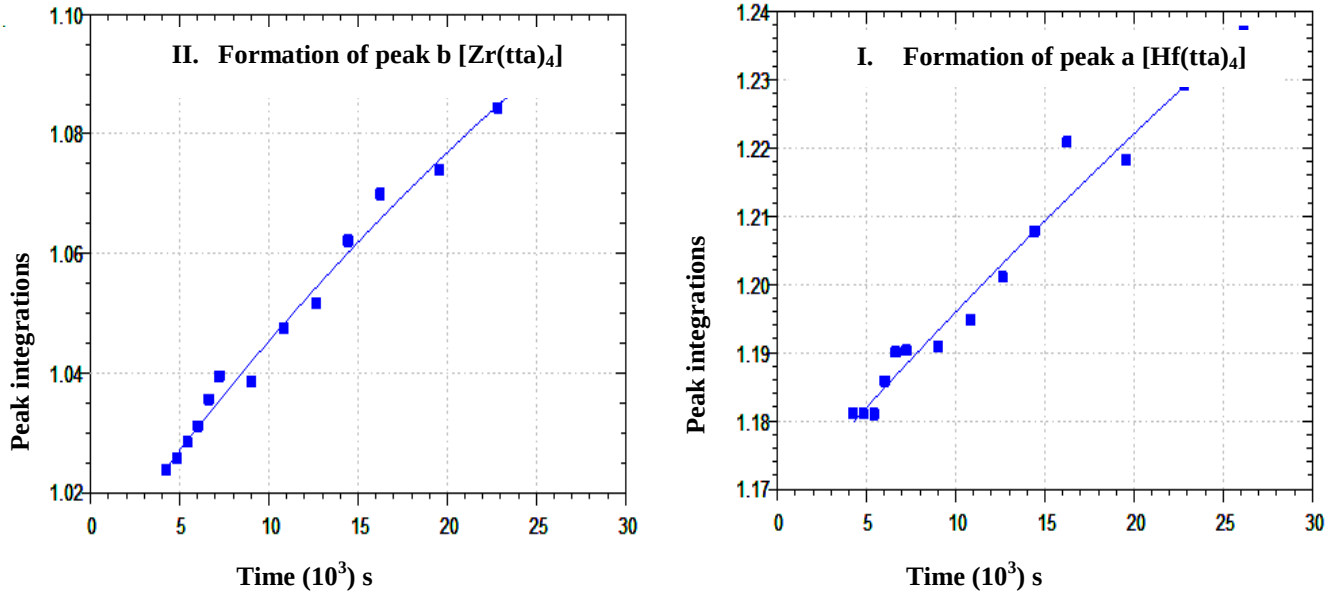

Figure 6.51: (I) ^{19}F-NMR peak intensity *vs* time data for the product formation of the second reaction, [HfCl$_4$]= 0.043 M, [ZrCl$_4$]= 0.044 M, [Na(tta)] = 0.435. in benzene at 20.0°C, k_{obs}= 2.0(1) x 10^{-5} (II) ^{19}F-NMR peak intensity *vs* time data for product formation of the second reaction [HfCl$_4$] = 7.75 x 10^{-3}, k_{obs} = 8.9(2) x 10^{-5} s^{-1}, in benzene at 20.0 °C. Total time represented on Micromath Scientist plot is of the combined first fast reaction and the second slow reaction.

A plot of the combined reactions, product formation of $[Zr(tta)_4]$ (blue block plot), $[Hf(tta)_4]$ and (orange cross plot) and the ligand consumption (red block plot) (Figure 6.51) has been constructed of the peak integrations *vs* time.

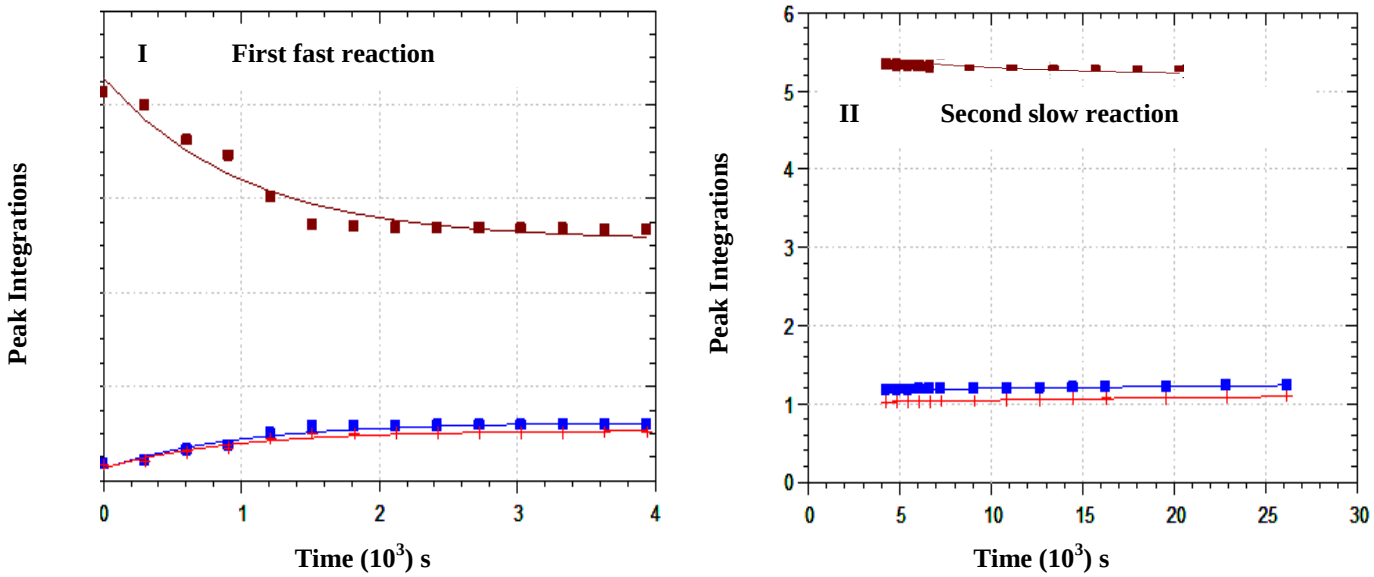

Figure 6.52: ^{19}F-NMR peak intensity *vs* time data for product formation $[Zr(tta)_4]$ and $[Hf(tta)_4]$ and ligand consumption for the first fast reaction (I) and the second slow reaction (II). [Hf : Zr] : [Na(tta)] = 0.5: 0.5 : 5 Entry 4, Table 6.1(b).

6.6 Summary of Rate data and Conclusion

Table 6.3 and Table 6.4 summarize the rate data for all the kinetic experiments that were performed in the study.

Table 6.3 : List of concentrations used for preliminary kinetic studies for the formation of tetrakis(thenoyltrifluoroacetylacetonato)zirconium(IV) and tetrakis(thenoyltrifluoroacetylacetonato) hafnium(IV) and calculated observed rate constants.

Entry No	k_{obs} $[Zr(tta)_4]$ Form.[b] $s^{-1} \times 10^3$	k_{obs} $[Hf(tta)_4]$ Form.[b] $s^{-1} \times 10^3$	[Metal] M	[Na(tta)] M	k_{obs} (Na(tta)) CONS.[a] 10^3	[M] : [tta]
1(FR)*	1.5(9)	-	0.118	0.481	1.08(9)	1 : 4
1(SR)*	0.29(6)	-	0.118	0.481	0.19(6)	1 : 4
2(FR)	0.64(6)	-	0.119	0.596	0.71(6)	1 : 5
2(SR)	0.28(3)	-	0.119	0.596	0.17(2)	1 : 5
3(FR)	0.053(1)	-	0.095	0.385	0.049(1)	1 : 4
3(SR)	0.019(3)	-	0.095	0.385	0.011(3)	1 : 4
4(FR)	-	3.7(8)	0.0869	0.347	3.2(2)	1 : 4
4(SR)	-	2.9(1)	0.0869	0.347	2.0(1)	1 : 4
5(FR)	-	1.4(1)	0.0855	0.435	1.8(1)	1 : 5
5(SR)	-	1.07(1)	0.0885	0.435	1.0(1)	1 : 5

*FR= (Fast reaction) SR= (Slow reaction)

a. CONSP. = Consumption of ligand.

b. Form = Formation of product.

Table 6.4: Rate data for the competition studies between ([$ZrCl_4$] + [$HfCl_4$]) and Na(tta).

Entry No	k_{obs} [$Zr(tta)_4$] form. 10^3	k_{obs} [$Hf(tta)_4$] form. 10^3	[Metal] M $ZrCl_4$;$HfCl_4$	[Na(tta)] M	k_{obs} [Na(tta)] Cons. 10^3	[M] : [Na(tta)]	Integ.[a] Values Zr;Hf;Ligand
1(FR)*	0.48(3)	0.49(3)	49.6 ; 48.8	197	0.062(4)	0.5: 0.5: 2	0.8 ; 1.3
1(SR)*	9.3(3)	1.56(2)	49.6 ; 48.8	197	0.062(4)	0.5: 0.5: 2	1.40 ; 0.84
2(FR)	0.09(2)	0.015(2)	49.6 ; 48.8	197	0.022(3)	0.5: 0.5: 4	1.00 ; 2.50
2(SR)	2.4(4)	2.85(4)	49.6 ; 48.8	197	0.022(3)	0.5: 0.5: 4	1.94 ; 1.70
3(FR)	0.78(4)	0.70(3)	48.8 ; 48.9	394	0.062(7)	0.5: 0.5: 4.5	0.55 ; 3.03
3(SR)	4.88(4)	4.9(4)	48.8 ; 48.9	394	0.062(7)	0.5: 0.5: 4.5	1.84 ; 1.74
4(FR)	0.24(4)	0.28(4)	48.8 ; 48.9	394	0.10(1)	0.5: 0.5: 5	0.66 ; 1.8
4(SR)	2.0(1)	8.9(2)	48.8 ; 48.9	394	0.10(1)	0.5: 0.5: 5	1.32 ; 1.14

*FR= (Fast reaction) *SR= (Slow reaction)
a. Integration of the last spectrum for the respective peak, Zr = [$Zr(tta)_4$] formation peak and Hf = [$Hf(tta)_4$] formation peak

In general, the observed rate constant is the same for [$HfCl_4$] and [$ZrCl_4$] in the first reaction. In the second reaction it is about 7 times faster favoring [$HfCl_4$].

The kinetic data obtained from ^{1}H-NMR experiments do not completely agree with the above data (Entry 3 in Table 6.1a). This is possibly due to the fast reaction that the changes in the spectra was not clearly identifiable as in the ^{19}F-NMR spectra.

The competition studies between [$HfCl_4$] and [$ZrCl_4$] yielded interesting results. The observed rate constants for both the fast and slow reactions were comparable in each case and do not reflect the observations made in the paragraph above. The hafnium(IV) complex are favored over the zirconium complex by about 10%, with even 30% at lower [tta]. However the integration values of the final spectra shows that slightly more [$Zr(tta)_4$] than [$Hf(tta)_4$] formed. This information yields exciting prospects for future separation studies.

This preliminary study indicates strongly that there are small differences in the way that the Hf and Zr complexes with Na(tta) as ligand are formed. A detailed mechanistic study by ^{19}F-NMR

and an internal standard (Ref in the spectra) would shed more light on the intimate mechanisms of these reactions and also the equilibria that exist when competition studies are conducted.
To our knowledge, this is the first study of its kind where ^{19}F-NMR was employed to evaluate the kinetics of Hf(IV) and Zr(IV) competition reactions.

The following observations and conclusions can be made from the previous paragraphs and table 6.3 and 6.4 for the reactions between [$HfCl_4$], [$ZrCl_4$] and Na(tta) as well as the competition studies.

- The starting materials and formed complexes were characterized with ^{19}F-NMR and ^{1}H-NMR.
- ^{19}F-NMR and ^{1}H-NMR kinetic studies were conducted in this chapter; they proved to be more accurate since the UV/Vis kinetic studies that were attempted were inconclusive.
- Valuable information was gathered from the NMR kinetic experiments with regards to the coordination mechanism, competition studies and the changes that occurred over time of the two metal complexes (zirconium and hafnium).
- The external probe, a reference solution of potassium fluoride was used with some success. This is not the ideal way to conduct kinetic studies, because the position of the probe in the NMR tube will not be the same in each case. However, the foundation for future in depth studies have been laid.
- Two reactions were observed for the reactions between both [$ZrCl_4$] and [$HfCl_4$] with Na(tta). The overall observed rate constants, k_{obs}, as observed by ^{19}F-NMR spectroscopy varied between 0.64(6) x 10^{-3} s^{-1} and 1.5(9) x 10^{-3} s^{-1} for the fast reaction and between 0.28(2) x 10^{-3} s^{-1} and 0.29(3) x 10^{-3} s^{-1} for the slow reaction when [$ZrCl_4$] was the starting material. For [$Hf(Cl)_4$] the variations were between 1.4(1) x 10^{-3} s^{-1} and 3.7 x 10^{-3} s^{-1} for the fast reaction and between 1.2(1) x 10^{-3} s^{-1} and 1.07(1) x 10^{-3} s^{-1} for the slow reaction.
- In general, the rate of formation of the resonance spectra for the formed complexes agrees well with the rate of disappearance of the ligand resonance spectra.

7 Evaluation of Study

7.1 Evaluation and Perspective of Study

The study was another step forward towards comprehending the intricate chemistry exhibited by zirconium and hafnium. The aim was to spectroscopically study the behaviour of these two metals individually and together. Hafnium and zirconium complexes with a *O,O'*-bidentate ligand coordinated to it was synthesized and characterised using XRD, UV/Vis spectroscopy, IR spectroscopy and NMR spectroscopy. This allowed for identifying possible subtle differences between the two complexes in solid state. It also allowed for certain predictions and explanations to be made in the solution study. ^{1}H-NMR and ^{19}F-NMR were used to follow the formation kinetics of these complexes. The ultimate goal of these efforts was to contribute to the very limited information available and to the development of a novel, economically viable and environmentally friendly separation method for zirconium and hafnium.

The aim to conduct a spectroscopic mechanistic study of zirconium(IV) and hafnium(IV) complexes was successful, bearing in mind that this was a preliminary mechanistic study. A significant amount of information was obtained from this study, with regards to how these metals behave at varying initial ratios between metal and the ligand. It should also be stressed that with this new information gained, many questions are raised that will need to be answered in the future. As expected there were many similarities between the two compounds. But some significant differences were identified which makes the future of separating these two metals brighter.

The crystal structure of $[Zr(tta)_4].H_2O$ was successfully obtained and characterised (see Chapter 5). Its counterpart $[Hf(tta)_4]$ was also successfully synthesised but unfortunately the solid state characterization *via* XRD was unsuccessful due to continuous decomposition and instability of the crystalline compound.

The competition studies showed that there is a slight difference in the rate of the reaction. It also showed that the formation of the respective products could be traced and quantified. Keeping in

mind that the kinetic investigations were only preliminary, more work is needed for further comprehension of this complex system so that the reaction can be fine-tuned to optimize the ligand selectivity of this reaction.

This study was successful in meeting the basic aims that were stipulated in the introductory chapter.

7.2 Future Research

To complete this preliminary study, recommendations based on the results obtained are listed as follows:

- To perform ^{1}H-NMR and possibly ^{13}C-NMR kinetic studies at the same ratios as was performed in the current study.
- To seek methods to grow good quality crystals and also to find conditions under which the synthesized complexes can be stored to avoid decomposition. This will in turn result in a successful comparison of the respective zirconium(IV) and hafnium(IV) complexes.
- Tailoring of other ligand systems that will prove more effective in achieving what was aimed for in the current study, without precipitation during formation reactions. This will lead to more accurate integration values to be determined and consistent Micromath plots with the rate constants.
- Ultimately all the findings gathered through the parallel studies by M. Steyn and J. A. Viljoen and this current and future studies need to be aggregated and a separation method need to be developed.

APPENDIX

Table 1. Atomic coordinates (x 10^4) and equivalent isotropic displacement parameters ($Å^2$x 10^3) for $[Zr(tta)]\cdot H_2O$.

	x	y	z	U(eq)
Zr(1)	8747(1)	7199(1)	875(1)	32(1)
S(2)	8110(2)	2900(3)	1624(3)	68(1)
S(4)	9390(2)	2889(3)	210(3)	72(1)
S(3)	10138(2)	4382(3)	2374(2)	71(1)
S(1)	7322(2)	4486(4)	-627(3)	80(1)
C(3)	6836(4)	6319(9)	-1655(5)	37(2)
O(7)	9246(3)	5558(6)	365(4)	40(1)
O(4)	7831(4)	7896(6)	1324(5)	49(2)
O(5)	9371(3)	6435(6)	1790(4)	42(1)
O(3)	8241(3)	5581(6)	1379(4)	38(1)
O(8)	9665(3)	7910(6)	443(5)	45(2)
O(6)	8961(4)	8768(7)	1653(4)	48(2)
F(5)	6139(4)	7883(8)	1551(9)	94(4)
F(10)	11368(4)	7841(7)	184(8)	87(3)
C(27)	10646(5)	3451(8)	-199(7)	46(2)
F(8)	9969(7)	10536(8)	2841(9)	133(5)
F(12)	10748(4)	9169(8)	765(7)	99(3)
O(1)	8121(3)	6480(7)	-39(4)	43(2)
O(2)	8531(4)	8817(6)	124(4)	47(2)
F(4)	6818(5)	8948(11)	2227(8)	113(4)
F(1)	8111(7)	11149(8)	-77(8)	119(4)
C(4)	7317(4)	6007(10)	-936(6)	43(2)
C(29)	9820(4)	5248(10)	255(6)	40(2)
F(7)	8924(7)	10589(14)	2829(9)	134(6)
C(7)	8098(5)	9017(10)	-373(6)	46(2)
C(11)	6878(6)	3455(10)	1917(8)	59(3)
C(5)	7718(4)	6912(9)	-537(6)	39(2)
F(6)	6749(5)	9221(9)	1014(9)	111(4)
F(2)	7557(6)	10637(8)	-1089(8)	118(5)
C(2)	6580(6)	4989(15)	-1784(8)	64(4)
F(9)	9463(9)	11089(9)	1823(9)	143(6)
C(12)	7500(5)	3988(10)	1673(6)	45(2)
C(22)	9837(5)	8121(11)	2453(7)	51(2)

C(30)	10354(5)	6158(9)	246(7)	47(2)
F(11)	10665(5)	9005(11)	-435(7)	111(4)
C(14)	7144(5)	6191(10)	1495(7)	51(2)
F(3)	8547(8)	10667(11)	-1076(8)	125(5)
C(28)	9989(5)	3971(9)	108(6)	44(2)
C(24)	9466(7)	10286(13)	2410(9)	73(4)
C(32)	10746(6)	8333(12)	209(10)	68(4)
C(6)	7676(6)	8172(11)	-710(7)	54(3)
C(19)	10624(6)	6037(13)	3258(7)	58(3)
C(20)	10197(5)	5900(10)	2647(7)	49(3)
C(13)	7641(4)	5276(10)	1500(5)	36(2)
C(23)	9422(5)	8951(10)	2141(7)	48(2)
C(31)	10224(5)	7393(9)	325(6)	45(2)
C(15)	7277(4)	7402(10)	1455(6)	42(2)
C(26)	10487(8)	2116(11)	-255(12)	77(5)
C(17)	10687(7)	3970(14)	3091(10)	74(4)
C(21)	9781(4)	6831(10)	2279(5)	41(2)
C(1)	6775(7)	4065(14)	-1303(9)	71(4)
C(16)	6732(5)	8372(10)	1558(9)	61(3)
C(10)	6998(8)	2148(10)	2009(11)	74(4)
C(18)	10917(7)	4951(16)	3463(10)	73(4)
C(25)	9874(8)	1744(12)	-56(10)	75(4)
C(8)	8059(7)	10387(12)	-623(10)	71(4)
C(9)	7585(8)	1744(12)	1893(10)	70(3)

Table 2. Bond lengths [Å] and angles [°] for [Zr(tta)]·H_2O.

Zr(1)-O(4)	2.156(8)
Zr(1)-O(8)	2.157(7)
Zr(1)-O(1)	2.167(7)
Zr(1)-O(5)	2.183(7)
Zr(1)-O(6)	2.193(7)
Zr(1)-O(3)	2.197(6)
Zr(1)-O(2)	2.208(7)
Zr(1)-O(7)	2.215(6)
S(2)-C(9)	1.703(13)
S(2)-C(12)	1.709(10)
S(4)-C(25)	1.641(14)

S(4)-C(28)	1.695(11)
S(3)-C(20)	1.699(12)
S(3)-C(17)	1.722(15)
S(1)-C(1)	1.673(16)
S(1)-C(4)	1.717(12)
C(3)-C(2)	1.536(18)
C(3)-C(4)	1.614(13)
O(7)-C(29)	1.234(11)
O(4)-C(15)	1.268(12)
O(5)-C(21)	1.261(11)
O(3)-C(13)	1.285(10)
O(8)-C(31)	1.284(12)
O(6)-C(23)	1.276(12)
F(5)-C(16)	1.318(14)
F(10)-C(32)	1.375(14)
C(27)-C(26)	1.472(15)
C(27)-C(28)	1.545(13)
F(8)-C(24)	1.294(16)
F(12)-C(32)	1.311(17)
O(1)-C(5)	1.275(11)
O(2)-C(7)	1.248(12)
F(4)-C(16)	1.318(18)
F(1)-C(8)	1.25(2)
C(4)-C(5)	1.442(14)
C(29)-C(28)	1.436(13)
C(29)-C(30)	1.462(14)
F(7)-C(24)	1.36(2)
C(7)-C(6)	1.378(16)
C(7)-C(8)	1.533(15)
C(11)-C(10)	1.432(16)
C(11)-C(12)	1.455(16)
C(5)-C(6)	1.386(14)
F(6)-C(16)	1.305(17)
F(2)-C(8)	1.327(16)
C(2)-C(1)	1.35(2)
F(9)-C(24)	1.33(2)
C(12)-C(13)	1.442(15)
C(22)-C(23)	1.342(16)

C(22)-C(21)	1.421(15)
C(30)-C(31)	1.359(13)
F(11)-C(32)	1.331(18)
C(14)-C(15)	1.330(14)
C(14)-C(13)	1.411(13)
F(3)-C(8)	1.300(19)
C(24)-C(23)	1.508(17)
C(32)-C(31)	1.480(14)
C(19)-C(18)	1.357(18)
C(19)-C(20)	1.373(17)
C(20)-C(21)	1.454(13)
C(15)-C(16)	1.534(14)
C(26)-C(25)	1.36(2)
C(17)-C(18)	1.32(2)
C(10)-C(9)	1.29(2)

Table 3.angles [°] for $[Zr(tta)_4]\cdot H_2O$

O(4)-Zr(1)-O(8)	138.9(2)
O(4)-Zr(1)-O(1)	82.6(3)
O(8)-Zr(1)-O(1)	112.9(3)
O(4)-Zr(1)-O(5)	112.3(3)
O(8)-Zr(1)-O(5)	82.7(3)
O(1)-Zr(1)-O(5)	137.1(2)
O(4)-Zr(1)-O(6)	71.9(3)
O(8)-Zr(1)-O(6)	76.4(3)
O(1)-Zr(1)-O(6)	146.4(3)
O(5)-Zr(1)-O(6)	74.5(3)
O(4)-Zr(1)-O(3)	74.1(2)
O(8)-Zr(1)-O(3)	145.5(2)
O(1)-Zr(1)-O(3)	74.2(3)
O(5)-Zr(1)-O(3)	72.2(2)
O(6)-Zr(1)-O(3)	117.4(3)
O(4)-Zr(1)-O(2)	76.3(3)
O(8)-Zr(1)-O(2)	72.2(3)
O(1)-Zr(1)-O(2)	74.8(3)
O(5)-Zr(1)-O(2)	146.4(3)
O(6)-Zr(1)-O(2)	78.0(2)
O(3)-Zr(1)-O(2)	139.3(2)

O(4)-Zr(1)-O(7)	144.7(2)
O(8)-Zr(1)-O(7)	75.2(2)
O(1)-Zr(1)-O(7)	72.6(3)
O(5)-Zr(1)-O(7)	73.6(3)
O(6)-Zr(1)-O(7)	139.4(3)
O(3)-Zr(1)-O(7)	75.16(19)
O(2)-Zr(1)-O(7)	119.0(3)
C(9)-S(2)-C(12)	91.5(7)
C(25)-S(4)-C(28)	92.9(7)
C(20)-S(3)-C(17)	90.2(7)
C(1)-S(1)-C(4)	92.2(7)
C(2)-C(3)-C(4)	97.1(9)
C(29)-O(7)-Zr(1)	135.4(6)
C(15)-O(4)-Zr(1)	133.7(6)
C(21)-O(5)-Zr(1)	137.9(7)
C(13)-O(3)-Zr(1)	135.4(6)
C(31)-O(8)-Zr(1)	132.3(6)
C(23)-O(6)-Zr(1)	131.7(7)
C(26)-C(27)-C(28)	100.5(9)
C(5)-O(1)-Zr(1)	137.6(7)
C(7)-O(2)-Zr(1)	132.6(7)
C(5)-C(4)-C(3)	124.7(9)
C(5)-C(4)-S(1)	119.3(7)
C(3)-C(4)-S(1)	116.0(7)
O(7)-C(29)-C(28)	120.8(9)
O(7)-C(29)-C(30)	122.0(9)
C(28)-C(29)-C(30)	117.2(8)
O(2)-C(7)-C(6)	128.1(10)
O(2)-C(7)-C(8)	113.2(10)
C(6)-C(7)-C(8)	118.7(10)
C(10)-C(11)-C(12)	105.5(11)
O(1)-C(5)-C(6)	122.5(9)
O(1)-C(5)-C(4)	116.1(9)
C(6)-C(5)-C(4)	121.3(9)
C(1)-C(2)-C(3)	119.6(12)
C(13)-C(12)-C(11)	127.6(9)
C(13)-C(12)-S(2)	120.0(8)
C(11)-C(12)-S(2)	112.4(8)

C(23)-C(22)-C(21)	120.8(10)
C(31)-C(30)-C(29)	120.4(9)
C(15)-C(14)-C(13)	122.2(10)
C(29)-C(28)-C(27)	127.8(9)
C(29)-C(28)-S(4)	117.6(7)
C(27)-C(28)-S(4)	114.5(7)
F(8)-C(24)-F(9)	107.7(15)
F(8)-C(24)-F(7)	107.0(14)
F(9)-C(24)-F(7)	104.1(14)
F(8)-C(24)-C(23)	114.8(11)
F(9)-C(24)-C(23)	112.5(12)
F(7)-C(24)-C(23)	110.0(14)
F(12)-C(32)-F(11)	103.6(12)
F(12)-C(32)-F(10)	106.5(11)
F(11)-C(32)-F(10)	107.3(12)
F(12)-C(32)-C(31)	111.7(11)
F(11)-C(32)-C(31)	113.0(12)
F(10)-C(32)-C(31)	114.0(10)
C(7)-C(6)-C(5)	120.9(9)
C(18)-C(19)-C(20)	112.8(14)
C(19)-C(20)-C(21)	129.0(12)
C(19)-C(20)-S(3)	111.0(8)
C(21)-C(20)-S(3)	119.8(9)
O(3)-C(13)-C(14)	120.5(9)
O(3)-C(13)-C(12)	117.8(8)
C(14)-C(13)-C(12)	121.6(8)
O(6)-C(23)-C(22)	128.8(10)
O(6)-C(23)-C(24)	113.1(10)
C(22)-C(23)-C(24)	118.1(10)
O(8)-C(31)-C(30)	127.6(9)
O(8)-C(31)-C(32)	111.5(9)
C(30)-C(31)-C(32)	120.7(10)
O(4)-C(15)-C(14)	126.9(9)
O(4)-C(15)-C(16)	112.6(9)
C(14)-C(15)-C(16)	120.5(9)
C(25)-C(26)-C(27)	118.2(11)
C(18)-C(17)-S(3)	112.0(10)
O(5)-C(21)-C(22)	121.5(9)

O(5)-C(21)-C(20)	116.5(10)
C(22)-C(21)-C(20)	122.1(9)
C(2)-C(1)-S(1)	115.0(12)
F(6)-C(16)-F(4)	107.1(12)
F(6)-C(16)-F(5)	107.2(12)
F(4)-C(16)-F(5)	108.4(12)
F(6)-C(16)-C(15)	111.8(11)
F(4)-C(16)-C(15)	108.8(11)
F(5)-C(16)-C(15)	113.3(9)
C(9)-C(10)-C(11)	118.1(12)
C(17)-C(18)-C(19)	113.7(13)
C(26)-C(25)-S(4)	113.9(10)
F(1)-C(8)-F(3)	103.5(14)
F(1)-C(8)-F(2)	112.7(14)
F(3)-C(8)-F(2)	100.6(13)
F(1)-C(8)-C(7)	114.3(12)
F(3)-C(8)-C(7)	110.5(13)
F(2)-C(8)-C(7)	113.8(11)
C(10)-C(9)-S(2)	112.4(10)

Table 4. Anisotropic displacement parameters ($Å^2 x\ 10^3$) for $[Zr(tta)]\cdot H_2O$.

	U^{11}	U^{22}	U^{33}	U^{23}	U^{13}	U^{12}
Zr(1)	29(1)	30(1)	35(1)	0(1)	-5(1)	1(1)
S(2)	69(2)	45(2)	90(2)	8(1)	18(2)	4(1)
S(4)	76(2)	49(2)	90(3)	-1(2)	13(2)	-1(1)
S(3)	78(2)	59(2)	74(2)	1(2)	-13(2)	23(2)
S(1)	90(3)	73(2)	77(2)	-5(2)	-13(2)	-19(2)
C(3)	27(3)	57(5)	26(4)	-17(3)	-5(3)	-12(3)
O(7)	32(3)	39(3)	48(3)	-4(3)	4(3)	0(2)
O(4)	42(4)	34(3)	71(5)	0(3)	5(4)	1(3)
O(5)	40(3)	43(3)	44(3)	0(3)	-10(3)	3(3)
O(3)	33(3)	39(3)	41(3)	9(3)	1(2)	5(2)
O(8)	37(3)	37(3)	63(5)	1(3)	0(3)	-6(2)
O(6)	48(4)	49(4)	46(4)	-11(3)	-16(3)	8(3)
F(5)	50(4)	73(6)	161(11)	5(5)	22(5)	14(3)
F(10)	40(4)	73(5)	148(10)	-9(5)	11(5)	-7(3)

C(27)	51(5)	23(4)	65(6)	-2(4)	5(5)	15(4)
F(8)	160(10)	69(5)	170(12)	-46(7)	-98(9)	7(7)
F(12)	70(5)	82(5)	146(9)	-56(6)	14(6)	-29(4)
O(1)	42(3)	45(3)	43(3)	-3(3)	-12(3)	4(3)
O(2)	43(4)	46(4)	54(4)	9(3)	-10(3)	-10(3)
F(4)	109(8)	95(7)	136(10)	-45(7)	33(7)	29(6)
F(1)	192(12)	46(4)	118(9)	6(5)	-35(9)	5(6)
C(4)	33(4)	63(6)	32(4)	-2(4)	0(3)	-2(4)
C(29)	41(5)	42(4)	37(5)	-1(4)	-1(4)	9(4)
F(7)	130(8)	129(11)	142(11)	-90(9)	-28(9)	45(8)
C(7)	48(5)	46(5)	43(5)	5(4)	-7(4)	-1(4)
C(11)	66(7)	34(5)	77(7)	13(5)	14(6)	-12(5)
C(5)	33(4)	46(4)	39(4)	2(4)	-4(3)	4(4)
F(6)	74(5)	82(6)	178(12)	49(7)	14(7)	33(4)
F(2)	130(8)	68(5)	155(11)	47(6)	-84(8)	-16(6)
C(2)	50(7)	105(11)	37(6)	-9(5)	-6(6)	-9(6)
F(9)	273(18)	46(4)	111(9)	1(6)	-43(11)	-20(7)
C(12)	40(5)	48(5)	48(5)	1(4)	-1(4)	9(4)
C(22)	46(5)	59(6)	48(5)	1(5)	-16(5)	1(5)
C(30)	35(4)	41(5)	64(6)	-6(4)	-3(5)	6(4)
F(11)	97(7)	105(7)	132(9)	53(7)	17(7)	-29(6)
C(14)	35(4)	41(5)	76(7)	6(5)	8(5)	7(4)
F(3)	170(11)	82(7)	124(10)	43(7)	23(10)	-28(7)
C(28)	43(5)	40(4)	47(5)	-1(4)	14(4)	12(4)
C(24)	91(9)	62(7)	66(8)	-20(7)	-37(7)	13(7)
C(32)	41(6)	55(6)	108(11)	0(7)	15(7)	-12(5)
C(6)	54(6)	53(6)	55(6)	8(5)	-23(5)	8(5)
C(19)	45(5)	80(8)	48(6)	7(5)	-9(5)	13(5)
C(20)	41(5)	58(6)	49(6)	19(5)	8(4)	15(4)
C(13)	24(4)	52(5)	33(4)	3(4)	2(3)	6(4)
C(23)	49(5)	44(5)	51(6)	-16(4)	-11(4)	-5(4)
C(31)	43(5)	42(4)	51(5)	-3(4)	2(4)	-5(4)
C(15)	32(4)	48(5)	47(5)	3(4)	3(4)	4(4)
C(26)	71(9)	46(6)	115(13)	-22(7)	18(9)	13(5)
C(17)	69(8)	72(8)	81(9)	16(7)	-11(7)	31(7)
C(21)	38(4)	55(5)	28(4)	5(4)	-1(3)	3(4)
C(1)	61(7)	78(9)	73(9)	-9(7)	13(7)	-15(6)
C(16)	44(5)	37(5)	104(10)	6(6)	9(6)	5(4)

C(10)	72(8)	42(6)	108(12)	9(6)	9(9)	-12(5)
C(18)	65(9)	97(11)	57(8)	20(7)	-13(8)	34(7)
C(25)	97(11)	41(6)	86(10)	-8(6)	18(8)	-2(6)
C(8)	76(8)	54(7)	82(9)	28(8)	-25(7)	-4(6)
C(9)	76(8)	46(6)	88(9)	0(6)	5(7)	-12(6)

Table 5. Hydrogen coordinates (x 10^4) and isotropic displacement parameters ($Å^2$x 10^3) for $[Zr(tta)]\cdot H_2O$.

	x	y	z	U(eq)
H(3)	6743	7064	-1910	44
H(27)	11034	3866	-315	55
H(11)	6485	3875	1997	71
H(2)	6293	4821	-2190	77
H(22)	10166	8393	2787	61
H(30)	10784	5889	185	56
H(14)	6709	5938	1522	61
H(6)	7359	8450	-1058	65
H(19)	10703	6793	3505	69
H(26)	10798	1543	-423	93
H(17)	10807	3153	3201	89
H(1)	6617	3254	-1345	85
H(10)	6662	1606	2147	88
H(18)	11250	4903	3832	87
H(25)	9740	916	-70	90
H(9)	7708	914	1950	84